Environmentally induced changes to the diatom cell wall and the implications of these changes on biogeochemical cycles

Colleen Andrea Durkin

A dissertation

submitted in partial fulfillment of the

requirements for the degree of

Doctor of Philosophy

University of Washington

2012

Reading Committee:

E. Virginia Armbrust, Chair

Anitra Ingalls

Gabrielle Rocap

Program Authorized to Offer Degree:

Oceanography

University of Washington

Abstract

Environmentally induced changes to the diatom cell wall and the implications of these changes on biogeochemical cycles

Colleen Andrea Durkin

Chair of the Supervisory Committee:
Professor E. Virginia Armbrust
Oceanography

Diatoms are responsible for 20% of global primary production, control the marine silicon cycle, and are a major constituent of the organic matter that sinks into the deep ocean. Diatom cell walls, or frustules, are composed of silica and additional organic components, and the formation of the frustule is genetically controlled. Changes in frustule formation in response to shifting nutrient conditions can affect biogeochemical cycles due to the physiological responses of individual species and changes in the composition of species with diverse frustules and physiologies. To disentangle these factors, species-specific molecular approaches and fluorescent stains were used to identify changes to the diatom frustule in response to changing environmental conditions. First, the unknown aspects of cell wall formation were explored and chitin was discovered in the cell wall of several diatom species. The transcript abundance of chitin synthase gene was correlated with the timing of maximum labeling of cellular chitin using a fluorescent probe. Chitin synthesis appeared to change when cells experienced silicic acid or iron starvation. Next, multiple genes related to frustule formation were studied in a community at the iron-limited Station Papa in the NE Pacific Ocean before and after iron-enrichment. The species-

specific influence on silica precipitation was evaluated with a quantitative fluorescent silica stain and was also evident from the diverse genetic potential among species. Changes in the transcript abundance of silicon transporters indicate that iron-enrichment may induce a functional shift in how silicon is taken up by the dominant species present. This was the first study to identify genetic patterns of frustule formation in natural diatom communities. Finally, the influence of silicic acid availability on coastal biogeochemistry was explored in natural communities and laboratory isolates. Growth experiments indicated that cellular silicification is highly influenced by the concentration of silicic acid available. Transcription of silicon transporters did not correlate with the changes in silicification, suggesting that diffusion of silicic acid into the cell may be important. When more silicic acid is available, cells are more silicified and sink faster. These changes in diatom frustule formation affect in the potential export of carbon from the surface ocean.

TABLE OF CONTENTS

Page

List of Figures ii

List of Tables iii

Introduction 1

Chapter 1: Chitin in Diatoms and its Association with the Cell Wall 12

1.1 Abstract 12

1.2 Introduction 12

1.3 Methods 15

1.4 Results 21

1.5 Discussion 26

1.6 Acknowledgments 32

1.7 Bibliography 33

Chapter 2: Frustule-related Gene Transcription and the Influence of Diatom Community Composition on Silica Precipitation in an Iron-limited Environment 52

2.1 Abstract 52

2.2 Introduction 52

2.3 Methods 55

2.4 Results 61

2.5 Discussion 69

2.6 Acknowledgments 74

2.7 Bibliography 75

Chapter 3: Silicic Acid Supplied to Coastal Diatom Communities Influences Cellular Silicification and the Potential Export of Carbon 88

3.1 Abstract 88

3.2 Introduction 88

3.3 Methods 91

3.4 Results 97

3.5 Discussion 105

3.6 Acknowledgments 110

3.7 Bibliography 112

Conclusion 125

LIST OF FIGURES

Figure Number		Page
1.1	Phylogenetic tree of translated diatom chitin synthase gene sequences	43
1.2	Protein domains from different chitin synthase clades	44
1.3	Transcript abundance of chitin synthase genes	45
1.4	Growth and gene expression characteristics of cultures	46
1.5	Transcript abundance of the *T. pseudonana* reference genes	47
1.6	Fluorescence of FITC-WGA in the presence of a competitive binding substrate	48
1.7	Fluorescent signal of cells in silicic acid replete and limited conditions	49
1.8	Micrographs of exponentially growing and silicic acid starved *T. pseudonana* cells	50
1.9	Micrographs of silicic acid starved diatoms incubated with FITC-WGA	51
2.1	Boxplot of integrated PDMPO fluorescence of individual cells at Sta. Papa	82
2.2	Contribution of different phytoplankton to total new silica precipitated	83
2.3	Proportion of *Pseudo-nitzschia* frustule parts labeled with PDMPO	84
2.4	Mean fluorescent intensity of fully labeled diatom cells	85
2.5	Phylogenetic trees of frustule-related genes, including environmental transcripts	86
2.6	Transcriptional response of *Pseudo-nitzschia multiseries* to low nutrients	87
3.1	Map of the coastal study region	117
3.2	Chlorophyll *a* vs. biogenic silica concentrations in deck-board incubations	118
3.3	Diatom community composition determined by flow cytometry	119
3.4	Diatom community composition determined by microscopy	120
3.5	Silica per cell of cultured isolates acclimated to different silicic acid concentrations	121
3.6	Fluorescence of PDMPO labeled cultures in different growth conditions	122
3.7	PDMPO fluorescence vs. silica per cell of cultures in different growth conditions	122
3.8	Transcript abundance of different silicon transporters	123
3.9	Sinking speeds of cultures acclimated to different concentrations of silicic acid	124

LIST OF TABLES

Table Number Page

1.1 Organisms tested by PCR for the presence of chitin synthase genes 40

1.2 Oligonucleotide primers used for amplifying chitin synthase genes 41

1.3 Genomic characteristics of chitin synthase genes ……..... 42

2.1 Transcripts measured by RT-qPCR …….....81

2.2 Genes related to frustule formation in four diatom genomes ……..81

3.1 Deck-board incubations conducted in coastal waters ……...…….116

Acknowledgments

Many people have contributed ideas, labor, influence, and encouragement to this thesis work and I am grateful for their contributions. Ginger has been a patient advisor, a skillful guide, a brilliant problem solver, and an inspirational scientist. I began this work because I wanted to learn how to do science and think scientifically, and Ginger has been a skilled teacher and inspiration in this regard. I am also thankful to those who have served on my committee; Gabrielle Rocap, John Baross, Anitra Ingalls, Rose Ann Cattolico, Jim Murray, and Jim Thomas.

This work was funded through the support of the Gordon and Better Moore Foundation, the University of Washington School of Oceanography, and a grant from the National Science Foundation to the Center for Coastal Margin Observation and Prediction (CMOP).

All of this work has been completed in collaboration with a team of scientist and would not be possible without the contributions of Thomas Mock, Adrian Marchetti, Sara Bender, Tiffany Truong, Rhonda Morales, Kelsey Gaessner, Karen Chan, and Danny Grünbaum. Additional technical help was provided by Chris Berthiaume, Dave Schruth, Ellen Ostlund Lin, Claire Ellis, Jarred Swalwell, Francois Ribalet, Gwenn Hennon, Robin Kodner, and Irina Oleinikov. The ideas from each of these people have influenced the evolution of this project. Others whose ideas have been particularly helpful include Julie Koester, Vaughn Iverson, Micaela Parker, and Shady Amin.

An important part of this thesis is the work conducted at sea, and I am thankful to those who accommodated me on their cruises and the crews of the ships. The work conducted in the subarctic north Pacific was made possible by Marie Robert, the scientists at Oceans and Fisheries Canada, and the officers and crew of the R/V J.P. Tully. The work conducted along the Washington and Oregon coast was made possible by the CMOP scientists (particularly Byron Crump, Tawnya Peterson, Lydie Herfort, and Fred Prahl) and the crews of the R/V New Horizon and R/V Wecoma.

I am also thankful to those scientists who gave me opportunities to explore research early in my education. Rose Ann Cattolico, Eric Sotka, Christiane Biermann, Linda Rhodes, and Piet Spaak guided me toward the path of research science.

This work could not have been completed without the encouragement from friends and family. For that I am grateful to Tom Connolly, Julie Koester, Sara Bender, Kate Hubbard, Karen Chan, Eric Collins, John Kirkpatrick, Rhonda Morales, Steve Morales, Cecilia Peralta

Ferriz, Sally Warner, Greg Curtis, David Thurman, Monica Shoemaker, Chris Shoemaker, Tim Durkin, Brigitte Durkin, and Brian Durkin.

Introduction

Diatoms have long been a source of scientific and artistic inspiration because they create intricately patterned silica cell walls (frustules) that occur in seemingly endless variations (Leeuwenhoek 1712; Haeckel 1904). The shape and pattern of these frustules are used to identify diatom species, which are one of the most species-rich lineages of eukaryotes. Diatoms are engineers of microscopic processes and drivers of global processes, and perhaps an ideal example of the interconnectedness of the earth's biology, geophysics, chemistry, and geology. Diatoms particularly influence these systems, and are influenced by them, because they precipitate silica frustules and because they are highly productive. Carbon is fixed into organic matter by photosynthesis as diatom cells grow and divide and this carbon becomes encapsulated by the silicon of the frustule; a fate for about 20% of the carbon fixed on earth and 75% of the carbon fixed in the coastal ocean (Nelson et al. 1995; Field et al. 1998). When carbon is fixed by diatoms the marine carbon and silicon cycles become coupled. This is a significant event because it affects the distribution of carbon on earth; whether it is likely to be respired and return to the atmosphere as carbon dioxide, to be recycled in the surface waters as dissolved organic carbon, to support the growth of higher trophic levels in the form of particulate organic carbon, or to be transported into the deep ocean. The carbon fixed into a diatom cell is more likely to follow one of these last two paths. Because diatoms are encased in a relatively heavy silica frustule, some of this production sinks to deeper waters before it can be eaten, or after it is eaten and is aggregated inside zooplankton fecal pellets (Smetacek 1999). The greatest export of particles in the ocean is associated with diatom blooms, which sink faster than other phytoplankton types, allowing them to escape the surface waters before they can dissolve, be eaten by zooplankton, or be decomposed and recycled by bacteria (Buesseler 1998). Diatom-bound carbon that is either respired in the deep ocean or becomes buried in the sediments will not immediately return to the atmosphere, and reduces the atmospheric reservoir of carbon dioxide, a gas with a warming forcing on the climate. Changes in the growth and chemical composition of diatoms, their metabolic functions, and their tendency to sink will alter these global scale processes, and these biological changes occur at the cellular and microscopic level.

To parameterize and predict how diatoms respond to environmental change, or how they may alter the environment, we must know their biological capabilities and the mechanisms responsible for them. Robust generalizations about how diatoms respond to environmental conditions are complicated by the scale of diversity within this group that evolved ~240 million years ago and has diversified faster than many other eukaryotic lineages (Round et al. 1990; Kooistra and Medlin 1996). The evolution of these species has produced cells of vastly different sizes, chemical contents, life histories, and capabilities. The first group to evolve were the radial centric diatoms, followed by the multi-polar centric diatoms (Sims et al. 2006). The clade of *Thalassiosirales* diatoms diverged from the clade of multi-polar centric diatoms, although they are morphologically similar to the radial centric diatoms (Kaczmarska et al. 2005). The last major group of diatoms to evolve was the pennate diatoms. Extant species from each of these lineages thrive and coexist in the modern ocean, in a world much different from the one the first emerged in, with perhaps the most important difference being the availability of silicic acid in seawater (Siever 1991). When centric diatoms evolved, the average concentration of silicic acid in the ocean was ~600 μM. Throughout the period of diatom evolution, diversification, and increasing ecological success, the average silicic acid concentrations in the ocean were drawn down to the modern day average of 70 μM. Today the largest photosynthetic habitats in the ocean, the tropical and subtropical oceans, contain <2 μM silicic acid (Treguer et al. 1995). Higher concentrations, sometimes >100 μM, are found in the coastal, temperate, and polar waters where winter mixing and upwelling brings nutrient-rich deep water to the surface. Diatoms are responsible for the current distribution of silicic acid in the ocean and, overall, diatoms control the marine silicon cycle (Siever 1991; Treguer et al. 1995). Their resilience in a world in which the availability of this critical nutrient has drastically changed illustrates the potential metabolic flexibility and functional diversity which has evolved among modern day diatoms. The biological mechanisms responsible for the continued resilience of diatoms may have evolved differently among species, and therefore the influence of diatoms on biogeochemistry will heavily depend on which species are present, what biological capabilities they have, and how they regulate those abilities when environmental conditions change. Since precipitation of the silica frustule is a key aspect

of how diatoms influence global processes, characterizing the formation of diatom frustules in diverse communities experiencing changing conditions is necessary to reconstruct past and predict future biogeochemical and climatic states.

The application of genetics in the field of oceanography has created a powerful way to discover what metabolisms different diatom species are capable of and to detect the response of these metabolisms to changing conditions. Identifying the pathways responsible for the formation of the silica frustule has been slow and difficult because this characteristic is not homologous to the cell walls of more well-studied organisms (Knoll 2003; Raven and Giordano 2009). The first discoveries about how the frustule is formed came from extracting proteins and other molecules from the cell membrane and the silica frustule. Long-chain polyamines and highly modified proteins, called silaffins and silacidins, are embedded within the silica of the frustule and biochemically capable of controlling the precipitation of silica (Kroger et al. 1999; Kroger et al. 2000; Wenzl et al. 2008). Frustulins, pleuralins, and a family of chitin-binding proteins called p150 are attached to, but not embedded in, the frustule (Kroger et al. 1996; Kroeger and Wetherbee 2000; Davis et al. 2005). Frustulins likely serve as a coat to prevent the dissolution of the frustule in seawater that is under-saturated with silicic acid, and pleuralins help to differentiate between the two halves of the frustule during cell division. The function of the p150 proteins was not determined but they respond to nutrient stresses and are localized in the girdle bands. The silicic acid transporters (SITs) are responsible for transporting silicic acid into the cell and were identified by characterizing silicon-responsive mRNA transcripts (Hildebrand et al. 1993; Hildebrand et al. 1998). These transporters are embedded in the outer cell membrane. The sequences of silicic acid transporters and p150 proteins appear to be relatively conserved and SIT gene sequences have been identified in diatoms representing each of the major lineages by targeting conserved nucleotides (Thamatrakoln et al. 2006). The other known frustule-related proteins (eg. silafins, silacidins, pleuoralins, frustulins) are defined by the chemical properties at the amino acid level, but are not conserved at the level of gene sequences. Consequently, identify and measuring these genes or protein products in diverse species is difficult.

The availability of the *T. pseudonana* genome sequence (Armbrust et al. 2004), followed by the *Phaeodactylum tricornutum* (Bowler et al. 2008), *Fragilariopsis cylindrus*, and *Pseudo-nitzschia multiseries* genome sequences, has revealed previously unidentified genes whose protein products may be involved in frustule-related processes. For example, since long chain polyamines are not proteins, their synthesis depends upon a metabolic pathway whose enzymes are encoded by genes. These unusually long molecules are hypothesized to be synthesized by a metabolic pathway similar to typical polyamines, but with an additional step involving specific aminopropyltransferases found in the diatom genome (Anthony 2011). One of these translated aminopropyltransferase genes contains both a spermidine synthase-like and a SAM decarboxylase protein domain, and is hypothesized to synthesize the long chain polyamines embedded within the silica frustule. A second type of aminopropyltransferase gene, whose protein product is predicted to contain a single spermidine synthase-like domain, is hypothesized to be involved in creating a polyamine modification of silifins. While the long chain polyamines themselves can be extremely diverse, the gene sequences encoding the protein pathway for their synthesis is relatively conserved, with motifs homologous to those found in all other domains of life. To identify additional genes and pathways involved in cell wall formation, several studies have employed whole genome transcription to identify genes whose expression is correlated with conditions that specifically affect frustule formation (Mock et al. 2008; Sapriel et al. 2009). The availability of the genome sequence has also been used to identify more genes with poorly conserved sequence but defined by the predicted amino acid characteristics of their protein products. This type of analysis enabled the discovery of cingulins, proteins that serve as a scaffold onto which silica is precipitated (Scheffel et al. 2011). Advances are happening much faster with the help of genome information, but the known pathway of silicon from the point it enters the cell to when it is precipitated into intricate shapes and patterns around the cell is still largely unknown. For this reason, genetic information must continue to be mined into order to develop tools capable of detecting how frustule formation changes in different conditions and among species.

Molecular tools capable of detecting changes in diverse communities are most likely to be developed with genes that are conserved at the nucleotide level. These

include the silicic acid transporters, the gene products involved in the polyamine synthesis pathway, and many with a hypothesized but uncharacterized role in frustule formation identified by whole cell transcriptomics. Interestingly, many of these genes are part of multi-copy gene families. If frustule formation involves proteins that are part of gene families, it introduces a possible mechanism for flexible responses to changing environments and functional differentiation among species. This is possible because only one must gene copy must retain its original functionality while random mutation can alter the other gene copies without harming the organism. This random mutation can by chance change the function of these gene copies. Because diatom species are extremely diverse and many of the known frustule-related genes are part of gene families, the evolution of functionally divergent genes could play a large role in the evolved response of each species to environmental change.

Measuring frustule formation at the molecular level may enable oceanographers to explain patterns and detect changes that are presently confounded by insensitive method and complicated by the presence of diverse species. These limitations need to be resolved to fully parameterize the carbon and silicon cycle in different ocean regions. The iron-limited open ocean and high nutrient coastal ocean are two regions where the diatoms link between the carbon and silicon cycles is particularly sensitive to change. The subarctic north Pacific, equatorial Pacific, and Southern Ocean all contain relatively high concentrations of nitrate that is not utilized by phytoplankton communities. In these regions that cover ~40% of the surface ocean, low availability of iron limit primary production and potential carbon export (Moore et al. 2002; De Baar et al. 2005). Changes in the availability of iron across glacial and interglacial time scales are hypothesized to have changed production by diatoms and the export of carbon in these regions (Martin 1990). Today, pulse inputs of iron also induce diatom blooms, illustrating the dynamic ecological state of these regions that can alter biogeochemistry (De Baar et al. 2005; Blain et al. 2007; Hamme et al. 2010). In coastal upwelling zones nutrient-rich deep water is brought to the surface, fueling diatom-dominated blooms. This deep water contains high concentrations of carbon dioxide that outgas into the atmosphere. Because production by diatoms is more likely to sink and return carbon to deeper waters, upwelling coastal zones can be both a source of carbon to the atmosphere

and a potential sink (Borges et al. 2005; Hales et al. 2005; Ianson et al. 2009). Therefore, the details of carbon fixation, silica precipitation, and sinking potential of these blooms are important biological details controlling the biogeochemistry of coastal regions. Furthermore, climate induced changes in patterns of upwelling and human impacts on coastal nutrient runoff make coastal regions a place where diatoms may change the future biogeochemical balance.

This thesis investigates the mechanisms and evolution of frustule formation in diverse diatom species and applies this information to better characterize the activity of diatom communities in environments with high potential for change. This thesis tests the overall hypothesis that changes in the environment will affect diatom frustule formation and alter the role of diatoms in biogeochemical cycles. Chapter 1 addresses the gap in knowledge related to diatom cell wall formation and composition, details which must be known if changes to the frustule and their biogeochemical consequences are to be measured. This first study hypothesizes that chitin is a component of the diatom cell wall, a hypothesis formed because of the presence of chitin-synthesizing genes in diatom genomes. This hypothesis is tested by correlating transcriptional c of these genes in cultured isolates with the localization of chitin-binding fluorescent cellular stains. In chapter 2 this new discovery and existing knowledge about frustule formation is applied to study natural communities in the iron-limited subarctic Pacific. This second chapter tests the hypothesis that silicon cycling in iron-limited environments will be largely influenced by diatom species composition due to the diversity of silica requirements among species and the species-specific responses of the frustule to iron limitation. In chapter 3 we shift our focus to the influence of diatoms on the biogeochemistry of the coastal ocean. This third chapter tests the hypothesis that high concentrations of silicic acid will increase the relative silicification of coastal phytoplankton communities and lead to a more efficient export of organic matter to deeper waters. These studies are among the first to apply molecular techniques to detect changes in frustule formation in the natural environment. This work improves the existing knowledge about diatom frustule formation and its effect on biogeochemical cycles, which will help detect and parameterize changes that influence global biogeochemistry.

Introduction Bibliography

Anthony, M. 2011. Molecular machines encoded by bacterially-derived multi-domain gene fusions that potentially synthesize, N-methylate and transfer long chain polyamines in diatoms. Febs Letters **585:** 2627-2634.

Armbrust, E. V., J. A. Berges, C. Bowler, B. R. Green, D. Martinez, N. H. Putnam, S. G. Zhou, A. E. Allen, K. E. Apt, M. Bechner, M. A. Brzezinski, B. K. Chaal, A. Chiovitti, A. K. Davis, M. S. Demarest, J. C. Detter, T. Glavina, D. Goodstein, M. Z. Hadi, U. Hellsten, M. Hildebrand, B. D. Jenkins, J. Jurka, V. V. Kapitonov, N. Kroger, W. W. Y. Lau, T. W. Lane, F. W. Larimer, J. C. Lippmeier, S. Lucas, M. Medina, A. Montsant, M. Obornik, M. S. Parker, B. Palenik, G. J. Pazour, P. M. Richardson, T. A. Rynearson, M. A. Saito, D. C. Schwartz, K. Thamatrakoln, K. Valentin, A. Vardi, F. P. Wilkerson, and D. S. Rokhsar. 2004. The genome of the diatom *Thalassiosira pseudonana*: Ecology, evolution, and metabolism. Science **306:** 79-86.

Blain, S., B. Queguiner, L. Armand, S. Belviso, B. Bombled, L. Bopp, A. Bowie, C. Brunet, C. Brussaard, F. Carlotti, U. Christaki, A. Corbiere, I. Durand, F. Ebersbach, J. L. Fuda, N. Garcia, L. Gerringa, B. Griffiths, C. Guigue, C. Guillerm, S. Jacquet, C. Jeandel, P. Laan, D. Lefevre, C. Lo Monaco, A. Malits, J. Mosseri, I. Obernosterer, Y. H. Park, M. Picheral, P. Pondaven, T. Remenyi, V. Sandroni, G. Sarthou, N. Savoye, L. Scouarnec, M. Souhaut, D. Thuiller, K. Timmermans, T. Trull, J. Uitz, P. Van Beek, M. Veldhuis, D. Vincent, E. Viollier, L. Vong, and T. Wagener. 2007. Effect of natural iron fertilization on carbon sequestration in the Southern Ocean. Nature **446:** 1070-U1071

Borges, A. V., B. Delille, and M. Frankignoulle. 2005. Budgeting sinks and sources of CO2 in the coastal ocean: Diversity of ecosystems counts. Geophys. Res. Lett. **32:** L14601

Bowler, C., A. E. Allen, J. H. Badger, J. Grimwood, K. Jabbari, A. Kuo, U. Maheswari, C. Martens, F. Maumus, R. P. Otillar, E. Rayko, A. Salamov, K. Vandepoele, B. Beszteri, A. Gruber, M. Heijde, M. Katinka, T. Mock, K. Valentin, F. Verret, J. A. Berges, C. Brownlee, J. P. Cadoret, A. Chiovitti, C. J. Choi, S. Coesel, A. De

Martino, J. C. Detter, C. Durkin, A. Falciatore, J. Fournet, M. Haruta, M. J. J. Huysman, B. D. Jenkins, K. Jiroutova, R. E. Jorgensen, Y. Joubert, A. Kaplan, N. Kroger, P. G. Kroth, J. La Roche, E. Lindquist, M. Lommer, V. Martin-Jezequel, P. J. Lopez, S. Lucas, M. Mangogna, K. Mcginnis, L. K. Medlin, A. Montsant, M. P. Oudot-Le Secq, C. Napoli, M. Obornik, M. S. Parker, J. L. Petit, B. M. Porcel, N. Poulsen, M. Robison, L. Rychlewski, T. A. Rynearson, J. Schmutz, H. Shapiro, M. Siaut, M. Stanley, M. R. Sussman, A. R. Taylor, A. Vardi, P. Von Dassow, W. Vyverman, A. Willis, L. S. Wyrwicz, D. S. Rokhsar, J. Weissenbach, E. V. Armbrust, B. R. Green, Y. Van De Peer, and I. V. Grigoriev. 2008. The *Phaeodactylum* genome reveals the evolutionary history of diatom genomes. Nature **456:** 239-244.

Buesseler, K. O. 1998. The decoupling of production and particulate export in the surface ocean. Global Biogeochemical Cycles **12:** 297-310.

Davis, A. K., M. Hildebrand, and B. Palenik. 2005. A stress-induced protein associated with the girdle band region of the diatom Thalassiosira pseudonana (Bacillariophyta). Journal of Phycology **41:** 577-589

De Baar, H. J. W., P. W. Boyd, K. H. Coale, M. R. Landry, A. Tsuda, P. Assmy, D. C. E. Bakker, Y. Bozec, R. T. Barber, M. A. Brzezinski, K. O. Buesseler, M. Boye, P. L. Croot, F. Gervais, M. Y. Gorbunov, P. J. Harrison, W. T. Hiscock, P. Laan, C. Lancelot, C. S. Law, M. Levasseur, A. Marchetti, F. J. Millero, J. Nishioka, Y. Nojiri, T. Van Oijen, U. Riebesell, M. J. A. Rijkenberg, H. Saito, S. Takeda, K. R. Timmermans, M. J. W. Veldhuis, A. M. Waite, and C. S. Wong. 2005. Synthesis of iron fertilization experiments: From the iron age in the age of enlightenment. Journal of Geophysical Research-Oceans **110:** C09S16, doi:10.1029/2004JC002601

Field, C. B., M. J. Behrenfeld, J. T. Randerson, and P. Falkowski. 1998. Primary production of the biosphere: Integrating terrestrial and oceanic components. Science **281:** 237-240.

Haeckel, E. 1904. Kunstformen der Natur. Verlag des Bibliographischen Instituts.

Hales, B., T. Takahashi, and L. Bandstra. 2005. Atmospheric CO2 uptake by a coastal upwelling system. Global Biogeochemical Cycles **19:**

Hamme, R. C., P. W. Webley, W. R. Crawford, F. A. Whitney, M. D. Degrandpre, S. R. Emerson, C. C. Eriksen, K. E. Giesbrecht, J. F. R. Gower, M. T. Kavanaugh, M. A. Peña, C. L. Sabine, S. D. Batten, L. A. Coogan, D. S. Grundle, and D. Lockwood. 2010. Volcanic ash fuels anomalous plankton bloom in subarctic northeast Pacific. Geophys. Res. Lett. **37:** L19604

Hildebrand, M., K. Dahlin, and B. E. Volcani. 1998. Characterization of a silicon transporter gene family in *Cylindrotheca fusiformis*: Sequences, expression analysis, and identification of homologs in other diatoms. Molecular and General Genetics MGG **260:** 480-486.

Hildebrand, M., D. R. Higgins, K. Busser, and B. E. Volcani. 1993. Silicon-responsive cDNA clones isolated from the marine diatom Cylindrotheca fusiformis. Gene **132:** 213-218

Ianson, D., R. A. Feely, C. L. Sabine, and L. W. Juranek. 2009. Features of Coastal Upwelling Regions that Determine Net Air-Sea CO2 Flux. Journal of Oceanography **65:** 677-687

Kaczmarska, I., M. Beaton, A. C. Benoit, and L. K. Medlin. 2005. Molecular phylogeny of selected members of the order Thalassiosirales (Bacillariophyta) and evolution of the fultoportula. Journal of Phycology **42:** 121-138

Knoll, A. H. 2003. Biomineralization and evolutionary history. Biomineralization **54:** 329-356

Kooistra, W. H. C. F., and L. K. Medlin. 1996. Evolution of the diatoms (Bacillariophyta): IV. A reconstruction of their age from small subunit rRNA coding regions and the fossil record. Molecular Phylogenetics and Evolution **6:** 391-407.

Kroeger, N., and R. Wetherbee. 2000. Pleuralins are Involved in Theca Differentiation in the Diatom Cylindrotheca fusiformis. Protist **151:** 263-273

Kroger, N., C. Bergsdorf, and M. Sumper. 1996. Frustulins: Domain conservation in a protein family associated with diatom cell walls. European Journal of Biochemistry **239:** 259-264

Kroger, N., R. Deutzmann, C. Bergsdorf, and M. Sumper. 2000. Species-specific polyamines from diatoms control silica morphology. Proceedings of the National Academy of Sciences of the United States of America **97:** 14133-14138.

Kroger, N., R. Deutzmann, and M. Sumper. 1999. Polycationic peptides from diatom biosilica that direct silica nanosphere formation. Science **286:** 1129-1132.

Leeuwenhoek, A. V. 1712. A Letter from Mr. Anthouy Van Leeuwenhoek, F. R. S. containing Some Further Microscopical Observations on the Animalcula Found Upon Duckweed, &c. Philosophical Transactions **28:** 160-164

Martin, J. H. 1990. Glacial-interglacial CO_2 change: The iron hypothesis. Paleoceanography **5:** 1-13.

Mock, T., M. P. Samanta, V. Iverson, C. Berthiaume, M. Robison, K. Holtermann, C. Durkin, S. S. Bondurant, K. Richmond, M. Rodesch, T. Kallas, E. L. Huttlin, F. Cerrina, M. R. Sussmann, and E. V. Armbrust. 2008. Whole-genome expression profiling of the marine diatom *Thalassiosira pseudonana* identifies genes involved in silicon bioprocesses. Proceedings of the National Academy of Sciences of the United States of America **105:** 1579-1584.

Moore, J. K., S. C. Doney, D. M. Glover, and I. Y. Fung. 2002. Iron cycling and nutrient-limitation patterns in surface waters of the World Ocean. Deep-Sea Research Part II **49:** 463-507.

Nelson, D. M., P. Treguer, M. A. Brzezinski, A. Leynaert, and B. Queguiner. 1995. Production and dissolution of biogenic silica in the ocean- Revised global estimates, comparison with regional data and relationship to biogenic sedimentation. Global Biogeochemical Cycles **9:** 359-372.

Raven, J. A., and M. Giordano. 2009. Biomineralization by photosynthetic organisms: Evidence of coevolution of the organisms and their environment? Geobiology **7:** 140-154

Round, F. E., R. M. Crawford, and D. G. Mann. 1990. The Diatoms : biology & morphology of the genera. Cambridge University Press.

Sapriel, G., M. Quinet, M. Heijde, L. Jourdren, V. Tanty, G. Z. Luo, S. Le Crom, and P. J. Lopez. 2009. Genome-wide transcriptome analyses of silicon metabolism in

Phaeodactylum tricornutum reveal the multilevel regulation of silicic acid transporters. Plos One **4:** e7458, doi: 7410.1371/Journal.Pone.0007458

Scheffel, A., N. Poulsen, S. Shian, and N. Kroeger. 2011. Nanopatterned protein microrings from a diatom that direct silica morphogenesis. Proceedings of the National Academy of Sciences **108:** 3175-3180.

Siever, R. 1991. Silica in the oceans: biological-geochemical interplay, p. xxii, 433 p. *In* S. H. Schneider and P. J. Boston [eds.], Scientists on Gaia. MIT Press.

Sims, P. A., D. G. Mann, and L. K. Medlin. 2006. Evolution of the diatoms: insights from fossil, biological and molecular data. Phycologia **45:** 361-402

Smetacek, V. 1999. Diatoms and the ocean carbon cycle. Protist **150:** 25-32

Thamatrakoln, K., A. J. Alverson, and M. Hildebrand. 2006. Comparative sequence analysis of diatom silicon transporters: Toward a mechanistic model of silicon transport. Journal of Phycology **42:** 822-834.

Treguer, P., D. M. Nelson, A. J. Vanbennekom, D. J. Demaster, A. Leynaert, and B. Queguiner. 1995. The Silica Balance in the World Ocean - a Reestimate. Science **268:** 375-379

Wenzl, S., R. Hett, P. Richthammer, and M. Sumper. 2008. Silacidins: Highly acidic phosphopeptides from diatom shells assist in silica precipitation in vitro. Angewandte Chemie-International Edition **47:** 1729-1732.

Chapter 1

Chitin in diatoms and its association with the cell wall

1.1 Abstract

Chitin is a globally abundant polymer widely distributed throughout eukaryotes that has been well characterized in only a few lineages. Diatoms are members of the eukaryotic lineage of stramenopiles. Of the hundreds of diatom genera, two produce long fibers of chitin that extrude through their cell walls of silica. Here we identify and describe genes encoding putative chitin synthases in a variety of additional diatom genera indicating that the ability to produce chitin is more widespread and likely plays a more central role in diatom biology than previously considered. Diatom chitin synthases fall into four phylogenetic clades. Protein domain predictions and differential gene expression patterns provide evidence that chitin synthases have multiple functions within a diatom cell. *Thalassiosira pseudonana* possesses 6 genes encoding three types of chitin synthases. Transcript abundance of the gene encoding one of these chitin synthase types increases when cells resume division after short-term silicic acid starvation and during short-term limitation by silicic acid or iron, two nutrient conditions connected in the environment and known to affect the cell wall. During long-term silicic acid starvation transcript abundance of this gene and one additional chitin synthase gene increased at the same time a chitin binding lectin localized to the girdle band region of the cell wall. Together, these results suggest that the ability to produce chitin is more widespread in diatoms than previously thought and that a subset of the chitin produced by diatoms is associated with the cell wall.

1.2 Introduction

Chitin is the most abundant polymer in the ocean and the second most abundant polymer on earth, exceeded only by cellulose (eg. Gooday 1990; Jeuniaux and Vossfoucart 1991; Aluwihare et al. 2005). The pervasiveness of chitin is attributed to its use by diverse eukaryotic organisms, including fungi, insects, mollusks, crustaceans, algae, and protists. These diverged lineages commonly use chitin to strengthen their cell walls or skeletons. Chitin synthase is used by all chitin producing organisms to generate the β-(1→4) linked N-acetylglucosamine

polymers. The universality of this enzyme suggests an ancient eukaryotic origin (Ruiz-Herrera et al. 2002). Chitin synthases are identified by the conserved amino acid motifs QXXEY, EDR, QXRRW, and additional lineage specific motifs that together are responsible for substrate specificity and reaction catalysis (Ruiz-Herrera et al. 2002; Merzendorfer 2006). Chitin synthases are embedded across the cell membrane and it is at the membrane junction that N-acetylglucosamine monomers are added to a growing polymer while it is transported across the membrane (Saxena et al. 1995). While maintaining these general features, chitin synthases have also diverged and diversified within and between eukaryotic lineages. These enzymes have been most extensively studied within fungi where sequence phylogenies identify two major divisions of chitin synthases, with additional classes within these divisions. Phylogenetically distinct chitin synthases produce chitin at different cellular locations and for different biological functions (Roncero 2002). Thus, an individual organism often contains multiple types of chitin synthases.

Diatoms are known chitin producers that are of significant ecological importance. Globally, these unicellular algae are responsible for about 20% of annual primary production (Nelson et al. 1995; Field et al. 1998) and support the most biologically productive regions of the ocean. Evolutionarily distinct from plants and metazoans, diatoms are members of the stramenopiles, a major eukaryotic lineage that includes plant pathogens, flagellates, and brown macro-algae. The most distinctive characteristic of diatoms is the nano-patterned silica cell wall, which is composed of two halves (thecae) connected by hoop-like silica structures called girdle bands. Diatom cell wall formation and eventual dissolution controls the biogeochemical cycling of silicon in the ocean, and because it is required for growth, silicon availability affects carbon and other nutrient cycles (Dugdale et al. 1995). The formation of these intricate inorganic nanostructures has been studied intensively due to potential applications in nanotechnology that require controlled synthesis of microscopic structures (Parkinson and Gordon 1999; Brott et al. 2001). These topics have motivated more detailed analysis of the biological mechanisms controlling cell wall formation (Hildebrand et al. 2006) and molecules associated with the silica (Kroger et al. 1999; Kroger et al. 2000; Frigeri et al. 2006; Tesson et al. 2008). The centric diatom *Thalassiosira pseudonana* has emerged as a powerful model for understanding silica biomineralization because of the availability of whole genome sequence (Armbrust et al. 2004).

Thalassiosira and *Cyclotella* are the two diatom genera known to produce chitin (Mclachlan and Craigie 1966). Both are members of the order Thalassiosirales, which falls within the multipolar diatoms (class Mediophyceae). Interestingly, this class is evolutionarily intermediate to the more ancient centric diatoms (class Coscinodiscophyceae) and the more derived pennate diatoms (class Bacillariophyceae) (Medlin and Kaczmarska 2004) (see inset, Fig. 1.1). *Thalassiosira* and *Cyclotella* both produce long thin chitin fibers that extend from the theca through specialized pores within the silica known as fultoportulae (Herth and Schnepf 1982; Round et al. 1990; Kaczmarska et al. 2005). The chitin fibers are arranged in an unusual highly crystalline beta configuration, in which all polymers lie parallel to one another and are not associated with other molecules (Mclachlan et al. 1965; Dweltz et al. 1968; Sugiyama et al. 1999). Specialized vesicles targeted to an invaginated membrane just below the fultoportulae have been identified and were proposed to carry the molecular and chemical machinery necessary for chitin synthesis, which likely includes the chitin synthases (Herth 1979). In *T. weissflogii*, chitin synthases are estimated to generate 700,000 N-aceytlglucosamine linkages sec^{-1} μm^{-2} of specialized membrane (Herth 1979).

Analysis of the whole genome sequences for *T. pseudonana* (Armbrust et al. 2004) and the pennate diatom *Phaeodactylum tricornutum* (Bowler et al. 2008) suggests a previously unsuspected and complex role for chitin-related processes in diatoms. All genes necessary for chitin synthesis were found in *T. pseudonana* as well as *P. tricornutum*, despite the fact that *P. tricornutum* does not produce chitin fibers. Both diatoms appear to encode multiple chitin synthases; *T. pseudonana* additionally possesses over 20 genes that encode putative chitin-degrading chitinases and over 20 genes that encode putative proteins with chitin-binding domains. Two of the putative chitin binding proteins in *T. pseudonana* localize to the girdle band region of the cell wall, a region not previously suspected to contain chitin (Davis et al. 2005). The genes encoding these chitin binding proteins, named p150 and p150-like, are highly expressed when cells are grown in the presence of high concentrations of copper or when cells are starved of silicic acid or iron, conditions that all result in abnormally elongated theca (Davis et al. 2005; Mock et al. 2008). We recently identified 84 genes upregulated when cells were deprived of iron or silicic acid; many of these co-regulated genes encode proteins known to be involved in cell wall processes (Mock et al. 2008). Surprisingly, a gene encoding a chitin synthase was among this subset of upregulated genes, suggesting that chitin may play a role in

diatom cell wall processes. Additional support for this possibility comes from a recent analysis of the organic composition of *T. pseudonana* cell walls using solid state NMR (Tesson et al. 2008). This study identified chitin as the main carbohydrate component embedded within the silica cell walls, although the authors attributed this presence to contaminating chitin fibers.

The genetic complexity of chitin related genes in *T. pseudonana*, the identification of potential chitin synthases in *P. tricornutum*, and the unexpected expression pattern of one chitin synthase gene in *T. pseudonana* suggests a more complex role of chitin synthesis in diatoms than previously thought. Here, we describe our characterization of diatom chitin synthase genes through comparative genetics and physiological experimentation to understand the evolution, function, and ecological consequences of chitin synthesis in diatoms.

1.3 Methods

In silico analyses

Putative chitin synthase genes were identified in the *T. pseudonana* and *P. tricornutum* genomes by combining automated gene predictions (www.doe.jgi.gov) and homology of predicted proteins to known chitin synthases in the NCBI non-redundant database based on nBLAST and pBLAST tools (ncbi.nlm.nih.gov/blast/Blast.cgi). BLAST identification of chitin synthases was considered significant when e values were $\leq 10^{-15}$ and when a majority of identified homologs were annotated as chitin synthases. Domain structures of chitin synthases were analyzed by Interpro (ebi.ac.uk/InterProScan/), Prodom (prodom.prabi.fr/prodom/current/html/form.php), NCBI Conserved Domain Database (ncbi.nlm.nih.gov/Structure/cdd/wrpsb.cgi), and TMHMM (cbs.dtu.dk/services/TMHMM-2.0/). Domain predictions were considered significant when $e \leq 10^{-5}$.

Phytoplankton cultures and experimental set up

An isolate of *Thalassiosira punctigera* and *T. rotula* was provided by P. von Dassow (Von Dassow et al. 2008) and an isolate of *Ditylum brightwellii* was provided by J. Koester; both isolates were collected from Puget Sound, WA, USA. An isolate of *Pseudo-nitzschia multiseries* from the North Atlantic was provided by S. Bates and C. Leger. All other phytoplankton isolates (Table 1.1) were purchased from the Provasoli-Guillard National Center for Culture of Marine Phytoplankton (ccmp.bigelow.org). Cultures were maintained exponentially at 100-200 µmol

photons m^{-2} s^{-1} in 250-500 ml f/2-amended seawater (Guillard and Ryther 1962; Guillard 1975) that had been filtered through a 0.45 μm polycarbonate filter (Millipore).

Silicic acid starvation and recovery were monitored on both short and long time scales. Short term recovery from silicic acid starvation was analyzed by first growing triplicate cultures in Aquil medium (Price N. M. et al. 1988/89) under continuous light at 100 μmol photons m^{-2} s^{-1} and constant bubbling with sterile air until the middle of the exponential growth phase. In a manner similar to those described by Hildebrand et al. (2007), cells were harvested by centrifugation at 4500 x g for 15 minutes, washed once with and inoculated into Aquil medium without silicic acid at a final concentration of 0.6 x 10^6 cells ml^{-1}. At t=48 hr, silicic acid was added to the cultures at a final concentration of 200 μM and the cultures were monitored for an additional 8 hr as they recovered from silicic acid starvation and resumed cell division. Long-term responses to silicic acid starvation were monitored in triplicate cultures transferred from exponential growth in fully amended f media into f media (Guillard and Ryther 1962) with low silicic acid (0.067 μM) at 175-275 μmol photons m^{-2} s^{-1}. Changes in chlorophyll *a* fluorescence over time were measured with a fluorometer (Turner) and cell concentrations were determined with an InFlux Cell Sorter flow cytometer (Cytopeia) equipped with a 488 nm laser. An aliquot of 2 μm fluorescent bead stock (Polysciences) of known concentration was added to 1 ml of culture and the particles were counted together. Photosynthetic capacity (Fv/Fm) was determined with a PhytoPAM fluorometer (Walz). To confirm that cell division had ceased due to silicic acid starvation, a final concentration of 214 μM silicic acid was added to a 50 ml aliquot of each triplicate culture and relative fluorescence was monitored for a day. Aliquots of the culture media on day 4 were also filtered through a 0.2 um filter and analyzed for dissolved silicic acid content using the molybdate method (Brzezinski and Nelson 1986). A pulse of silicic acid similar to the short-term experiment (214 μM) was added to the silicic acid starved cultures after six days in stationary phase and the response of the cells was monitored 24 and 48 hours later. Samples were collected from both types of experiments for quantitative reverse transcriptase PCR (qRT-PCR) by filtering between 200 and 1000 ml of culture onto four 2 μm polycarbonate filters (Millipore) (see below). Filtered cells were also collected from previously described experiments (Mock et al. 2008) with nutrient replete cultures and short-term (<1 day) silicic acid, iron, and nitrate limited cultures.

DNA and RNA extraction and cDNA synthesis

DNA was extracted with the Plant DNA Extraction kit (Qiagen) from exponentially maintained cultures (Table 1.1) that had been concentrated and frozen onto 0.45 μm polycarbonate filters (Millipore). RNA was extracted with the Plant RNA Isolation Reagent (Invitrogen) from frozen cells on 2 μm polycarbonate filters. Contaminating DNA was eliminated by incubating the isolated RNA with DNAse I (Ambion) at 37º C for 1-2 hrs; DNA-free RNA was purified with the RNeasy MiniElute Clean up kit (Qiagen). cDNA was synthesized from 2 μg purified RNA with Superscript III First Strand Synthesis System for RT-PCR (Invitrogen). The 20 μL of cDNA was subsequently diluted with water to 100 μL. One microliter of RNA was used in PCRs (see below) to ensure that all contaminating DNA had been eliminated.

Determination of full-length gene sequences

Full-length sequence of the *T. pseudonana* chitin synthase cDNAs was determined by DNA sequencing of PCR-generated fragments using a total of 40 primers (not listed) designed across the entire length of the modeled gene sequences (www.doe.jgi.gov), and open reading frames that appeared to extend up or downstream of gene models. PCRs consisted of 1 μL cDNA, 1 μL 10x Taq buffer, 3.125 mM $MgCl_2$, 0.7 units Taq (Promega and Gene Choice), 0.4 mM dNTPs, 0.5 μM forward and reverse primers. Amplifications consisted of a denaturation at 94 °C for 2 minutes followed by 30 cycles of 94 °C for 10 sec, between 55 and 62 °C for 30 sec depending on annealing temperature of the primer set, and 72 °C for 90 sec. Amplified fragments were separated on an agarose gel and fragments of the appropriate size were cut out of the gel and extracted with the QiaQuick Gel extraction kit (Qiagen). Between 50 and 100 ng of purified PCR product was cycle sequenced with DYEnamic ET Dye Terminator Cycle Sequencing Kit (GE Healthcare Bio-sciences Corp) and analyzed on a MegaBACE 1000 (GE Healthcare Bio-sciences Corp). Rapid Amplification of cDNA Ends (RACE) was performed with First Choice RLM-RACE kit (Ambion) to identify the 5' and 3' ends of the gene encoding protein 7305. RACE primers are listed in Table 1.2. All sequences were analyzed and aligned in Sequencher version 4.6 and compared to the *T. pseudonana* genome with BLAST.

Gene expression

Transcript abundances in *T. pseudonana* were determined by qRT-PCR. Primers (Table 1.2) were designed to amplify a 100-250 bp fragment for four reference genes encoding the actin-like protein (protein id 269504), actin (protein id 25772), 40S rRNA (protein id 31084), and beta tubulin (protein id 31569). Primers were also designed to amplify a 100 bp fragment from genes encoding three chitin synthases (protein ids 7305, 6575, and 4368) and two genes encoding girdle band-associated chitin-binding proteins p150 and p150-like (protein ids 12594 and 26041). Triplicate qRT-PCRs included 2 μL cDNA, 0.8 μM forward and reverse primers, 10, 20, or 25 μL iQ Supermix (BioRad, California) in a 20, 40, or 50 uL reaction volume. Amplifications were carried out in an iCycler (Biorad, California) and consisted of an initial denaturation at 95 ºC for 3 minutes followed by 45 cycles of 95 ºC for 10 sec, 60 ºC for 30 sec, and 72 ºC for 50 sec, followed by a step-wise increase in melting temperature to verify the presence of a single melt peak fluorescent signal. Threshold cycle (CT) values were calculated with iCycler software and the PCR amplification curves were imported into LinReg (Ramakers et al. 2003) to calculate amplification efficiency. Efficiency calculations were based on at least 4 points and only values with $R \geq 0.998$ and efficiency between 1.7 and 2.2 were considered. Efficiencies calculated from all qRT-PCR reactions for a single primer set were averaged to yield a single efficiency for use in expression calculations. These averages were between 1.92 and 1.98 determined from between 34 and 187 separate PCRs, depending on the gene. Relative transcript abundance was calculated with the equation $(E_{ref}^{CTref})/(E_{target}^{CTtarget})$ where E_{ref} is the reference gene efficiency, E_{target} is the target gene efficiency, CT_{ref} is the threshold cycle of the reference gene, and CT_{target} is the threshold cycle of the target gene (Pfaffl 2001). Relative transcript abundance measured in triplicate cultures entering silicic acid-, iron-, or nitrate-limitation were compared to the control condition using a student's T test. Relative transcript abundance in triplicate cultures in the hours after silicic acid replenishment or the days of growth in silicic acid deplete media were log transformed and time points were compared using an ANOVA test ($\alpha < 0.05$) in SPSS version 16. Time points with significant differences were identified using a Tukey test (Zar 1996).

Phylogenetic analysis

ClustalW (Thompson et al. 1994) was used to align translated *T. pseudonana* chitin synthase genes with fungal chitin synthase protein sequences (GenBank ID O13353, P29465, P30573, Q01285, P78611, O13394) and PCR primers (Table 1.2) were designed using CODEHOP (Rose et al. 1998). Primers were designed to target the region encoding conserved chitin synthase motifs $G(X)_4(Y/F)R$ and SWG and spanned the sequence encoding EDR and QRRRW residues, which define the enzyme (Nagahashi et al. 1995; Ruiz-Herrera et al. 2002; Merzendorfer 2006). Reactions included 1-25 ng DNA, 0.5 μM forward and reverse primers, 1μL 10x buffer, 3.125 mM $MgCl_2$, 0.4 mM dNTPs , and 0.7 units taq (Promega and Gene Choice). Amplifications consisted of an initial denaturation of 95 ºC for 2 minutes followed by 30 cycles of 94 ºC for 10 sec, 55 or 60 ºC for 30 seconds, and 72 ºC for 2 minutes. Amplified DNA fragments were separated and purified from an agarose gel as described above, ligated into the TOPO vector (Invitrogen), and used to transform *Escherichia coli* TOP 10 cells. Plasmids from 3-10 positive transformants were amplified with TempliPhi (GE Healthcare Bio-sciences Corp) and sequenced with M13 forward and reverse primers as described above. Resulting DNA sequences were analyzed in Sequencher and aligned with ClustalW. Positive identification of fragments corresponding to chitin synthase genes were based on the presence of sequence that encoded EDR and QRRRW motifs. Sequences that differed by three or more nucleotides were considered distinct. A maximum likelihood tree was calculated in proml in the phylip software package (Felsenstein 1989) based on alignment of all translated sequence fragments amplified with CODEHOP primers, *T. pseudonana* and *P. tricornutum* sequences, with *Saccharomyces cerevisiae* chitin synthase 3 (P29465) as an outgroup. Sequence alignment was anchored by the EDR, QRRRW, and SWG motifs. A region corresponding to amino acids 1007-1073 in *T. pseudonana* 7305, 573-770 in *P. tricornutum* 37908, and 1,012-1,078 in *S. cerevisiae* P29465 was eliminated due to the uncertainty of alignment in this region. The resulting alignment was 111 amino acids long and bootstrap values were calculated from the construction of 1000 trees.

Localizing and quantifying chitin and silica deposition

Silica deposition was determined by incubating 50 ml aliquots of cultures with 0.5 μM 2-(4-pyridyl)-5 oxazole (PDMPO) (Invitrogen) for 12-14 hours in the same light and temperature conditions as the experimental conditions (Shimizu et al. 2001). Cells were analyzed with an

Influx Cell Sorter Flow Cytometer (Cytopeia) equipped with a 355 nm UV laser. Fluorescent emission was detected at 460 nm (50 nm bandpass). Internal standards of 3 μm UV beads (Spherotech) were used for calibration. Epifluorescence was also visualized with an i80 microscope (Nikon) after excitation at 300-400 nm and emission detected with a 420 nm longpass filter (Chroma). Potential chitin localization was determined by incubating cells with 4 μg fluorescein isothiocyanate-labeled wheat germ agglutinin (FITC-WGA) (Sigma) for 15-30 minutes. Cells were centrifuged at 15,000 x g for 5 minutes and resuspended in 1 ml f/2 media or PBS buffer (137 mM NaCl, 2.7 mM KCl, 10.4 mM Na_2HPO_4, 1.8 mM KH_2PO_4) to remove unbound FITC-WGA. The resulting fluorescent signal was quantified by flow cytometry after excitation with a 488 nm laser and 2 μm yellow-green beads (Polysciences) were used as internal standards. Emission was detected at 530 nm (40 nm bandpass). Localization of FITC-WGA binding was visualized by fluorescence microscopy with a 500-570 nm wavelength filter (Chroma) after excitation at 455-500 nm. Competitive binding experiments with chitotriose and N-acetylglucosamine (Montgomery et al. 1990; Peters and Latka 1997) were used to determine if the FITC-WGA bound specifically to chitin in *T. pseudonana*. First, 4 μg FITC-WGA was incubated with 1 μg-2.4 mg chitotriose in 100 μL water for 3 hours followed by a 30 minute incubation with 100 μL of cell culture at $>10^6$ cells ml^{-1}. Excess FITC-WGA was washed from the cells as described above and the amount of FITC-WGA bound to cells was quantified by flow cytometry and microscopy. Second, similar incubations were conducted using 1μg-9.6 mg of N-acetylglucosamine as the competitive binding substrate. Flow cytometry signal comparisons were calculated in MatLab using a two sided Kolmogorov-Smirnov test with a 95% confidence interval. Modes were determined by creating a histogram of the 65,000 possible fluorescent intensities detected by the flow cytometer with a bin size of 200. If a distribution had two modes the average of the two numbers was used. Distributions were visualized using FlowJo (Tree Star Inc.).

Exponentially growing and silicic acid starved *T. pseudonana* cells were also incubated with FITC-labeled chitin binding probe (FITC-chb) purified from *Bacillus circulans* (New England Biolabs) by first pelleting cells in a centrifuge at 15,000 x g for 10 minutes, resuspending them in 500 uL of TBS (0.05 M Tris base, 0.15 M NaCl), and incubating them with 1 μL FITC-chb for at least 3 hrs. Cells were washed and FITC-chb localization was visualized as described above. Cells were also stained with 10 μg Calcofluor white (Sigma) for 30 minutes

and visualized after excitation at 300-400 nm and emission detected with a 420 nm longpass filter (Chroma). Additional diatom species *T. punctigera*, *T. rotula*, and *S. costatum* were also silicic acid starved and stained with FITC-WGA as described above.

Genetic sequences

Chitin synthase sequence fragments amplified from CODEHOP primers were deposited in the NCBI database with the following accession numbers; *C. socialis* (FJ544943 - FJ544945), *L. undulatum* (FJ544946, FJ544947), *S. costatum* (FJ544948 - FJ544952), *T. guillardii* (FJ544953 - FJ544960), *T. minuscula* (FJ544961 - FJ544965), *T. oceanica* (FJ544966 - FJ544974), *T. punctigera* (FJ544975 - FJ544977), *T. wiessfloggii* (FJ550076 - FJ550085).

1.4 Results

In silico and phylogenetic analyses of putative chitin synthases in diatoms

Automated annotation of *T. pseudonana* whole genome sequence identified six genes that encoded putative chitin synthases (Table 1.3) based on detection of the chitin synthase active site domain with the conserved amino acid motifs EDR, QRRRW, and SWG. Full-length sequences and intron locations of the identified genes were confirmed through a combination of cDNA sequencing and RACE. The six *T. pseudonana* genes are located on 3 chromosomes. Chitin synthase genes occur as inverted repeats once on chromosome 4 and again on chromosome 7. Because the genes in both inverted repeats are identical to each other, it was not possible to determine whether retrieved cDNA sequences corresponded to both members of a repeat. Automated gene model predictions from version 3 of the *T. pseudonana* genome were consistent with transcribed regions confirmed by cDNA sequencing and RACE, except modeled protein ID 4368 incorrectly predicted a short exon at the 3' end.

Automated annotation of *P. tricornutum* whole genome sequence identified two genes that encoded putative chitin synthases (Table 1.3) that also contained the chitin synthase active site domain with conserved amino acid motifs, despite the fact that this diatom is not known to produce chitin. The gene model for one chitin synthase (44759) displayed EST support without additional open reading frames detected either upstream or downstream of the modeled gene and was therefore assumed to be accurate. The second gene (37908) lacked EST support, but

displayed 61% nucleotide sequence identity and 57% translated nucleotide identity to the gene encoding 44759.

PCR products from the active site region of chitin synthase genes were successfully amplified from a variety of multipolar species including the known chitin fiber producers *T. oceanica*, *T. punctigura*, *T. minuscula*, *T. guillardii*, and *T. weissflogii* as well as species not known to produce fibers including *Skeletonema costatum*, *Chaetoceros socialis*, and *Lithodesmium undulatum*. PCR products were not successfully amplified from the other examined phytoplankton (Table 1.1). Phylogenetic analyses grouped the diatom chitin synthases into three clades with bootstrap support of 96, 71, and 100; a fourth potential clade has weaker bootstrap support of 45 (Fig. 1.1). The two *P. tricornutum* sequences formed a clade, identified here as clade D. The multipolar diatom sequences were distributed among three clades, identified here as clades A, B, and C. Each of these three clades contained sequences from multiple species. Moreover, most examined multipolar species encoded proteins that fell into more than one clade. Although clone libraries were not sequenced to saturation, it is of interest to note that only species possessing fultoportula encoded proteins associated with clade A sequences.

The large sequence divergence of clade D from clades A, B, and C is similar to the divergence between division 1 and division 2 fungal chitin synthases. The *P. tricornutum* chitin synthases do not have transmembrane domains N-terminal to the QRRRW motif. This motif is also located relatively near the N-terminal end, which is typical of division 1 fungal and oomycete chitin synthases. In contrast, the *T. pseudonana* chitin synthases possess additional transmembrane domains and a cytochrome b5 domain toward the N-terminal end and their QRRRW motif is located closer towards the C-terminal end, features that characterize division 2 fungal chitin synthases (Ruiz-Herrera et al. 2002) (Fig. 1.2). The chitin synthases from clades A and C contain a myosin motor head domain and have identical protein domain predictions overall. The clade B chitin synthase lacks the myosin motor head domain and has an additional transmembrane domain. The three different protein domain structures further support the identification of phylogenetically distinct clades A, B, and D.

Differential expression of chitin synthase genes in *T. pseudonana*

Relative transcript abundance for the chitin synthase genes from the three clades was not significantly different ($p > 0.01$) under nutrient-replete or nitrate-depleted conditions (Fig 1.3A). Relative transcript abundance for the genes from clades A and C was also not significantly different when growth was slowed by iron or silicic acid depletion relative to nutrient replete conditions ($p > 0.01$). In contrast, the gene from clade B was upregulated by 7.6 ± 0.5 fold and 4.9 ± 0.5 fold ($p<0.01$) relative to the control after experiencing less than 24 hrs of silicic acid or iron depletion, respectively. This treatment is expected to stop growth of a portion of cells in the same phase of the cell cycle (Hildebrand et al. 2007).

To assess transcript abundance in synchronized cells, cells were first starved of silicic acid for 48 hrs to block the majority of cells in the same phase of the cell cycle, and then replenished with sufficient silicic acid to resume cell division. This is similar to a treatment shown to synchronize *T. pseudonana* (Hildebrand et al. 2007), modified in this study with an additional day of silicic acid starvation. Transcript abundance of genes from Clades A and C did not differ significantly ($p > 0.01$) among the 11 time points examined during the eight hours after replenishment of silicic acid. In contrast, transcript abundance of the clade B gene remained significantly lower ($p < 0.01$) during the early time points (5 min, 0.5, 1, 2 hrs) after addition of silicic acid than during the later time points (4, 6, 8 hrs); transcript abundance also differed significantly between the 5 minute and 7 hour time points (Fig. 1.3B). This treatment appears to influence transcription of the clade B chitin synthase gene once cells reach a particular stage in cell division.

The effects of long-term silicic acid starvation and recovery were also examined. Asynchronous cells maintained in media with growth limiting concentrations of silicic acid increased exponentially ($\mu=1.8$ day^{-1}) for 3 days, after which point silicic acid was depleted to 0 μM in all bottles. Photosynthetic capacity decreased in these silicic acid starved cells, as measured by a drop in Fv/Fm from 0.64 ± 0.02 to 0.5 ± 0.05 (Fig 1.4A), cell division was blocked, and cells began to display aberrant morphology and aggregation. The chlorophyll *a* RFUs doubled in 50 mL aloquots from each day-4 culture one day after adding 214 μM silicic acid. Together these data indicate that growth of cells was stopped by silicic acid depletion. The tendency for aggregation persisted until the starved culture was replenished with silicic acid

on day 9. By day 10, Fv/Fm had increased to 0.62 ± 0.03 and cultures resumed asynchronous exponential growth (μ=1.1 day^{-1}) (Fig 1.4A).

During the 3 days of exponential growth, relative transcript abundance was low for the chitin synthase genes from clades A, B, and C and the two genes encoding chitin binding proteins, p150 and p150-like, that localize to the girdle bands (days 2 and 3, Fig. 1.4B and 1.4C). A slight yet significant increase of Clade B and decrease of Clade A chitin synthases occurred on day three suggesting that cells were beginning to experience silicic acid depletion. On day 4,when silicic acid was depleted and cell division stopped, relative transcript abundance of both the clade B and C chitin synthases increased by 4.9 ± 0.6 and 2.3 ± 0.4 fold respectively, relative to the previous day. This increased transcript abundance was significantly maintained through Day 10 for the Clade C chitin synthase and through day 11 for the Clade B chitin synthase, although levels did begin to drop as cells resumed unsynchronized division. Transcript abundance of the chitin binding gene p150 also increased 3.8 ± 0.8 fold on day 4. In contrast, transcript abundance of the clade A chitin synthase gene and p150-like gene did not increase during the period of silicic acid starvation. When related to different reference genes, the absolute value of transcript abundance, but not the direction of the daily changes, was affected by the choice of reference gene (Fig. 1.5). Transcript abundance of the actin-like gene (269504) appeared to maintain constant expression or increase during silicic acid starvation and decrease during exponential growth depending on reference gene used (Fig. 1.5A), and was thus identified as the most conservative reference gene for target gene expression. This gene was previously shown to have similar expression levels in different growth conditions (Mock et al. 2008).

Chitin localization in diatoms

Competitive binding experiments were conducted to determine whether FITC-labeled wheat germ agglutinin (FITC-WGA) binds specifically to *T. pseudonana* chitin and thus can be used to determine chitin localization. As concentrations of chitotriose pre-incubated with FITC-WGA increased, reduced amounts bound to *T. pseudonana* cells, as detected with flow cytometry (Fig. 1.6A). Distributions of the FITC-WGA fluorescence of cells incubated with or without chitotriose were significantly different ($p<0.05$) at every concentration, and the mode consistently decreased as chitotriose concentrations increased, to a final mode 70% less than non-competitively bound cells. In contrast, the fluorescence distributions of FITC-WGA bound

cells with and without N-acetylglucosamine were not significantly different ($p > 0.05$) until concentrations of 22 mM and the mode values varied by no more than ± 5% (Fig. 1.6B). These results suggested that the FITC-WGA bound specifically to *T. pseudonana* chitin.

The impact of silicic acid starvation and recovery on silica deposition and chitin localization were examined by staining cells with FITC-WGA and PDMPO, a stain that incorporates into newly deposited silica (Shimizu et al. 2001). During the transition of *T. pseudonana* from exponential growth to silicic acid depletion, silica deposition and chitin exposure on the cell wall were inversely correlated. Exponentially growing cells had a relatively narrow distribution of high intensity (mode=135 ± 5 RFUs) PDMPO staining as detected with flow cytometry (Fig. 1.7A). Epifluorescent microscopy confirmed that these exponentially growing cells were depositing silica at valves and girdle bands (Fig. 1.7B,C). In contrast, FITC-WGA fluorescence of exponentially growing cells was slightly higher (mode=66 ± 4 RFUs) than unstained cells (mode=46 ± 2); FITC-WGA staining of cells was not detectable with epifluorescent microscopy. As cells entered silicic acid depletion on day four (Fig. 1.4A), the distribution of PDMPO fluorescence broadened, with more cells displaying lower intensity fluorescence and the average mode decreased by 35% (Fig. 1.7A). Microscopic examination of cells indicated that many still deposited silica at the girdle bands but not the valves. Mode fluorescence of FITC-WGA per cell increased on day four by 35%. Microscopy revealed lectin localization around the girdle bands (Fig. 1.7C). PDMPO fluorescent intensity per cell continued to decrease until the average mode was 1% of the original intensity on day 5 and no staining of cells was observed (Fig. 1.7C). The distribution of FITC-WGA fluorescence shifted to a higher intensity with the highest average mode on day 9 about twice the original intensity. Most cells had FITC-WGA bound to the girdle-band region. These cells also had an elongated and bent phenotype. This was particularly evident in the highest fluorescing cells where this exposed bent joint between the two thecae appeared to be larger (Fig 1.7C). No binding of FITC-WGA was seen at the chitin fibers. After silicic acid replenishment on day nine, the mode of PDMPO fluorescence increased significantly (119 ± 5 RFUs) and the mode of FITC-WGA fluorescence decreased significantly (72 ± 1 RFUs) ($p<0.01$).

To confirm the localization of chitin at the girdle bands additional fluorescent chitin binding probes were used to label both exponentially growing and silicic acid starved *T. pseudonana* cultures. Cells were incubated with FITC-WGA, calcofluor white and the

commercially available chitin binding protein derived from bacteria, FITC-chb. All three stains localized to the girdle-band regions of these cells, and were especially visible on silicic acid starved cells with elongated morphologies (Fig. 1.8). FITC-chb and calcofluor white also labeled the girdle bands of cells that were in the process of separating (Fig. 1.8). FITC-chb and calcofluor white also localized to the chitin fibers of *T. pseudonana* while FITC-WGA did not (data not shown), illustrating differences in their chitin binding mechanisms and access to the substrate.

The localization of chitin at the girdle band region in additional species of diatoms was confirmed by labeling silicic acid starved *T. punctigera*, *T. rotula*, and *S. costatum* with FITC-WGA (Fig. 1.9). All three species displayed an abnormal phenotype elongated at the theca. As in *T. pseudonana*, FITC-WGA localized to these elongated regions.

1.5 Discussion

The discovery of chitin synthase genes in a variety of diatoms emphasizes the wide-spread distribution of chitin throughout eukaryotic lineages. Stramenopile chitin synthases have been sparsely characterized and this study provides a more complete picture of the evolutionary history of this polymer. Chitin is often widely distributed within lineages due to its fundamental structural function in the organisms, however it can also evolve divergent functions and structures. For example, in fungi and insects chitin is a primitive, indispensable character that serves a fundamental structural role in forming the cell wall and exoskeleton and thus is present throughout these two groups of organisms. However, within the fungi, chitin has different functions during cell wall formation, bud scar formation, and cell division (Roncero 2002). In mollusks, chitin is also widely distributed and is used for diverse structural functions, such as the formation of the shells in bivalves (Levi-Kalisman et al. 2001), the structural pens in squid (Hunt and Sherief 1990), and the radula of snails (Sollas 1907). Identification of chitin synthase genes in diatom genera (*Phaeodactylum*, *Lithodesmium*, *Chaetoceros*, and *Skeletonema)* that do not produce chitin fibers and the apparent localization of chitin to the cell wall suggests that a similar pattern of evolution has occurred within the diatoms. Our data suggests a broad distribution of chitin in diatoms due to a fundamental structural function in the cell wall with cases of additional functional diversification, such as fiber production. Consequently, the discovery of chitin as the

major carbohydrate component in silica frustules by Tesson et al. (2008) is possibly a true measurement rather than solely due to contamination from residual fibers.

The chitin synthase gene sequences from the representative pennate and multipolar centric species examined here are widely diverged, as expected for diatoms from evolutionarily distant lineages (Medlin and Kaczmarska 2004; Bowler et al. 2008). The predicted chitin synthases from *P. tricornutum* and *T. pseudonana* have different numbers and positions of transmembrane domains and thus are expected to assume different folded structures across the membrane. In addition, only the *T. pseudonana* chitin synthase genes encode a cytochrome b5 domain, which can anchor proteins into lipid bilayers (George et al. 1989) and may have served as a template for the evolution of a lipid binding site (Mifsud and Bateman 2002). This difference in the presence of cytochrome b5 domains is also observed between the two divisions of fungal chitin synthases. The acquisition or loss of this N-terminus from the ancestral chitin synthase is hypothesized to have driven the divergence of the two fungal chitin synthase divisions (Ruiz-Herrera et al. 2002). Fungi often contain chitin synthases from both divisions. In contrast, the few stramenopile lineages that have been examined do not contain this level of diversity within a single organism. The other chitin synthases identified in stramenopiles are from oomycetes, whose sequences are phylogenetically similar to division one fungal chitin synthases (Ruiz-Herrera et al. 2002). In diatoms, *T. pseudonana* chitin synthases appear to be similar to division 2 fungal chitin synthases, while *P. tricornutum* chitin synthases are more similar to those of division 1. It is unclear whether *P. tricornutum* lost the cytochrome b5 domain or *T. pseudonana* gained it. Clearly there are interesting parallels to fungal chitin synthases within the stramenopiles and the mechanism of this evolutionary connection may be clarified as more stramenopile chitin synthases are examined.

Three clades of chitin synthase genes were detected in multipolar diatoms; two were supported by high bootstrap values and the distinctiveness of the third was supported by additional gene expression data. This suggests different evolutionary histories and possibly different functions for chitin within the cells. Each clade contains sequences from multiple species and a single species commonly has chitin synthase genes in multiple clades. The lone exception to this is *T. weissfloggi*, with multiple sequences all assigned only to clade A; this could be due to insufficient sampling of clone libraries, and the large number of copies may be related to the large genome size of this strain (Von Dassow et al. 2008). Clades B and C contain

gene fragments from all successfully tested genera including the chitin-producing *Thalassiosira* species and the non-chitin fiber producing *C. socialis, L. undulatum*, and *S. costatum*. Representatives from these two gene clades were likely present in the common ancestor prior to the evolution of the chitin-fiber producing species. Interestingly, the encoded proteins from these two clades in *T. pseudonana* appear to utilize different modes of intracellular transport: the clade C protein possesses a myosin motor head domain N terminal to the cytochrome b5 domain whereas the clade B protein lacks this domain. Clade A sequences are dominated by members of the genus *Thalassiosira*. The single exception is a gene fragment from *Skeletonema costatum*. This genus is derived from *Thalassiosira* (Kaczmarska et al. 2005) and also has fultoportula, the specialized pores in the silica wall through which chitin fibers emerge. However, rather than chitin fibers extending from the fultoportula, the *S. costatum* silica structures instead remain fused between divided cells and create distinctive chains of cells. Currently only species with fultoportula contain Clade A chitin synthases. Therefore, Clade A gene products are likely associated with the fultoportula structures including the synthesis of the long chitin fibers. The clade A chitin synthase also possesses a myosin motor head domain in a similar location as the protein from clade C, suggesting a similar evolutionary history for these two gene families.

Support for functional differences between chitin synthases also comes from the differential transcription of genes in *T. pseudonana* cells exposed to different nutrient conditions. Relative transcript abundance of the clade B gene is particularly sensitive to short-term depletion of either silicic acid or iron. These conditions resulted in an increased transcript abundance of this clade B gene, but not the clade A or C genes. Co-regulation of transcript abundance by silicic acid and iron depletion has been linked to cell wall processes (Mock et al. 2008). Transcript abundance of only the clade B gene varied depending on the amount of time elapsed since synchronized cells resumed division after short term silicic acid starvation (Hildebrand et al. 2007), suggesting that the clade B gene may have a role during a particular part of the cell cycle and particularly under silicic acid and iron stresses. When cells were submitted to longer term silicic acid starvation, a response from both the clade B and clade C chitin synthases was detected, but the clade C response was of a much smaller magnitude. This gene may also be related to cell wall processes, although it appears to have less sensitivity to changing silicic acid conditions. Interestingly, similar differences in transcription level was found for the two genes encoding girdle-band associated chitin binding proteins both in this study and others (Davis et al.

2006). None of the tested conditions affected the transcript abundance of the clade A chitin synthase, suggesting that it is not directly related to these cell wall processes.

The chitin-specific lectin WGA was used to correlate clade B and C transcript abundance with chitin synthesis. The lectin bound to the girdle band region of cells. WGA can bind to multiple substrates so its specificity for chitin on the cell was confirmed both by competitive binding experiments and by similar localization patterns using two additional chitin-binding probes with different binding mechanisms and access to the binding substrate. Interestingly, the lectin was not visibly bound to the chitin fibers extruded from the fultoportula. This might be due to the pure beta configuration of the fiber polymers, whose highly crystalline parallel arrangement may not be accessible to the lectin binding sites. In contrast, both the chitin-binding probe and calcofluor white were visible on both the girdle-bands and the fultoportula chitin fibers, indicating a more general binding mechanism that does not exclude specific forms of chitin. When cells experienced silicic acid depletion and longer term starvation, transcript abundance increased for the clade B and C chitin synthases and for a gene encoding a chitin-binding protein, p150, previously localized to cell wall girdle bands (Davis et al. 2005). The increase in transcripts corresponded to the increase in WGA binding at the girdle bands, which suggests that the clade B and C proteins are related to synthesis of chitin at the girdle bands in times of cell wall stress. The clade B gene also appears to be transcribed during normal progression through the cell cycle. The relative amount of transcript abundance of the clade B gene depended on length of exposure to silicic acid starvation and/or amount of time since recovery from different degrees of silcic acid starvation, events known to influence cell cycle progression (Hildebrand et al. 2007). Further experiments are needed to determine the exact relation between chitin synthesis and cell cycle progression. However, both the chitin binding probe and calcofluor white localized to the girdle band region of exponentially growing cells preparing to separate after completing division. This supports a connection between chitin synthesis with the cell cycle and suggests that chitin synthesis is enhanced in stressed cells unable to precipitate silica and divide.

The identification of chitin synthase genes in a wide variety of diatoms and the localization of chitin at the girdle bands of *T. pseudonana* suggests the possibility that this use for chitin may be more widespread in diatoms. Silicic acid starved *T. punctigera*, *T. rotula*, and *S. costatum* were labeled with WGA and similar localization patterns were identified. The

association of chitin with the cell wall should be considered in other diatom species; however more detailed analysis within each lineage is needed.

Chitin appears to be intimately connected with silica processes because of its relationship to the cell wall and this connection is illustrated in several ways. The distinctive fultoportula that serve as pores through the silica cell wall appear to have formed specifically to extrude chitin fibers (Hildebrand et al. 2006) implying that this structure likely coevolved with the ability to produce chitin fibers at this cellular location, perhaps with the evolution of the clade A chitin synthase genes. Interestingly, chitin and silica have also evolved to form structures of similar functions. Diatoms can be found as solitary cells or in chains depending on the species. Either chitin fibers or silica spines can extend out from the cell to increase drag in the water and also form the connections between chains of cells. The evolution of either chitin or silica connections between cells may result from the different costs associated with production of rigid silica spines versus flexible chitin fibers; for example, rigid chains experience larger shear flow compared to flexible chains, which has the potential to increase their encounter rate with other particles and nutrients (Karp-Boss and Jumars 1998). The discovery of chitin at the girdle band region reveals another connection between chitin and silica. Our results suggest that chitin is localized to the girdle band region as a normal function of cell division and also under conditions when the cells are unable to precipitate additional silica. This stress-induced localization of chitin around the girdle band region is associated with cells that are elongated and bent and that tend to aggregate and sink. The formation of both the organic and inorganic components of the cell wall must be coordinated which may explain how these relationships between chitin and silica evolved.

Chitin synthase is proposed to have been present in a primitive eukaryote because of its wide-spread distribution throughout the eukaryotic tree of life (Ruiz-Herrera et al. 2002). Thus, it seems probable that the ability to synthesize chitin was present in diatom ancestors as they evolved the ability to generate cell walls of silica. However further work is needed to investigate whether chitin synthases can be identified in the more primitive centric lineage or a sister group to diatoms. Perhaps chitin has been maintained as an essential component of the cell wall and it is only during times of cell wall stress or certain stages of the cell cycle that it can be detected through lectin binding at specialized locations. The use of chitin as a matrix for the precipitation of inorganic structures is a common strategy in eukaryotes (Wainwright 1963; Falini et al. 1996; Ehrlich et al. 2007) and the potential for chitin-silica structures specifically has been

demonstrated *in vitro* (Ogasawara et al. 2000). It is intriguing to speculate whether direct interactions between silica and chitin occur in diatoms, however the current understanding of diatom silica precipitation is that it occurs in an acidic vesicle and does not rely on chitin (Kroger et al. 1999; Kroger et al. 2000; Kroger et al. 2002). Interestingly, a recent microscopy-based study has shown that an uncharacterized organic matrix of fibers forms the core of the girdle bands onto which the silica structure is formed (Hildebrand et al. 2009). Our data indicate a role for chitin in the cell wall and future microscopy based studies are needed to clarify that role. Chitin may be a component of the cell wall that is linked to silica but functionally separate. For example, chitin, rather than silica, may be used for more flexible components of the cell wall during the cell division cycle. Similarly, the apparently larger quantities of chitin detected at the girdle bands during silicic acid starvation may serve as a replacement cell wall material during conditions in which silica can not be deposited. Notably, the increased synthesis of chitin at girdle bands in stressful conditions is reminiscent of chitinous cyst formation, a survival strategy used by other protists (Mulisch 1993).

The relationship between silica and chitin has ecological implications for both diatoms and the global ocean. Chitin is the most abundant polymer in the ocean and serves as an enormous reservoir of organic carbon and nitrogen. Diatoms have traditionally been excluded from considerations of chitin production (Jeuniaux and Vossfoucart 1991; Smucker 1991). Our work suggests that diatoms are likely larger contributors to this organic reservoir than previously thought. Chitin is an attractive source of nutrients for microbes (Nalin et al. 1979; Meibom et al. 2004), and deposition of chitin at diatom girdle bands has the potential to facilitate diatom-microbe interactions (Haines 1974; Hünken 2008). The morphology of cell-wall stressed, chitin producing cells is also of ecological importance. These cells are elongated and bent with a tendency to aggregate, which causes them to sink. If these processes observed in a laboratory translate to post-bloom environmental conditions, it suggests that production of chitin on the cell wall is enhanced when growth is no longer possible followed by sinking out of the surface layer. Sinking is proposed to be a survival strategy for cells in hostile surface environments, and enables them to persist at depth until upwelling brings them back into favorable conditions (Smetacek 1985). Thus, the deposition of chitin around the cell as it sinks to less hostile conditions may be a component of a survival strategy to persist through fluctuating ocean

conditions. Additionally, if cells sink below the mixing depth, sinking becomes a mechanism to pump carbon and other nutrients to the deep ocean (Smetacek 1999).

1.6 Acknowledgements

This work was supported by a Gordon and Betty Moore Foundation Marine Microbiology Investigator Award to E. V. Armbrust and conducted in collaboration with Thomas Mock and E. Virginia Armbrust. I would like to thank Rhonda Morales, Julie Koester, and Thomas Connolly for help with flow cytometry analysis, Ellen O. Lin and Audrey Djunaedi for help with sequencing, and Tiffany Truong for help with RNA extraction and qRT-PCR. I would also like to thank Julie Koester, Micaela Parker, and Nils Kröger for helpful comments and recommendations.

1.7 Bibliography

Aluwihare, L. I., D. J. Repeta, S. Pantoja, and C. G. Johnson. 2005. Two chemically distinct pools of organic nitrogen accumulate in the ocean. Science **308:** 1007-1010

Armbrust, E. V., J. A. Berges, C. Bowler, B. R. Green, D. Martinez, N. H. Putnam, S. G. Zhou, A. E. Allen, K. E. Apt, M. Bechner, M. A. Brzezinski, B. K. Chaal, A. Chiovitti, A. K. Davis, M. S. Demarest, J. C. Detter, T. Glavina, D. Goodstein, M. Z. Hadi, U. Hellsten, M. Hildebrand, B. D. Jenkins, J. Jurka, V. V. Kapitonov, N. Kroger, W. W. Y. Lau, T. W. Lane, F. W. Larimer, J. C. Lippmeier, S. Lucas, M. Medina, A. Montsant, M. Obornik, M. S. Parker, B. Palenik, G. J. Pazour, P. M. Richardson, T. A. Rynearson, M. A. Saito, D. C. Schwartz, K. Thamatrakoln, K. Valentin, A. Vardi, F. P. Wilkerson, and D. S. Rokhsar. 2004. The genome of the diatom *Thalassiosira pseudonana*: Ecology, evolution, and metabolism. Science **306:** 79-86.

Bowler, C., A. E. Allen, J. H. Badger, J. Grimwood, K. Jabbari, A. Kuo, U. Maheswari, C. Martens, F. Maumus, R. P. Otillar, E. Rayko, A. Salamov, K. Vandepoele, B. Beszteri, A. Gruber, M. Heijde, M. Katinka, T. Mock, K. Valentin, F. Verret, J. A. Berges, C. Brownlee, J.-P. Cadoret, A. Chiovitti, C. J. Choi, S. Coesel, A. De Martino, J. C. Detter, C. Durkin, A. Falciatore, J. Fournet, M. Haruta, M. J. J. Huysman, B. D. Jenkins, K. Jiroutova, R. E. Jorgensen, Y. Joubert, A. Kaplan, N. Kroger, P. G. Kroth, J. La Roche, E. Lindquist, M. Lommer, V. Martin-Jezequel, P. J. Lopez, S. Lucas, M. Mangogna, K. Mcginnis, L. K. Medlin, A. Montsant, M.-P. O.-L. Secq, C. Napoli, M. Obornik, M. S. Parker, J.-L. Petit, B. M. Porcel, N. Poulsen, M. Robison, L. Rychlewski, T. A. Rynearson, J. Schmutz, H. Shapiro, M. Siaut, M. Stanley, M. R. Sussman, A. R. Taylor, A. Vardi, P. Von Dassow, W. Vyverman, A. Willis, L. S. Wyrwicz, D. S. Rokhsar, J. Weissenbach, E. V. Armbrust, B. R. Green, Y. Van De Peer, and I. V. Grigoriev. 2008. The Phaeodactylum genome reveals the evolutionary history of diatom genomes. Nature**:**

Brott, L. L., R. R. Naik, D. J. Pikas, S. M. Kirkpatrick, D. W. Tomlin, P. W. Whitlock, S. J. Clarson, and M. O. Stone. 2001. Ultrafast holographic nanopatterning of biocatalytically formed silica. Nature **413:** 291-293

Brzezinski, M. A., and D. M. Nelson. 1986. A Solvent-Extraction Method for the Colorimetric Determination of Nanomolar Concentrations of Silicic-Acid in Seawater. Marine Chemistry **19:** 139-151

Davis, A. K., M. Hildebrand, and B. Palenik. 2005. A stress-induced protein associated with the girdle band region of the diatom Thalassiosira pseudonana (Bacillariophyta). Journal of Phycology **41:** 577-589

---. 2006. Gene expression induced by copper stress in the diatom Thalassiosira pseudonana. Eukaryotic Cell **5:** 1157-1168

Dugdale, R. C., F. P. Wilkerson, and H. J. Minas. 1995. The Role of a Silicate Pump in Driving New Production. Deep-Sea Research Part I-Oceanographic Research Papers **42:** 697-719

Dweltz, N. E., J. R. Colvin, and A. G. Mcinnes. 1968. Studies on chitan (beta-(1-]4)-linked 2-acetamido-2-deoxy-D-glucan) fibers of the diatom Thalassiosira fluviatilis Hustedt. 3. Structure of chitan from X-ray diffraction and electron microscope observations. Canadian Journal of Chemistry **46:** 1513-1521

Ehrlich, H., M. Krautter, T. Hanke, P. Simon, C. Knieb, S. Heinemann, and H. Worch. 2007. First evidence of the presence of chitin in skeletons of marine sponges. Part II. glass sponges (Hexactinellida : porifera). Journal of Experimental Zoology Part B-Molecular and Developmental Evolution **308B:** 473-483

Falini, G., S. Albeck, S. Weiner, and L. Addadi. 1996. Control of aragonite or calcite polymorphism by mollusk shell macromolecules. Science **271:** 67-69

Felsenstein, J. 1989. PHYLIP - Phylogeny Inference Package (Version 3.2). Cladistics **5:** 164-166

Field, C. B., M. J. Behrenfeld, J. T. Randerson, and P. Falkowski. 1998. Primary production of the biosphere: Integrating terrestrial and oceanic components. Science **281:** 237-240.

Frigeri, L. G., T. R. Radabaugh, P. A. Haynes, and M. Hildebrand. 2006. Identification of proteins from a cell wall fraction of the diatom Thalassiosira pseudonana - Insights into silica structure formation. Molecular & Cellular Proteomics **5:** 182-193

George, S. K., L. Najera, R. P. Sandoval, C. Countryman, R. W. Davis, and G. M. Ihler. 1989. The Hydrophobic Domain of Cytochrome-B5 Is Capable of Anchoring Beta-Galactosidase in Escherichia-Coli Membranes. Journal of Bacteriology **171:** 4569-4576

Gooday, G. W. 1990. The ecology of chitin degradation, p. 387-429. *In* K. C. Marshall [ed.], Advances in Microbial Ecology. Plenum Press.

Guillard, R. R., and J. H. Ryther. 1962. Studies of marine planktonic diatoms.1. *Cyclotella nana* Hustedt, and *Detonula confervacea* (Cleve) Gran. Canadian Journal of Microbiology **8:** 229-239.

Guillard, R. R. L. 1975. Culture of phytoplankton for feeding marine invertebrates, p. 26-60. *In* W. L. Smith and M. H. Chanley [eds.], Culture of Marine Invertebrate Animals. Plenum Press.

Haines, K. C., Robert R. L. Guillard. 1974. Growth of vitamin B_{12}-requiring marine diatoms in mixed laboratory cultures with vitamin B_{12}-producing marine bacteria. Journal of Phycology **10:** 245-252

Herth, W. 1979. Site of beta-chitin fibril formation in centric diatoms. 2. Chitin-forming cytoplasmic structures. Journal of Ultrastructure Research **68:** 16-27

Herth, W., and E. Schnepf. 1982. Chitin-fibril Formation in Algae, p. 184-206. *In* R. M. Brown [ed.], Cellulose and Other Natural Polymer Systems. Plenum Press.

Hildebrand, M., L. G. Frigeri, and A. K. Davis. 2007. Synchronized growth of Thalassiosira pseudonana (Bacillariophyceae) provides novel insights into cell-wall synthesis processes in relation to the cell cycle. Journal of Phycology **43:** 730-740

Hildebrand, M., S. Kim, D. Shi, K. Scott, and S. Subramaniam. 2009. 3D imaging of diatoms with ion-abrasion scanning electron microscopy. Journal of Structural Biology **166:** 316-328

Hildebrand, M., E. York, J. I. Kelz, A. K. Davis, L. G. Frigeri, D. P. Allison, and M. J. Doktycz. 2006. Nanoscale control of silica morphology and three-dimensional structure during diatom cell wall formation. Journal of Materials Research **21:** 2689-2698

Hünken, M., J. Harder, G. O. Kirst,. 2008. Epiphytic bacteria on the Antarctic ice diatom Amphiprora kufferathii Manguin cleave hydrogen peroxide produced during algal photosynthesis. Plant Biology **10:** 519-526

Hunt, S., and A. E. Sherief. 1990. A periodic structure in the 'pen' chitin of the squid Loligo vulgaris. Tissue Cell **22:** 191-197

Jeuniaux, C., and M. F. Vossfoucart. 1991. Chitin biomass and production in the marine environment. Biochemical Systematics and Ecology **19:** 347-356

Kaczmarska, I., M. Beaton, A. C. Benoit, and L. K. Medlin. 2005. Molecular phylogeny of selected members of the order Thalassiosirales (Bacillariophyta) and evolution of the fultoportula. Journal of Phycology **42:** 121-138

Karp-Boss, L., and P. A. Jumars. 1998. Motion of diatom chains in steady shear flow. Limnology and Oceanography **43:** 1767-1773

Kroger, N., R. Deutzmann, C. Bergsdorf, and M. Sumper. 2000. Species-specific polyamines from diatoms control silica morphology. Proceedings of the National Academy of Sciences of the United States of America **97:** 14133-14138.

Kroger, N., R. Deutzmann, and M. Sumper. 1999. Polycationic peptides from diatom biosilica that direct silica nanosphere formation. Science **286:** 1129-1132.

Kroger, N., S. Lorenz, E. Brunner, and M. Sumper. 2002. Self-assembly of highly phosphorylated silaffins and their function in biosilica morphogenesis. Science **298:** 584-586

Levi-Kalisman, Y., G. Falini, L. Addadi, and S. Weiner. 2001. Structure of the nacreous organic matrix of a bivalve mollusk shell examined in the hydrated state using Cryo-TEM. Journal of Structural Biology **135:** 8-17

Mclachlan, J., and J. S. Craigie. 1966. Chitan fibres in *Cyclotella cryptica* and growth of *C. cryptica* and *Thalassiosira fluviatilis*, p. 511-517. *In* H. Barnes [ed.], Some Contemporary Studies in Marine Science. George Allen and Unwin Ltd.

Mclachlan, J., A. G. Mcinnes, and M. Falk. 1965. Studies on chitan (chitin-poly-n-acetylglucosamine) fibers of diatom Thalassiosira fluviatilis Hustedt. 1. Production and isolation of chitan fibers. Canadian Journal of Botany **43:** 707-&

Medlin, L. K., and I. Kaczmarska. 2004. Evolution of the diatoms: V. Morphological and cytological support for the major clades and a taxonomic revision. Phycologia **43:** 245-270

Meibom, K. L., X. B. B. Li, A. T. Nielsen, C. Y. Wu, S. Roseman, and G. K. Schoolnik. 2004. The Vibrio cholerae chitin utilization program. Proceedings of the National Academy of Sciences of the United States of America **101:** 2524-2529

Merzendorfer, H. 2006. Insect chitin synthases: a review. Journal of Comparative Physiology B-Biochemical Systemic and Environmental Physiology **176:** 1-15

Mifsud, W., and A. Bateman. 2002. Membrane-bound progesterone receptors contain a cytochrome b5-like ligand-binding domain. Genome Biol **3:** RESEARCH0068

Mock, T., M. P. Samanta, V. Iverson, C. Berthiaume, M. Robison, K. Holtermann, C. Durkin, S. S. Bondurant, K. Richmond, M. Rodesch, T. Kallas, E. L. Huttlin, F. Cerrina, M. R. Sussmann, and E. V. Armbrust. 2008. Whole-genome expression profiling of the marine diatom Thalassiosira pseudonana identifies genes involved in silicon bioprocesses. Proceedings of the National Academy of Sciences of the United States of America **105:** 1579-1584

Montgomery, M. T., N. A. Welschmeyer, and D. L. Kirchman. 1990. A Simple Assay for Chitin - Application to Sediment Trap Samples from the Sub-Arctic Pacific. Marine Ecology-Progress Series **64:** 301-308

Mulisch, M. 1993. Chitin in protistan organisms- Distribution, synthesis and deposition. European Journal of Protistology **29:** 1-18

Nagahashi, S., M. Sudoh, N. Ono, R. Sawada, E. Yamaguchi, Y. Uchida, T. Mio, M. Takagi, M. Arisawa, and H. Yamadaokabe. 1995. Characterization of chitin synthase 2 of Saccaromyces cerevisiae- Implication of 2 highly conserved domains as possible catalytic sites. Journal of Biological Chemistry **270:** 13961-13967

Nalin, D. R., V. Daya, A. Reid, M. M. Levine, and L. Cisneros. 1979. Adsorption and Growth of Vibrio-Cholerae on Chitin. Infection and Immunity **25:** 768-770

Nelson, D. M., P. Treguer, M. A. Brzezinski, A. Leynaert, and B. Queguiner. 1995. Production and dissolution of biogenic silica in the ocean- Revised global estimates, comparison with regional data and relationship to biogenic sedimentation. Global Biogeochemical Cycles **9:** 359-372.

Ogasawara, W., W. Shenton, S. A. Davis, and S. Mann. 2000. Template mineralization of ordered macroporous chitin-silica composites using a cuttlebone-derived organic matrix. Chemistry of Materials **12:** 2835-+

Parkinson, J., and R. Gordon. 1999. Beyond micromachining: the potential of diatoms. Trends in Biotechnology **17:** 190-196

Peters, W., and I. Latka. 1997. Wheat germ agglutinin-gold labelling, p. 33-40. *In* R. A. A. M. a. M. G. Peters [ed.], Chitin Handbook. European Chitin Society.

Pfaffl, M. W. 2001. A new mathematical model for relative quantification in real-time RT-PCR. Nucleic Acids Research **29:** -

Price N. M., Harrison G. I, Hering J. G, Hudson R. J., Nirel P. M. V., Palenik B., and M. F. M. M. 1988/89. Preparation and chemistry of the artificial algal culture medium aquil. Biological Oceanography **6:** 443-461

Ramakers, C., J. M. Ruijter, R. H. L. Deprez, and A. F. M. Moorman. 2003. Assumption-free analysis of quantitative real-time polymerase chain reaction (PCR) data. Neuroscience Letters **339:** 62-66

Roncero, C. 2002. The genetic complexity of chitin synthesis in fungi. Current Genetics **41:** 367-378

Round, F. E., R. M. Crawford, and D. G. Mann. 1990. The Diatoms : biology & morphology of the genera. Cambridge University Press.

Ruiz-Herrera, J., J. M. Gonzalez-Prieto, and R. Ruiz-Medrano. 2002. Evolution and phylogenetic relationships of chitin synthases from yeasts and fungi. FEMS Yeast Res **1:** 247-256

Saxena, I. M., R. M. Brown, M. Fevre, R. A. Geremia, and B. Henrissat. 1995. Multidomain architecture of beta-glycosyltransferases- Implications for mechanism. Journal of Bacteriology **177:** 1419-1424

Shimizu, K., Y. Del Amo, M. A. Brzezinski, G. D. Stucky, and D. E. Morse. 2001. A novel fluorescent silica tracer for biological silicification studies. Chemistry & Biology **8:** 1051-1060

Smetacek, V. 1999. Diatoms and the ocean carbon cycle. Protist **150:** 25-32

Smetacek, V. S. 1985. Role of sinking in diatom life-history cycles - Ecological, evolutionary and geological significance. Marine Biology **84:** 239-251

Smucker, R. A. 1991. Chitin Primary Production. Biochemical Systematics and Ecology **19:** 357-369

Sollas, I. B. J. 1907. Memoirs: The Molluscan Radula: its Chemical Composition, and Some Points in its Development. Quarterly Journal of Microscopical Science **s2-51:** 115-136

Sugiyama, J., C. Boisset, M. Hashimoto, and T. Watanabe. 1999. Molecular directionality of beta-chitin biosynthesis. Journal of Molecular Biology **286:** 247-255

Tesson, B., S. Masse, G. Laurent, J. Maquet, J. Livage, V. Martin-Jezequel, and T. Coradin. 2008. Contribution of multi-nuclear solid state NMR to the characterization of the

Thalassiosira pseudonana diatom cell wall. Analytical and Bioanalytical Chemistry **390:** 1889-1898

Thompson, J. D., D. G. Higgins, and T. J. Gibson. 1994. CLUSTAL W: improving the sensitivity of progressive multiple sequence alignment through sequence weighting, position-specific gap penalties and weight matrix choice. Nucl. Acids Res. **22:** 4673-4680

Von Dassow, P., T. W. Petersen, V. A. Chepurnov, and E. V. Armbrust. 2008. Inter- and intraspecific relationships between nuclear DNA content and cell size in selected members of the centric diatom genus Thalassiosira (Bacillariophyceae). Journal of Phycology **44:** 335-349

Wainwright, S. A. 1963. Skeletal Organization in Coral, Pocillopora Damicornis. Quarterly Journal of Microscopical Science **104:** 169-&

Zar, J. H. 1996. Biostatistical analysis, 3rd ed. Prentice Hall.

Table 1.1. Organisms tested by PCR for the presence of chitin synthase genes and identification of those in which chitin synthase gene fragments were successfully amplified.

Organism	Source	Group	Known chitin producer?	Chitin synthase identified?
Phaeocystis globosa	CCMP 629	Prymnesiophyte	Yes	No
Gyrodinium sp.	CCMP 1737	Dinoflagellate	No	No
Choodactylon ramorsum	CCMP 1941	Red Algae	No	No
Thalassiosira pseudonana	CCMP 1335	Multipolar diatom	Yes	Yes
Thalassiosira guillardii	CCMP 988	Multipolar diatom	Yes	Yes
Thalassiosira minuscula	CCMP 1093	Multipolar diatom	Yes	Yes
Thalassiosira oceanica	CCMP 999	Multipolar diatom	Yes	Yes
Thalassiosira punctigura	P. von Dassow	Multipolar diatom	Yes	Yes
Thalassiosira weissflogii	CCMP 1336	Multipolar diatom	Yes	Yes
Skeletonema costatum	CCMP 780	Multipolar diatom	No	Yes
Chaetoceros socialis	CCMP 205	Multipolar diatom	No	Yes
Lithodesmium undulatum	CCMP 472	Multipolar diatom	No	Yes
Ditylum brightwellii	J. Koester	Multipolar diatom	No	No
Stephanopyxis palmeriana	CCMP 814	Radial centric diatom	No	No
Phaeodactylum tricornutum	CCMP 632	Pennate diatom	No	Yes (genome)
Entomoneis alata	CCMP 1522	Pennate diatom	No	No
Fragilaria pinnata	CCMP 395	Pennate diatom	No	No
Pseudo-nitzschia multiseries	C. Leger and S.S. Bates	Pennate diatom	No	No
Toxarium undulatum	CCMP 2277	Pennate diatom	No	No

Table 1.2. Oligonucleotide primers used for amplifying chitin synthase gene fragments in phytoplankton and cDNA fragments from various genes in *T. pseudonana*.

Method	Direction	Gene target/Protein ID	Sequence (5' to 3')
CODEHOP	F	Chitin synthase (general)	5'-TGCGTCACATGTTTG CCAGGAtgyttcwsgatgta-3'
CODEHOP	R	Chitin synthase (general)	5'-CGAACGAGTCTCACC CCAAGAraartcrtc-3'
5' RACE	R-inner	Chitin synthase/7305	5'-TCTCGCAGTGTTGTTGCTCT-3'
5' RACE	R-outer	Chitin synthase/7305	5'-GCGATAGCGTTCTTCTTCCA-3'
3' RACE	F	Chitin synthase/7305	5'-TGCCGGTGTTTTACTTCCTT-3'
qRT-PCR	F	Chitin synthase/6575	5'-GTAGAAGTTTGGTAGAGAGA-3'
qRT-PCR	R	Chitin synthase/6575	5'-ACTATTTGCTCGGACAGAAA-3'
qRT-PCR	F	Chitin synthase/7305	5'-GGTGTGCAGTTGGTGGTGTT-3'
qRT-PCR	R	Chitin synthase/7305	5'-CGCAGCAACCTTACGAGTCT-3'
qRT-PCR	F	Chitin synthase/4368	5'-TACGACCAGCAGTAGTACAA-3'
qRT-PCR	R	Chitin synthase/4368	5'-ACTCACTTTCATCATCACTA-3'
qRT-PCR	F	Actin-like/269504	5'-CTCCCAATCCTGGCAATAGA-3'
qRT-PCR	R	Actin-like/269504	5'-CGAAACCTATCCACGACGTT-3'
qRT-PCR	F	p150-like/12594	5'-GCGATTACAATGCTCCCACT-3'
qRT-PCR	R	p150-like/12594	5'-GTGAAGAGAACGCTTGGGTA-3'
qRT-PCR	F	p150/26041	5'-GTTGCTCAAAGTTCGGCTTC-3'
qRT-PCR	R	p150/26041	5'-TCGGTTGTTCCACACCTGTA-3'
qRT-PCR	F	Actin/25772	5'-ACCAACTGGGACGACATGGAGAAA-3'
qRT-PCR	R	Actin/25772	5'-TGTGGGTAACACCATCTCCCGAAT-3'
qRT-PCR	F	40S S11/31084	5'-CCAAAGACCATCGAAGGAGA-3'
qRT-PCR	R	40S S11/31084	5'-GACACGGACGAGGGTTTCT-3'
qRT-PCR	F	Beta tubulin/31569	5'-GCCTTTGATGCCAAGAACAT-3'
qRT-PCR	R	Beta tubulin/31569	5'-GATGGATGCCTTGAGGTTGT-3'

Table 1.3. Genomic characteristics of chitin synthase genes discovered in the *T. pseudonana* and *P. tricornutum* genomes.

Genome	Protein ID	Nucleotides (bp)	Intron length (bp)	Chromosome location	Confirmation method
T. pseudonana	6575	4,408	96, 99	6	cDNA sequencing
T. pseudonana	7305	3,887	143	7 (inverted repeat)	cDNA sequencing and RACE
T. pseudonana	7306	3,887	143	7 (inverted repeat)	cDNA sequencing
T. pseudonana	4368	4,374	none	4	cDNA sequencing
T. pseudonana	4413	3,012	none	4 (inverted repeat)	cDNA sequencing
T. pseudonana	4414	3,012	none	4 (inverted repeat)	cDNA sequencing
P. tricornutum	44759	2,806	91	5	EST coverage
P. tricornutum	37908	2,875	73	14	Similarity to 44759

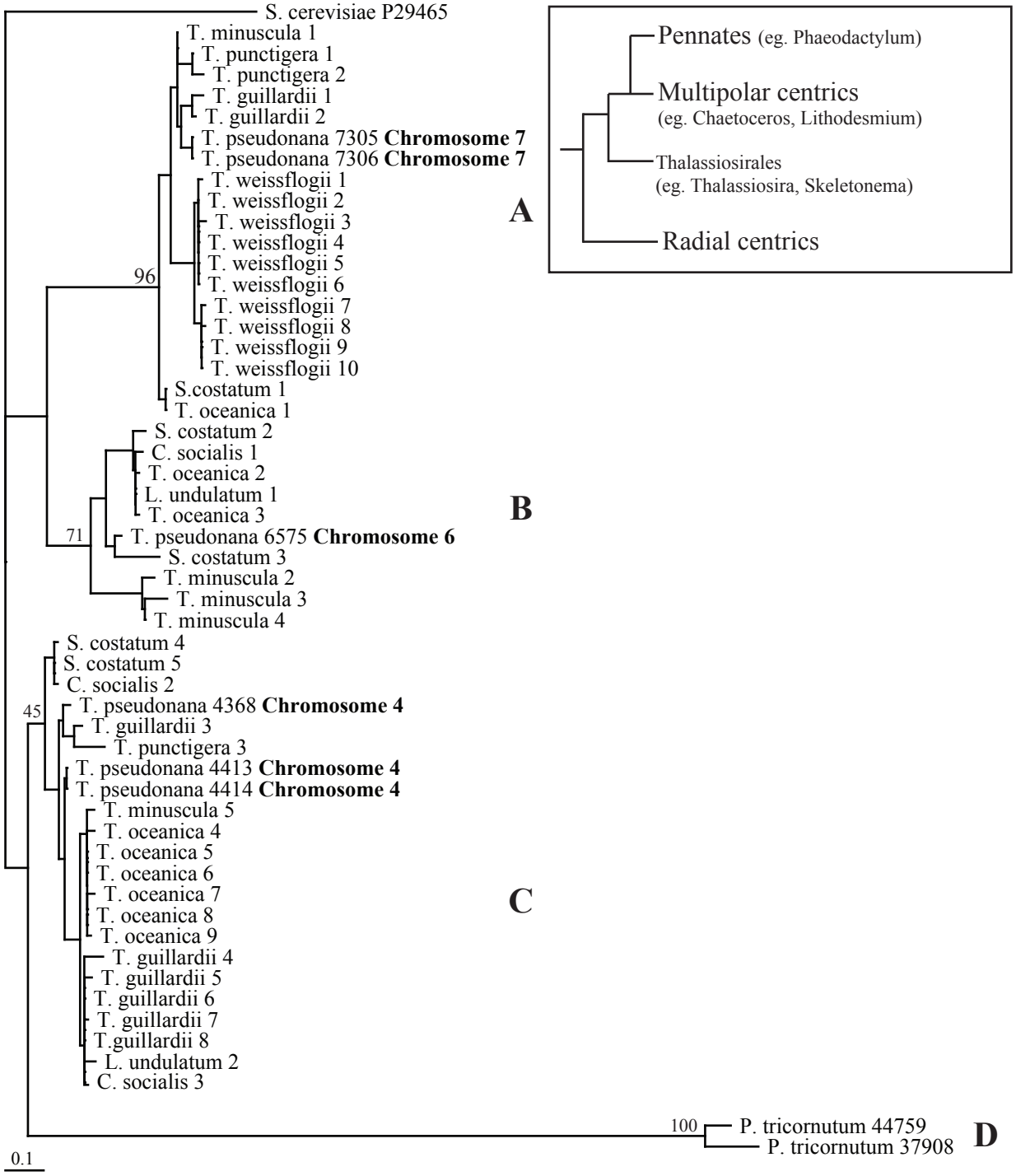

Figure 1.1 Maximum likelihood phylogenetic tree of translated diatom chitin synthase gene sequences. Sequences amplified by CODEHOP primers are followed by numerical identifiers 1 through10, while sequences identified from genomes are followed by their protein ID number. The outgroup S. cerevisiae chitin synthase 3 (NCBI accession P29465) was used to root the tree. Bootstrap values are indicated at nodes. Scale bar indicates number of amino acid changes. Inset is a simplified phylogeny of diatom evolution adapted from Medlin and Kaczmarska (2004) and genera listed in inset correspond to those present in the gene tree.

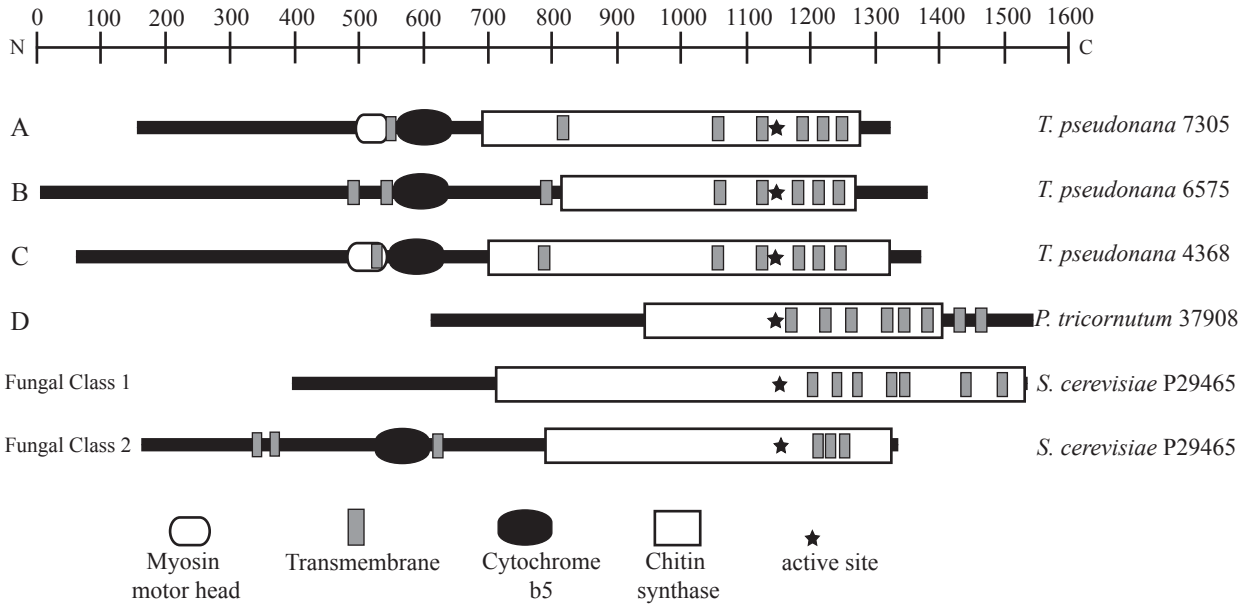

Figure 1.2 Schematic of predicted protein domains for representatives from the four diatom chitin synthase clades and two classes of fungal chitin synthases. Species and protein or NCBI ID is indicated to the right; clade or class designation is indicated to the left. Amino acid length is indicated by the top scale and represented in each protein by black lines. Functional domain symbols defined in the key at the bottom.

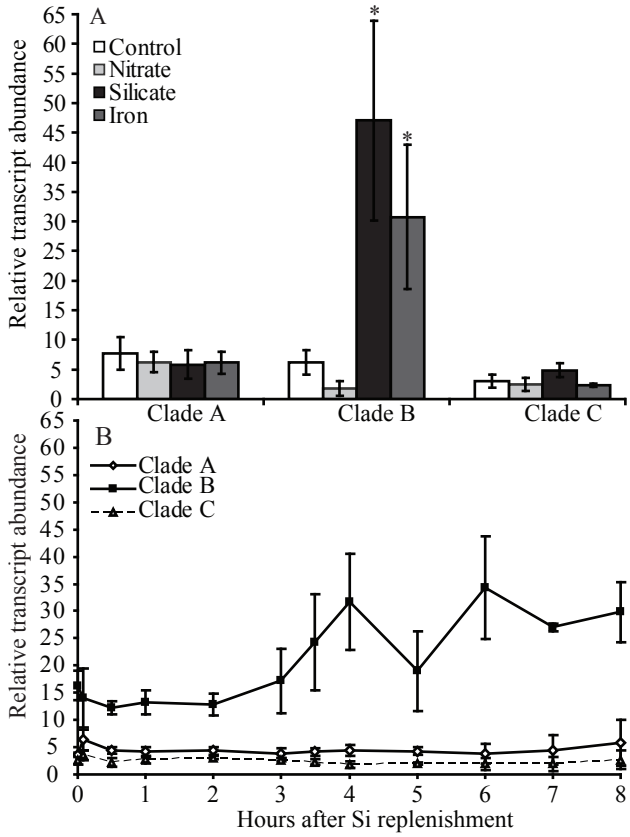

Figure 1.3 Transcript abundance of chitin synthase genes from clades A (protein id 7305), B (protein id 6575), and C (protein id 4368) relative to the actin-like gene (protein id 269504) in *T. pseudonana* cells under different nutrient conditions. A) Cells maintained under nutrient replete conditions or starved of nitrate, silicic acid, or iron for less than 1 day. B) Time course of relative transcript abundance after replenishment of silicic acid to cells starved for silicic acid for 2 days. In A, asterisks indicate a significant difference from the nutrient replete control condition. Error bars represent standard deviation of biological triplicates.

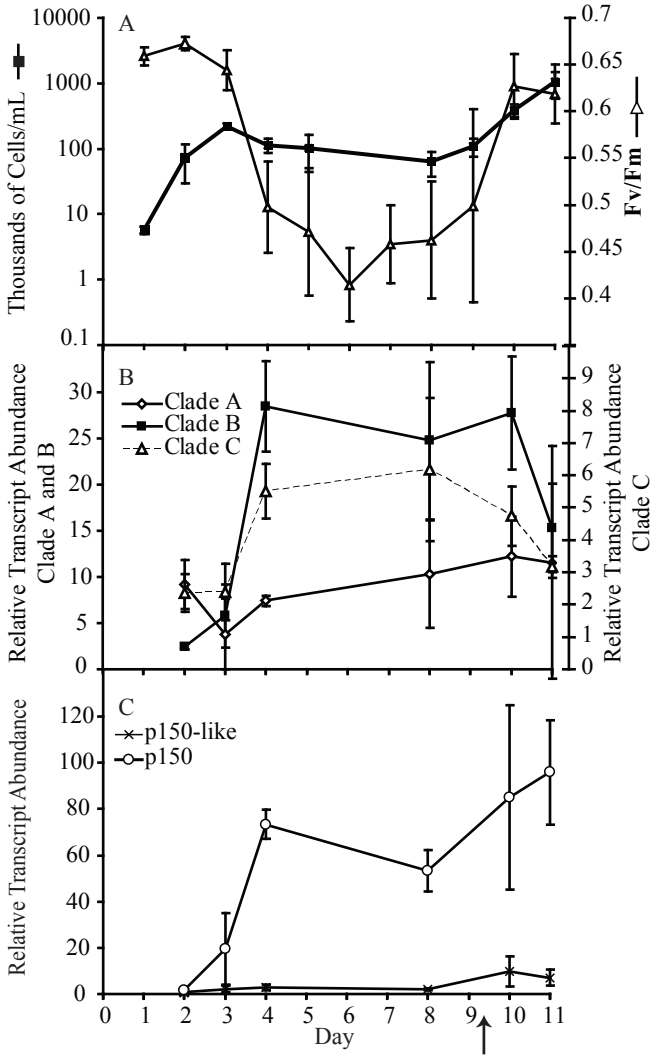

Figure 1.4 Growth and gene expression characteristics of cells grown in silicic acid deplete media and after replenishment of silicic acid on day 9, as indicated by x-axis arrow. A) Time course of cell concentration and Fv/Fm. Relative transcript abundance of chitin synthase genes (B) from clades A (protein id 7305), B (protein id 6575), and C (protein id 4368) and two girdle band associated chitin binding genes p150 and p150-like (protein ids 12594 and 26041) (C) relative to the actin-like gene (protein id 269504) (note change in scales). Error bars represent standard deviation of biological triplicates.

Figure 1.5 Transcript abundance of the *T. pseudonana* reference gene and target genes relative to different reference genes as cells grew in silicic acid deplete media. A) Transcript abundance of reference gene 269504 relative to four other house-keeping genes. B-F) Transcript abundance of three chitin synthases and two chitin binding genes relative to four different reference genes. Error bars represent the standard deviation between biological triplicates, except the single point in A on day 4 relative to 31569, which represents a single biological sample.

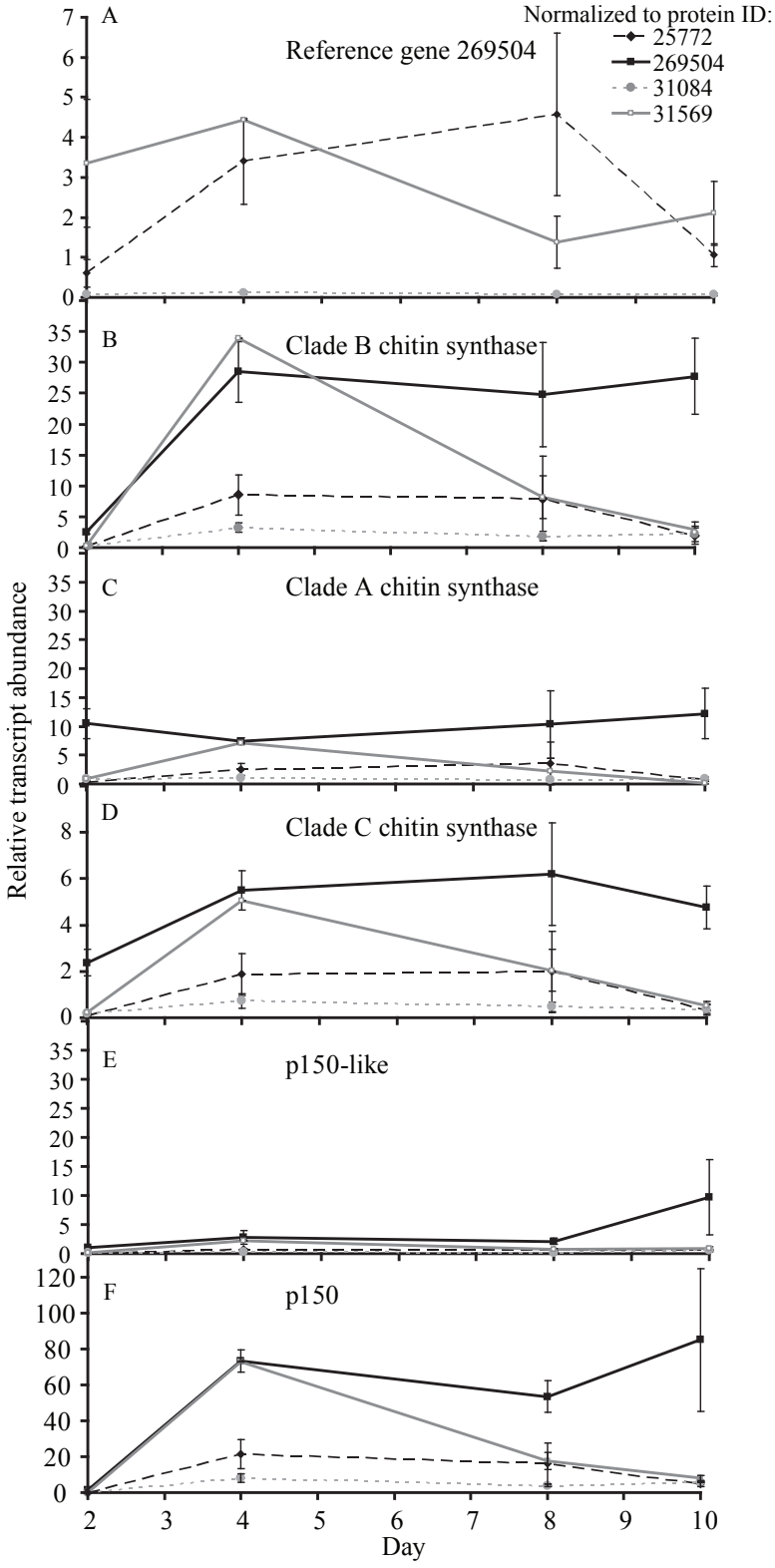
A
Reference gene 269504
Normalized to protein ID:
25772
269504
31084
31569
B
Clade B chitin synthase
C
Clade A chitin synthase
D
Clade C chitin synthase
E
p150-like
F
p150
Relative transcript abundance
Day

Figure 1.6 Distributions of fluorescent intensities from *T. pseudonana* cells bound with FITC-WGA in the presence of a competitive binding substrate. A) Cells bound with FITC-WGA pre-incubated with increasing concentrations of chitiotriose. B) Cells bound with FITC-WGA pre-incubated with increasing concentrations of N-acetylglucosamine. Concentrations of the competitive binding substrate are indicated in each panel. Thick black lines represent fluorescence of cells in the presence of the competitive substrate and thin gray lines represent fluorescence of cells bound with FITC-WGA without a competitive substrate. Asterisks indicate a significant difference between distributions.

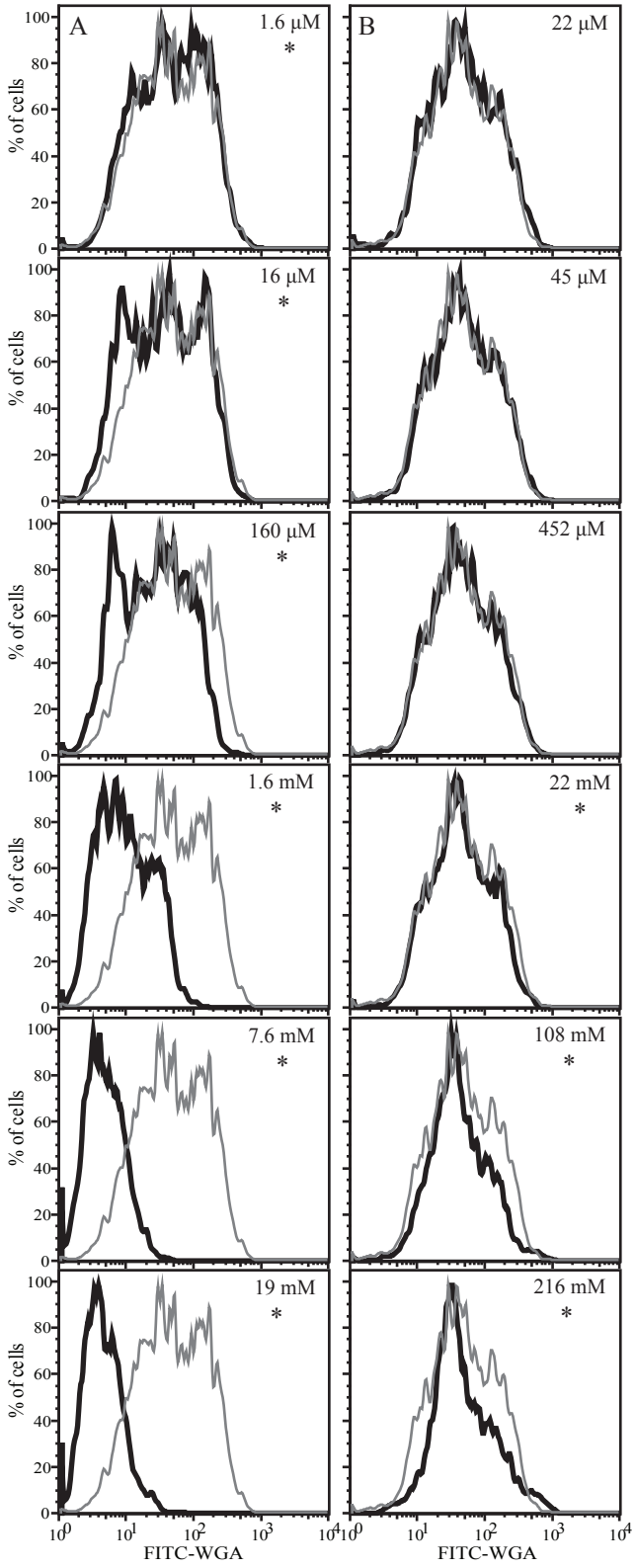
A
B
1.6 µM
22 µM
16 µM
45 µM
160 µM
452 µM
1.6 mM
22 mM
7.6 mM
108 mM
19 mM
216 mM
*
% of cells
FITC-WGA

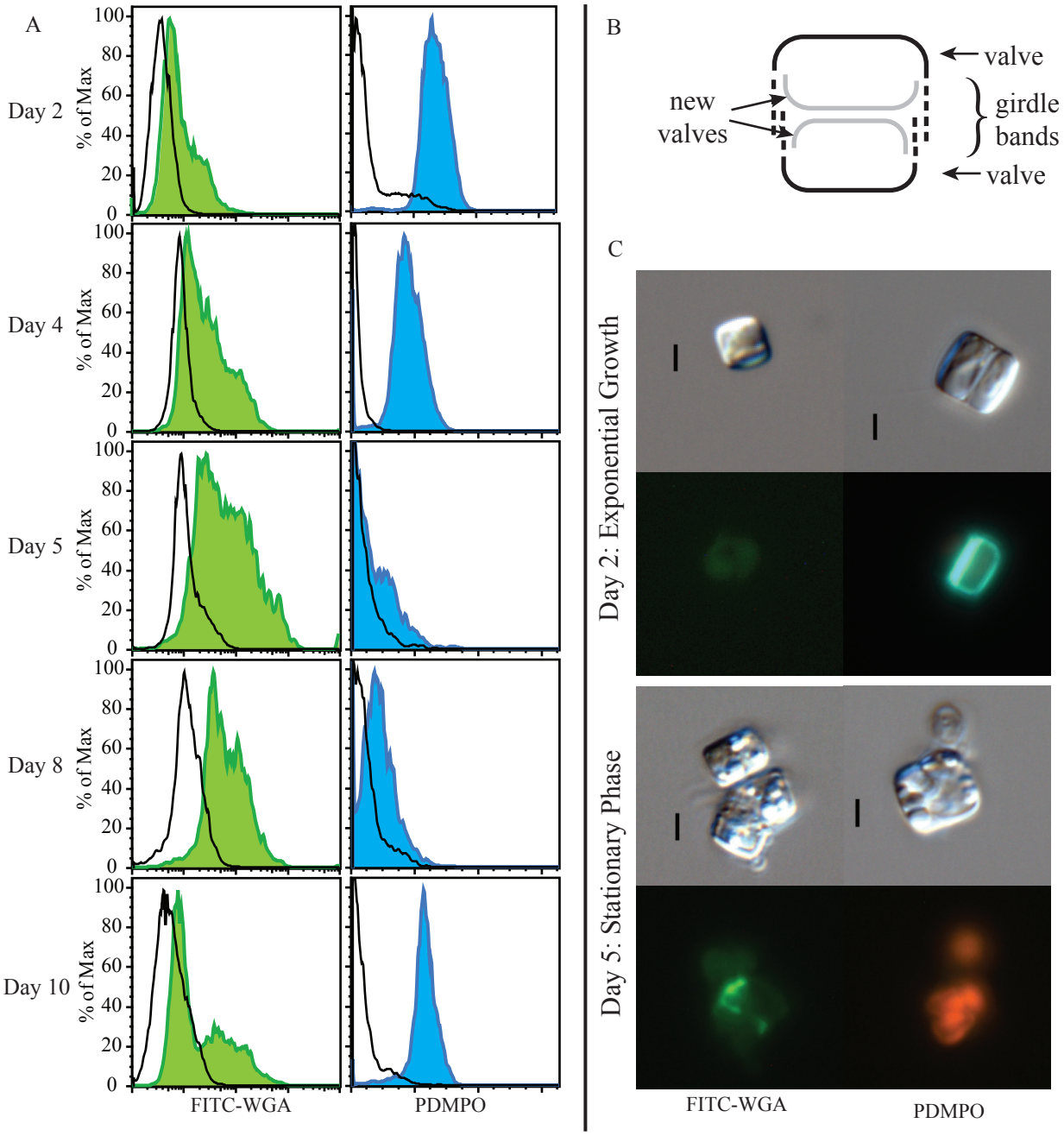

Figure 1.7 Fluorescent signal of *T. pseudonana* cells (A) bound with FITC-WGA (left column) and stained with PDMPO (right column) as measured by flow cytometry during transitions between silicic acid replete and limited conditions. The distribution of fluorescent signals from stained cells is indicated by colored histograms and from untreated cells by a black line. Silicic acid depletion was observed on day 4 and silicic acid was replenished on day 9. (B) Diagram of T. pseudonana frustules and (C) DIC and fluorescence micrographs of live cells during exponential growth (above) and stationary phase (below). Scale bars in light micrographs indicate 2 μm. FITC-WGA is localized by the intense green fluorescence while chlorophyll autofluorescence appears a diffuse green. PDMPO is localized by the blue fluorescence while chlorophyll autofluorescence appears red.

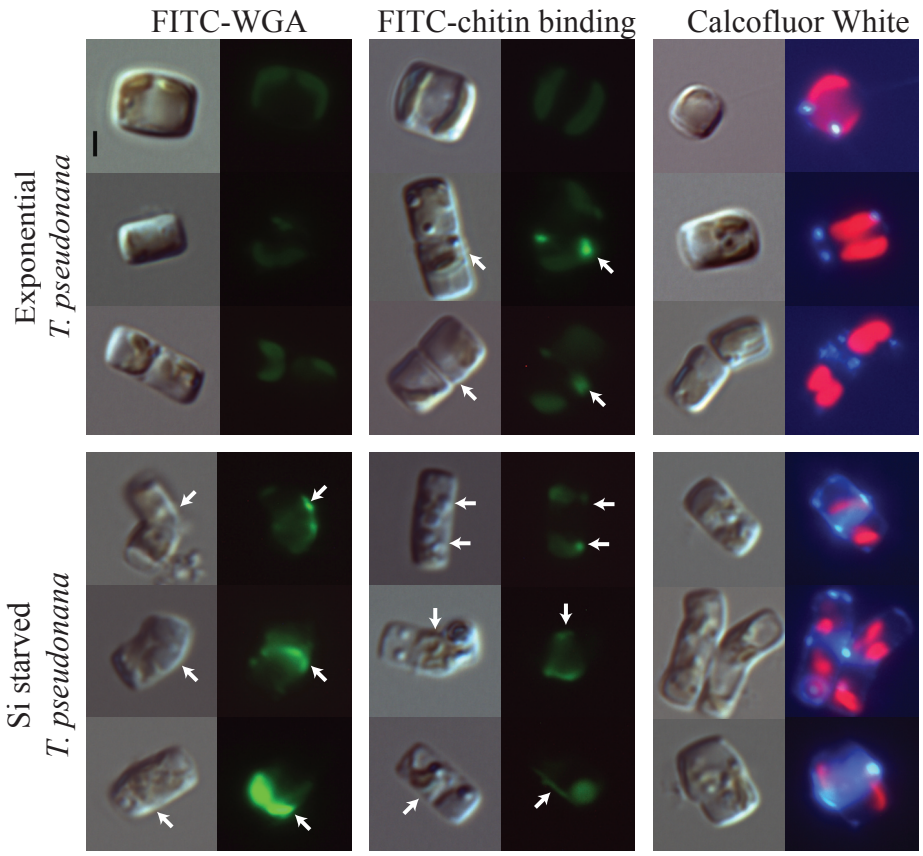

Figure 1.8 Light and fluorescent micrographs of exponentially growing (above) and silicic acid starved (below) *T. pseudonana* cells incubated with A) FITC-WGA, B) FITC-chb protein, or C) calcofluor white. Bar in the light micrograph indicate 2 um. Multiple cells are shown from each treatment to illustrate cells in different stages of division. For A and B, the brighter green fluorescence at the girdle bands (indicated with arrows) is the location of FITC-labeling while diffuse green is chlorophyll a autofluorescence. In C, calcofluor white appears blue and chlorophyll *a* autofluorescence appears red.

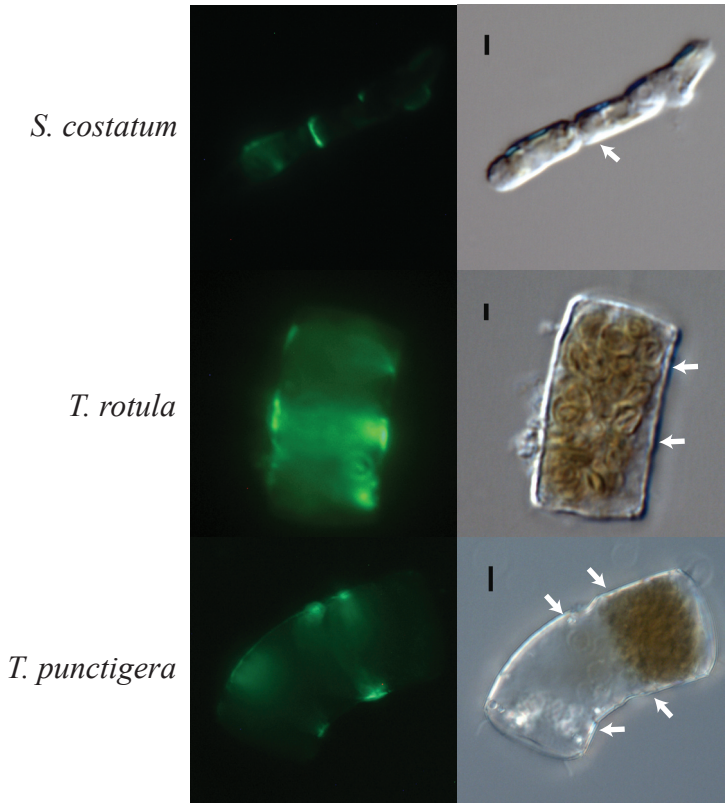

Figure 1.9 Light and fluorescent micrographs of silicic acid starved diatoms incubated with FITC-WGA. Arrows in the light micrographs indicate the location of FITC-WGA binding in fluorescent micrographs. Scale bars indicate 2 μm for *S. costatum* and *T. rotula* and 10 μm for *T. punctigera*.

Chapter 2

Frustule-related gene transcription and the influence of diatom community composition on silica precipitation in an iron-limited environment

2.1 Abstract

A microcosm study in iron-limited waters of the northeast subarctic Pacific Ocean was conducted to examine how iron-availability affects the frustule-related response of individual diatoms and thus the total quantity of silica precipitated by the community. New silica precipitated per cell was estimated using the fluorescent cell stain 2-(4-pyridyl)-5{[4-dimethylaminoethyl-aminocarbamoyl)-methoxy]phenyl}oxazole (PDMPO). Differences in new silica precipitation within a particular genus before and after iron enrichment were small compared to differences among genera indicating that the quantity of total silica precipitated is particularly sensitive to community composition. Transcriptional patterns of genes encoding silicon transporters, aminopropyltransferases, chitin synthases, and a protein with uncharacterized function were measured in natural populations to identify indicators of the frustule-related responses of different genera to iron-limitation. Transcripts associated with silicon transporters were the most readily detectable in three metatranscriptome datasets and were capable of resolving species composition shifts and physiological responses. Silicon transporter transcripts from a distinct phylogenetic clade were most abundant in the iron-limited community and transcripts from a separate clade were more abundant in the community that bloomed after iron enrichment. Transcripts of the gene present in the iron-limited community were also more abundant in iron-limited laboratory cultures of *Pseudo-nitzschia multiseries*, suggesting that this gene plays a role in silicon uptake during iron-limitation. The responses of individual cells, as detected in this study, determine how the community influences silicon cycling in iron-limited environments.

2.2 Introduction

Diatoms are unicellular silicified algae responsible for about one fifth of the total carbon fixed into organic matter each year (Nelson et al. 1995; Field et al. 1998). They are among the

most diverse groups of organisms in the ocean (Kooistra and Medlin 1996; Bowler et al. 2008), a characteristic realized in the diverse shapes and sizes of their silica cell walls (frustules). These relatively heavy frustules help to efficiently transport diatom organic matter into the deep ocean and onto the sea floor (Buesseler 1998). Diatom production is limited by the availability of iron in approximately 40% of the world's oceans (Moore et al. 2002; De Baar et al. 2005). In these regions, iron-limited diatoms commonly increase their silicic acid uptake relative to nitrate (Hutchins and Bruland 1998) through a variety of proposed mechanisms (Takeda 1998; De La Rocha et al. 2000; Marchetti and Harrison 2007). The resulting changes in silicon utilization may shift the stoichiometry of seawater and the distribution of nutrients throughout the global ocean (Brzezinski et al. 2002; Matsumoto et al. 2002). Additionally, iron-induced changes in primary production, nutrient consumption, and particle export are hypothesized to have influenced global climate across glacial and interglacial periods (Martin 1990). Vast differences in silicon content per cell, division rates, cell size, and grazing pressure make diatom species composition, at any given location and time, a determining factor in the fate of silicon and carbon in iron-limited regions of the world's oceans (Baines et al. 2010; Krause et al. 2010; Marchetti et al. 2010). Thus, relatively small changes in frustule formation by diatoms caused by shifting environmental conditions can have large-scale effects on biogeochemical cycles (Brzezinski et al. 2002).

To more fully understand how diatoms affect biogeochemistry in iron-limited environments, the influence of individual species' physiology must be disentangled from the influence of changes in community composition, a possibility offered through use of species-specific molecular approaches. To date, a handful of gene products with a role in frustule formation have been identified and characterized. The most well-characterized genes encode the silicic acid transporters (SIT), which are embedded within the outer membrane and transport silicic acid into the cell. Multiple copies of the SIT genes are found within each diatom species examined thus far and the pattern of gene divergence is generally congruent with diatom species divergence (Thamatrakoln et al. 2006). SIT genes in the centric diatom *Thalassiosira pseudonana* are differentially regulated across the cell cycle, suggesting that they serve different functions in the cell and/or the silicification process (Thamatrakoln and Hildebrand 2007). Among species, SIT genes appear to be regulated differently under iron or silicic acid-limited growth conditions. For example, the pennate diatom *Phaeodactylum tricornutum* differentially transcribes SIT genes while experiencing iron or silicic acid starvation (Allen et al. 2008; Sapriel

et al. 2009), whereas *T. pseudonana* upregulates SIT genes upon silicic acid starvation but not iron starvation (Mock et al. 2008). The evolutionary divergence of SIT genes among species and the regulatory diversity within a species likely contributes to the variety of frustule changes exhibited by iron-limited diatoms.

Upon transport of silicic acid into the cell, its precipitation and morphology are controlled by additional molecules that become embedded within the frustule. Silaffins, silacidins, and cingulins (Kroger et al. 1999; Wenzl et al. 2008; Scheffel et al. 2011) are proteins required for silica precipitation. These protein families contain common amino acid motifs (e.g., lysine-rich), but their limited nucleotide sequence conservation complicates gene identification and characterization across different species. Long-chain polyamines are also required for silica precipitation and also remain embedded within the silica frustule (Kroger et al. 2000). The pathway for long-chain polyamine synthesis is hypothesized to involve spermidine synthase-like genes (Frigeri et al. 2006; Knott et al. 2007; Knott 2009), or more generally aminopropyl transferases (APT) (Ikeguchi et al. 2006). APT genes are part of a multi-copy gene family in diatoms, which include two phylogenetically distinct groups of genes encoding proteins proposed to be responsible for long-chain polyamine synthesis and modification of silaffin proteins with polyamine side chains (Anthony 2011). In *T. pseudonana*, several of the APT genes proposed to be involved in long-chain polyamine synthesis due to their predicted protein domain structure (Anthony 2011) are upregulated by silicic acid and iron starvation, suggesting a potential role in the observed response of the frustule to iron starvation (Mock et al. 2008). Chitin is another compound embedded within the frustule of *T. pseudonana* (Brunner et al. 2009) and likely other members of the Thalassiosirales lineage. Chitin synthase genes are found in diverse diatoms and are also part of a multi-copy gene family (Durkin et al. 2009). Transcription of some chitin synthase gene copies in *T. pseudonana* is influenced by iron and silicic acid starvation, suggesting that chitin may also play a role in changing the cell wall morphology in iron-limited environments. Additionally, many genes without a known function are hypothesized to be involved in frustule formation due to transcriptional patterns that correlate with the transcription of other frustule-related genes (Frigeri et al. 2006; Mock et al. 2008).

We investigated the contribution of different diatoms to silicon cycling within an iron-limited community by using a fluorescent cellular label to quantify silica precipitation by individual genera. The physiological responses of diverse genera were further evaluated in both

field samples and a lab isolate based on transcriptional patterns of genes encoding SITs, APTs, chitin synthases, and a protein with unknown function. These genes were selected because they represent different processes related to frustule formation, are detectable in a range of species, and have previously been implicated in iron-limited frustule formation. This study aims to test the feasibility of using these genes as indicators of biogeochemically relevant processes in natural environments based on the correlation of their transcription with specific environmental conditions.

2.3 Methods

Collection of field samples

Field samples were collected at Ocean Sta. Papa (50° N, 145° W) on 8-13 June, 2008 during a Line P cruise aboard the R/V *J.P. Tully*. Concurrent with this study, a deck-board iron enrichment experiment was conducted and eukaryotic metatranscriptomes were sequenced by 454 (Roche) pyrosequencing from the ambient iron-limited community and from the iron-enriched incubations, as described by Marchetti et al. (2012). Metatranscriptomes from these conditions and additionally from an unamended control incubation were also sequenced by SOLiD (Life Technologies) sequencing. The SOLiD ribonucleic acid (RNA)-Seq reads were aligned to the transcripts from the two 454 metatranscriptomes to enhance the ability to detect differentially expressed genes among the treatments (Marchetti et al. 2012).

Fluorescent labeling of newly precipitated silica

Whole seawater samples were collected at Ocean Sta. Papa with a Niskin bottle at a depth of 5 meters. The ambient plankton populations were concentrated 5-fold (from 2 L to 400 mL) by inverse filtration in a graduated cylinder through a 3 μm polycarbonate filter attached to a peristaltic pump. For every 100 mL filtered, the flow was briefly reversed to wash plankton off the filter and return them to the seawater. A 1.8 mL aliquot was preserved with 0.2 mL fixative (10% formaldehyde, 0.5% glutaraldehyde, 40% phosphate buffered saline solution) (Andersen 2005) and stored in liquid nitrogen for future measurement by flow cytometry. Triplicate polycarbonate bottles containing 125 mL of the concentrated sample and 0.5 μmol L^{-1} 2-(4-pyridyl)-5{[4-dimethylaminoethyl-aminocarbamoyl)-methoxy]phenyl}oxazole (PDMPO) (Invitrogen) were incubated for 24 hours in deck-top incubators covered with neutral density

screening reducing irradiance to 30% of ambient light. After the 24 h incubation, a 1.8 mL aliquot of PDMPO-labeled seawater was preserved in fixative for later flow cytometry analysis and the remaining volume was filtered onto black 25 mm 0.2 μm polycarbonate filters and preserved in immersion oil on microscope slides with cover slips. The edges of the cover slips were sealed with nail polish and the slides were stored at -20°C. Triplicate 10 L cubitainers containing seawater either enriched with 4 nM $FeCl_3$ or without iron enrichment (unamended controls) were incubated in deck-top incubators and sampled after 98 h (Marchetti et al. 2012). Newly precipitated silica in these iron-enriched and control samples was labeled as above with 0.5 μmol L^{-1} PDMPO for 24 hours in 125 mL bottles, except without prior concentration. The PDMPO-labeled, iron-enriched and control samples were fixed and filtered as described above for the PDMPO-labeled, ambient seawater samples.

Quantifying new silica precipitation by flow cytometry

Abundance, chlorophyll *a* fluorescence, and PDMPO fluorescence of preserved cells was quantified with an Influx flow cytometer (Becton, Dickinson and Company). Chlorophyll *a* was excited by a 488 nm Coherent laser and fluorescence was detected at 692 nm (40 nm bandpass) and the newly precipitated silica labeled with PDMPO was excited by a 355 nm ultraviolet (UV) laser and detected at 460 nm (50 nm bandpass); a control sample without PDMPO labeling was similarly analyzed. One μm (Polysciences) and 3 μm (Spherotech) beads were added to each sample as relative size and fluorescence standards. Total measured sample volume was determined by change in weight during a known run time.

Cytometry measurements were visualized and quantified with tools in the FlowCore library for R. The bead subset was identified using tools in the Splancs library and fluorescence of all particles was normalized to the mode bead fluorescence. Silicifying phytoplankton were identified by their fluorescent PDMPO signal and these populations were further defined by chlorophyll *a* and forward scatter characteristics. Relative PDMPO fluorescent intensities for all particles in each population were combined to quantify their relative contribution to total new silica precipitation. Populations were sorted onto microscope slides and cells within each population were identified by microscopy. Quantifications by flow cytometry likely underestimate both the abundance and fluorescent intensity of cells with a length greater than the 20 μm laser diameter.

Quantifying new silica precipitation by microscopy

PDMPO-labeled cells frozen on filters and mounted on microscope slides were analyzed on a Nikon Eclipse 80i microscope with a Nikon Digital Sight-Qi1monochrome camera and Nikon Imaging Software (NIS) Elements. PDMPO labeled cells were excited at 300-400 nm and emission was detected with a 420 nm long-pass filter (Chroma). More than 100 photos were captured from each filter at a magnification of 400X. To determine fluorescence of newly precipitated silica quantitatively, exposure time remained constant for all photos and samples were photographed within one month of each other to minimize changes in lamp intensity. The locations of newly precipitated silica were noted (e.g., one valve, two valves, valve and girdle bands, four valves). Actively silicifying cells were enumerated from a separate set of more than 100 photos taken at random across the filter area with optimal exposure times. Cell concentrations were estimated from the fraction of total filter area photographed and the total volume of seawater filtered onto the membrane.

The relative amount of newly precipitated silica for individual cells was quantified using NIS Elements software by outlining fluorescent cell walls and recording both the mean and the integrated brightness of the fluorescent label. Triplicate values of integrated brightness were combined from either ambient samples or iron-enriched samples for each cell type to determine the distribution of total new silica precipitation before and after iron enrichment. Differences between samples were tested using a student's *t*-test. The contribution of each cell type to total new silica precipitation was determined by multiplying cell abundance by average new silica per cell. To determine whether relative silicification differed among each diatom genus, the individual mean brightness values of fully labeled cells were combined from triplicate iron-enriched samples. Mean brightness values represent the sum of each pixel's brightness within an outlined shape divided by the number of pixels. These values are assumed to be proportional to the amount of new silica deposited when normalized to valve surface area. Cells from iron-enriched samples were selected because these samples contained a higher proportion of fully labeled cells for each genus. Differences in mean brightness among genera were determined using an analysis of variance and a tukey test. Epifluorescent microscopy may underestimate the silica content of different cell types because their various shapes may have a tendency to lie in different ways on the two-dimensional filter membrane, but this does not affect comparisons of a single genus among conditions.

Gene identification and in silico characterization

Genes encoding silicic acid transporters (SIT), aminopropyl transferases (APT), chitin synthases, and a gene encoding a protein of unknown function were chosen for transcriptional analysis due to their proposed functions in different aspects of diatom cell wall formation (Table 2.1). Homologs of *T. pseudonana* sequences were identified in the whole genome sequences of *P. tricornutum*, *F. cylindrus*, and *P. multiseries* and the National Center for Biotechnology Information (NCBI) non-redundant (nr) database with Blastx (expect value < 10^{-5}) (Altschul et al. 1990). Due to the large number of known APT-like genes in the NCBI nr database, a subset of sequences representing different lineages was selected from the study by Minguet et al. (2008). Gene models from the *P. tricornutum*, *F. cylindrus, and P. multiseries* genomes (genome.jgi-psf.org) provided predictions of the start and end of genes.

Amino acid alignments were created using Muscle (Edgar 2004) for each predicted gene product including sequences from both the NCBI database and diatom genomes. For genes encoding SITs, chitin synthases, and a gene with unknown function, all regions of the known amino acid sequences were included in the alignment to ensure that sequence fragments from any region of the genes could be identified in environmental datasets. For the APT gene sequences, only the region homologous to a spermidine synthase domain was included in the alignment. Maximum likelihood-based phylogenetic trees were created for each alignment of each protein product using Randomized Axelerated Maximum Likelihood (RAxML) software (Stamatakis et al. 2005). To ensure that tree topology was not influenced by differences in sequence length or regions of the alignment with missing sequence data or gaps, a second tree was created based on a sequence alignment trimmed to include the most conserved and informative regions. With the full amino acid alignment as a reference, HMMer (hmmer.janelia.org) was used to perform hidden markov model (HMM) searches of six-frame translated *Pseudo-nitzschia granii* expressed sequence tags from a transcriptome library of an isolate obtained from the iron-enriched incubations (Marchetti et al. 2012), environmental eukaryotic metatranscriptome datasets from the ambient (iron-limited) and iron-enriched communities at Sta. Papa in the northeast subarctic Pacific (community cyberinfrastructure for advanced microbial ecology research and analysis, camera.calit2.net) (Marchetti et al. 2012), and a metatranscriptome dataset from the surface waters of the temperate Puget Sound estuary (T. Mock unpubl.). Translated environmental sequences that recruited to the amino acid reference

alignment were placed on the phylogenetic trees using pplacer software (Matsen et al. 2010). For simplicity, final trees included only sequences from sequenced diatom genomes and sequences most phylogenetically closely related to environmental transcripts. The phylogenetic tree of SIT genes includes sequences characterized in previous studies of *P. tricornutum* (Sapriel et al. 2009), *Cylindrotheca fusiformis* (Hildebrand et al. 1998), and *T. pseudonana* (Thamatrakoln et al. 2006), and are labeled as in these publications.

To provide statistical support for changing transcriptional patterns of genes related to frustule formation in the Sta. Papa metatranscriptomes, SOLiD sequence reads aligned to 454 sequences (Marchetti et al. 2012) were compared between the ambient iron-limited and iron-enriched metatranscriptomes. Additionally, to determine the influence of bottle incubation, the abundance of SOLiD sequence transcripts was compared between an unamended control incubation and the iron-enriched incubation. Significant differences between SOLiD transcript abundance for each gene were assessed with the edgeR package in R. SOLiD library sizes and the abundance of reads assigned to diatoms between the two libraries were adjusted by a trimmed mean of fold change (M) normalization (TMM) (Robinson and Oshlack 2010) and differential expression was considered significant at adjusted $p<0.05$ by Benjamini and Hochberg (1995) multiple testing correction with the 'p.adjust' function in R.

Culturing conditions and experiments

Pseudo-nitzschia multiseries (CLN 17) was obtained from S. Bates (Fisheries and Oceans Canada) and maintained in continuous light at 100 μmol photons m^{-2} s^{-1} in modified Enriched Seawater Artificial Water (ESAW) (Berges et al. 2001) amended with f/2 concentrations of nutrients (Guillard and Ryther 1962). Growth of triplicate cultures of *P. multiseries* at 20°C were monitored by measuring relative chlorophyll *a* fluorescence with a 10AU fluorometer (Turner). Cultures were considered acclimated to the growth conditions when the growth rates of 3 consecutive transfers were not significantly different from one another according to an analysis of covariance (Brand et al. 1981).

P. multiseries experimental treatments were conducted in 4 L of artificial seawater continuously bubbled with sterile air and mixed on a stir plate. Experimental cultures were grown in triplicate batch cultures with nutrient replete media (882 μmol L^{-1} $NaNO_3$, 106 μmol L^{-1} Na_2SiO_3, 36.2 μmol L^{-1} NaH_2PO_4), low nitrate media (55 μmol L^{-1} $NaNO_3$, 212 μmol L^{-1}

Na_2SiO_3, 72.4 μmol L^{-1} NaH_2PO_4), or low silicic acid media (1764 μmol L^{-1} $NaNO_3$, 53 μmol L^{-1} Na_2SiO_3, 72.4 μmol L^{-1} NaH_2PO_4). Photosynthetic yield of photosystem II (Fv:Fm) was monitored with a PhytoPAM fluorometer (Waltz). Macronutrient starvation was defined to be within 24 hours after chlorophyll *a* fluorescence no longer increased exponentially and Fv:Fm values decreased. Frozen RNA samples from cultures maintained in iron-replete (pFe19) or iron-limited (pFe21.4) conditions were used from a previous study (Marchetti et al. 2009).

Approximately 2 L of the experimental cultures were filtered onto 0.8 μm polycarbonate filters (Millipore) at the onset of stationary phase (macronutrient starvation), or during mid-exponential growth (nutrient replete). Filtered cells were immediately frozen in liquid nitrogen, and stored at -80°C until RNA extraction (*see* below). Depletion of either silicic acid or nitrate was confirmed by removing two 50 mL aliquots from the remaining macronutrient-starved culture and adding either 212 μmol L^{-1} Na_2SiO_3 or 1764 μmol L^{-1} $NaNO_3$ to one aliquot and to the remaining large volume culture. The chlorophyll *a* fluorescence of all cultures was monitored for at least two days to confirm that the nutrient addition allowed the limited culture to resume growth.

RNA extraction

RNA was extracted from cells on frozen filters using the Totally RNA extraction kit (Invitrogen). The RNA with incubated with dioxyribonuclease (DNase) I (Ambion) at 37°C for 2 hours and purified either by ethanol precipitation or by DNase inactivation reagent (Ambion). One μL of RNA was reserved for quantitative polymerase chain reaction (*see* below) to confirm that deoxyribonucleic acid (DNA) was removed. Two μg of DNA-free RNA were reverse transcribed into cDNA using Superscript III First Strand Synthesis System for reverse transcription quantitative polymerase chain reaction (RT-qPCR) (Invitrogen). cDNA aliquots were diluted with water five fold prior to use in RT-qPCR.

Quantification of gene transcripts

Primers for RT-qPCR (Table 2.1) were designed using Primer3 (Rozen and Skaletsky 2000) to amplify a 100-200 base pair fragment of each gene. Gene standards for qPCR were generated by PCR amplification consisting of an initial incubation at 94°C for 5 min, followed by 40 cycles of 94°C for 30 s, 60°C for 30 s, and 72°C for 50 s, followed by 72°C for 5 min.

Reactions consisted of 1 μL cDNA, 1X Taq Buffer, 2 mmol L^{-1} $MgCl_2$, 0.8 μmol L^{-1} forward and reverse primers, and 0.075 units μL^{-1} Taq polymerase (Gene Choice). Amplified fragments were purified using a PCR purification kit (Roche) and cloned and transformed into *Escherichia coli* using the TOPO TA Cloning Kit for Sequencing (Invitrogen). Colonies containing the cloned gene fragment were incubated at 37°C overnight in liquid luria broth media and plasmids were purified using the QIAprep Miniprep Kit (Qiagen). Plasmids were incubated with *SpeI* (New England Biolabs) at 37°C for 2 hours and linearization was confirmed by gel electrophoresis. Linearized plasmids were quantified on a Nanodrop spectrophotometer and the copy number per μL was calculated based on the known base pair length of the vector with insert and an average double stranded DNA weight of 660 g mol^{-1}.

Transcript copy number of selected genes was quantified by RT-qPCR in 30 μL reactions consisting of 2 μl cDNA or DNA standard, 0.8 μmol L^{-1} forward and reverse primer, and 15 μL of iQ Supermix (Biorad). Reactions were carried out on an iCycler thermocycler (BioRad) with an initial incubation at 95ºC for 3 minutes followed by 45 cycles of 95ºC for 10 s, 60ºC for 30 s, and 72ºC for 50 s, followed by a step-wise increase in melting temperature to verify the presence of a single melt peak fluorescent signal. A dilution series of standards were amplified at the same time as transcripts from experimental cDNA samples. Transcript copy numbers were calculated using iCycler software and normalized to actin copy numbers from the same cDNA sample. A previous study of silicic acid starved *T. pseudonana* identified actin as the most conservative housekeeping gene for normalization (Durkin et al. 2009), and also does not change transcription levels in our silicic acid-starved *P. multiseries* cultures according to an RNA-seq dataset (S. Bender unpubl.).

2.4 Results

Silica precipitation by diatoms at Sta. Papa before and after iron enrichment

The relative amount of newly precipitated silica per cell was quantified based on the incorporation of the fluorescent stain PDMPO into individual frustules after a 24 h incubation (Leblanc and Hutchins 2005). Members of the diatom community at the iron-limited Sta. Papa that were labeled with PDMPO consisted primarily of the genera *Pseudo-nitzschia*, *Fragilariopsis*, *Chaetoceros*, *Asteromphalus*, *Neodenticula*, and *Thalassiosira.* Silicoflagellates of the genera *Meringosphaera* and *Dictyocha* were also labeled with this stain (Fig. 2.1).

Because the PDMPO stain incorporates into the frustule as the silica precipitates, these genera were defined as the actively growing component of the silicifying phytoplankton community. The quantity of new silica precipitated by each genus was compared by microscopy for the two most extreme conditions, the iron-limited ambient and iron-enriched incubation (Figs. 2.1, 2.2A). To account for effects caused by incubation in bottles, the new silica precipitated by the community in the control bottles was compared to the ambient and iron-enriched communities by flow cytometry (Fig. 2.2B, 2.2C).

The relative amount of newly precipitated silica per cell at Sta. Papa varied across genera by three orders of magnitude (Fig. 2.1). The two categories of large centric diatoms (20-40 μm and >40 μm), including *Thalassiosira* cells and additional unidentified genera, displayed the greatest PDMPO fluorescence per cell (>40 μm: 836,486 ± 161, 795 relative fluorescence units (RFUs), 20-40 μm: 437,820 ± 307,881 RFUs, with standard deviations) and thus were assumed to have precipitated the greatest amount of new silica over 24 hours. *Asteromphalus* spp. precipitated the next largest quantity of new silica over 24 h (152,866 ± 45,696 RFUs), followed by *Chaetoceros* sp. (97,343 ± 80,501 RFUs), *Neodenticula*-like (74,966 ± 42,741 RFUs), *Pseudo-nitzschia* spp. (58,428 ± 18,789 RFUs), *Meringosphaera* sp. (23,006 ± 11,680 RFUs), large (10 μm) *Fragilaropsis* sp. (7983 ± 2480 RFUs), and small (5 μm) *Fragilariopsis* sp. (3749 ± 3549 RFUs).

After iron enrichment, the relative amount of newly precipitated silica per cell increased (p<0.05) in *Chaetoceros*, *Pseudo-nitzschia*, and both the 5 and 10 μm size categories of *Fragilariopsis*. The quantity of new silica precipitated by the large centric and *Neodenticula*-like cells decreased after iron enrichment (p<0.05), which may indicate a slower growth rate for these genera under this high iron condition. No significant change in silica precipitation was detected in *Asteromphalus* spp. or the silicoflagellate *Meringosphaera* sp. The changes in new silica precipitation per cell detected before and after iron addition within a given genus were minor relative to the differences across genera (Fig. 2.1).

The relative contribution of each genus to community-wide new silicification was determined by multiplying the estimated cell abundance of individual genera by the average quantity of new silica precipitated by that genus before and after iron enrichment (Fig. 2.2A). Prior to iron enrichment, the 5 μm *Fragilariopsis* sp. dominated cell abundance of the actively silicifying community (104 ± 65 cells mL^{-1}, 64% of total), but contributed only 13% to total new

silica precipitation (419,291 ± 383,305 RFU mL^{-1}). In contrast, *Pseudo-nitzschia* spp. accounted for 16% of the silicifying community cell abundance (26 ± 8 cells mL^{-1}) but contributed 46% to community new silica precipitation (1,473,917 ± 501,391 RFU mL^{-1}). Similarly, *Chaetoceros* sp. cells contributed 5% (8 ± 5 cells mL^{-1}) of total silicifying cell abundance and 28% (897,068 ± 705,553 RFU mL^{-1}) to new silica precipitation. The 10 μm *Fragilariopsis* sp. and *Meringosphera* sp. cells each contributed < 10% to both silicifying cell abundance and silica precipitation. The contribution of less abundant genera, like *Asteromphalus* spp. and *Neodenticula*-like cells when grouped together accounted for 9.4% of the total silicifying community (15 ± 10 cells mL^{-1}). After iron enrichment, *Pseudo-nitzschia* spp. dominated the composition of the silicifying community at 53% (2240 ± 308 cell mL^{-1}) and accounted for 76% (231,694,542 ± 107,948,281 RFU mL^{-1}) of new silica precipitation. *Chaetoceros* sp. cells accounted for 4.2% of the silicifying community (179 ± 48 cells mL^{-1}) and contributed 21% (62,608,180 ± 66,134,605 RFU mL^{-1}) of the total new silica precipitation, with large variability in RFUs per cell caused by large differences in cell sizes and the number of new valves and spines fluorescing per cell within a single sample. Actively growing cells of small *Fragilariopsis* (1459 ± 66 cells mL^{-1}), large *Fragilariopsis* (208 ± 43 cells mL^{-1}), and *Meringosphaera* (29 ± 6 cells mL^{-1}) all increased in cell abundance, but decreased in their percent contribution to the total silicifying community and combined accounted for only 3.4% percent of the newly deposited silica. Less abundant species were grouped as before and accounted for 2.7% of the total actively silicifying community (114 ± 52 cells mL^{-1}) (Fig. 2.2A).

To more accurately analyze the small (5 μm) and the weakly fluorescent, lightly silicified cells, the same samples plus the control incubation were quantified on a sorting-capable flow cytometer. Four distinct populations of actively silicifying phytoplankton were identified, quantified, and sorted to determine the dominant components of the populations (Fig. 2.2B, C). Population A contained cells with the greatest chlorophyll *a* fluorescence and light scatter and was composed of large (≥20 μm), chain-forming *Pseudo-nitzschia* spp. and *Chaetoceros* spp. Population B cells had comparable light scatter but less chlorophyll *a* fluorescence per cell than population A cells and included *Fragilariopsis* sp. Population C cells were the smallest (based on light scatter) with the least chlorophyll *a* fluorescence per cell and included *Meringosphaera* sp. Population D cells displayed reduced light scatter relative to chlorophyll *a* fluorescence, a characteristic of pennate diatoms, and included lightly silicified pennates, such as *Cylindrotheca*.

All communities examined (ambient iron-limited, iron-enriched, and control) contained a high proportion of cells from population C (iron-limited = 41%, 25 cells mL^{-1}; iron-enriched= 69%, 1416 cells mL^{-1}; control= 73%, 763 cells mL^{-1}) followed by population B (iron-limited = 45%, 27 cells mL^{-1}; iron-enriched= 16%, 333 cells mL^{-1}; control= 16%, 167 cells mL^{-1}). Actively silicifying cells from Population A were nearly absent in the control incubation (1%, 11 cells mL^{-1}) and in the ambient iron-limited community (8.9%, 5 cells mL^{-1}), and were more abundant after iron enrichment (12%, 248 cells mL^{-1}). Despite their relatively low abundance, these larger cells accounted for 45% (0.35 RFU mL^{-1}) and 72% (19 RFU mL^{-1}) of the total silica precipitated by the community before and after iron enrichment, respectively. In the control incubation, community silica precipitation was more equally distributed, with Populations A, B, C, and D contributing 17% (0.89 RFU mL^{-1}), 26% (1.4 RFU mL^{-1}), 36% (1.9 RFU mL^{-1}), and 21% (1.1 RFU mL^{-1}), respectively. Both microscopy and flow cytometry identified *Pseudo-nitzschia* spp. and *Chaetoceros* sp.*,* or the populations containing these genera, to be particularly influential on silica precipitation before and after iron enrichment. These consistent patterns were found in spite of the fact that the flow cytometer underestimates both abundance and fluorescence of chain-forming cells and cells larger than the laser diameter of 20 μm.

In *Pseudo-nitzschia*, a portion of this increase in new silica per cell 98 hours after iron enrichment (Fig. 2.1) was caused by a faster division rate over the 24 h PDMPO incubation period, and resulted in a greater number of fluorescing valves and girdle bands per cell (Fig. 2.3A). The increase in total *Pseudo-nitzschia* PDMPO fluorescence after iron-enrichment is also caused by an increase in the average fluorescence of either single valves or both valves by 29% and 42%, respectively, suggesting that the silica content per valve increases (Fig. 2.3B).

Mean fluorescence of individual cells fully labeled with PDMPO in the iron-enriched incubation was used as a proxy for surface area normalized silicification estimates to determine whether species composition may also affect silicon and other nutrient cycles due to differences in relative nutrient requirements (Fig 2.4). Despite large variability within a diatom category or genus, significant differences exist among the diatoms measured ($p<0.001$), caused by higher mean values of silicification in the centric diatoms and *Neodenticula*. The large centric diatoms had the highest mean PDMPO fluorescence (12.6 ± 1.3 RFUs), followed by *Neodenticula sp.* (11 ± 1.4 RFUs), medium sized centric diatoms (10.1 ± 1.9 RFUs), *Asteromphalus* (8.7 ± 1.1 RFUs),

Pseudo-nitzschia (8.7 ± 2.7 RFUs), *Chaetoceros sp.* (8 ± 2.4 RFUs), 5 μm *Fragiliriopsis* (7.9 ± 2.5 RFUs), and 10 μm *Fragilariopsis* (7.1 ± 0.8 RFUs).

Transcriptional responses related to frustule formation in field communities

To identify genetic signals of the physiological responses related to frustule formation in iron-limited communities, the phylogeny and transcription of key genes related to different aspects of frustule formation were investigated in the mixed field communities. Target genes that encode proteins potentially related to frustule formation were identified and characterized based on available diatom genomes and previously published sequences.

Transporters responsible for silicic acid uptake (SITs) are encoded by multiple genes based on analysis of the *T. pseudonana*, *F. cylindrus*, *P. tricornutum*, and *P. multiseries* genomes (Table 2.2). Additional SIT genes were identified in the *P. granii* transcriptome library and NCBI nr database. SIT sequences from the four diatom genomes fell into five major clades labeled A, B, C, D, and E (Fig. 2.5A), supported by bootstrap probability values >90 or in the case of clade C, lacking bootstrap support with any other clade. Clades A, B, and D consisted of sequences from the most derived group of diatoms, the pennate diatoms. Sequences from *F. cylindrus* and *P. multiseries*, but not *P. tricornutum* grouped with clades A and D, whereas sequences from all three pennates grouped with clade B (Table 2.2, Fig. 2.5A). One SIT gene copy in *P. multiseries* from clade B (protein identity 338018) was three times longer than a typical SIT gene and encoded three concatenated SIT domains. These three domains were aligned as separate sequences from each other for the phylogenetic analysis. Clade E consisted of SIT sequences from the Thalassiosirales, a subset of the multipolar centric diatoms that produce chitin fibers. Clade C appears to be the most basal clade because it contains SIT sequences derived from radial centric, multipolar centric, and pennate diatoms, although not all diatom species with known SIT sequences contain SITs from this clade. The amino acid alignment used to identify these clades was 911 amino acids long, including gaps. The same clades were identified based on a tree created from an alignment of only the most conserved regions of the amino acid alignments, with total length of 114 amino acids (data not shown).

To determine the environmental relevance of the SIT clades, three environmental metatranscriptomes consisting of 454-derived transcript fragments (~ 200 base pairs) were examined for the presence of SIT sequences. Twenty-six SIT sequences were identified in a

metatranscriptome derived from iron-limited surface water at Sta. Papa; 37 were identified in a metatranscriptome derived from iron enrichment of the Sta. Papa surface waters; and 37 were identified in a metatranscriptome derived from surface waters in Puget Sound, Washington (Fig. 2.5A). The majority (92%) of SIT sequences from Puget Sound were from clade C (Fig. 2.5A). In contrast, the vast majority of SIT sequences from Sta. Papa grouped with the A, B, and D clades. Seventy-nine percent of the clade A and D SIT sequences were from the iron-enriched community; 74% of clade B SIT sequences were from the iron-limited community (Fig. 2.5A). The majority of all SIT sequences identified in clades A, B, and D are more closely related to *Pseudo-nitzschia* SIT sequences than other known diatom SIT sequences. These *Pseudo-nitzschia* sequences include sequences from an oceanic *P. granii* isolate obtained from the same iron enrichment experiment (Marchetti et al. 2012).

To provide statistical support for the apparent bias in clade representation at Sta. Papa before and after iron enrichment, sequence reads of approximately 50 base pairs in length derived from a SOLiD sequence library from the RNA of the ambient iron-limited community, unamended control incubation, and iron-enriched incubation were mapped to the 454-derived SIT sequences (Marchetti et al. 2012). From 0 to 375 additional SIT sequence reads were detected for each 454-derived SIT sequence. Twenty-four 454-derived transcripts of the original 63 displayed significant differences ($p<0.05$) in the numbers of aligned SOLiD reads from the ambient vs. iron-enriched libraries (Fig. 2.5A). Thirteen of the 14 SOLiD-supported SIT sequences from clades A and D were found only in the library from the iron-enriched community. Eight of the SOLiD-supported SIT sequences were from clade B and of these, 7 were over-represented in the iron-limited library and were much less abundant after iron enrichment. One SIT sequence with a significant difference in SOLiD reads between the two conditions was identified in clade C and another in clade E. Both were over-represented in the metatranscriptome from the iron-limited sample. To account for transcriptional responses induced by bottle incubation, SOLiD transcripts from the control incubation were also compared to the iron-enriched incubation (Fig. 2.5A). Thirteen sequences from clades A and D were identified with a significant difference between the two incubation conditions, 9 of which were overrepresented in the iron-enriched incubation relative to the control incubation. One sequence from clade B and another from clade C were significantly over represented in the control incubation relative to the iron-enriched incubation. The similar relative abundance of SIT gene

transcripts in the ambient and control communities compared to the iron-enriched community indicates that changes in SIT transcript abundance after iron-enrichment are not an artifact of bottle incubation.

The controlled precipitation of silica likely involves aminopropyl transferases (APT) and the genes encoding these enzymes were identified in four diatom genomes (Table 2.2). Each of the four species contain multiple APT gene copies, including the two phylogenetically diverged clades hypothesized by Anthony (2011) to be involved in long-chain polyamine synthesis (Fig. 2.5B). One of these diverged clades was composed of predicted proteins containing both spermidine synthase-like and SAM decarboxylase domains. A second distinct diatom clade contained proteins with a single spermidine synthase-like domain. In addition to these diverged clades, sequences similar to known APTs in other organisms were also identified in diatoms. These clades were identified from amino acid alignment containing the region encoding the entire spermidine synthase-like domain (amino acid length 219) and also after cropping this domain to the most conserved parts of the alignment (amino acid length 106). A total of 24 APT sequences were identified in the three metatranscriptomes. Three of these sequences were most similar to the two diverged clades hypothesized to be involved in long-chain polyamine synthesis (Fig. 2.5B). One diatom-like APT transcript was detected in the 454 library from the iron-enriched community, and was significantly more abundant in the SOLiD library derived from the community in the iron-enriched vs. the control incubation (Fig. 2.5B).

Chitin is an organic component of the silica cell wall of *T. pseudonana*, and chitin synthase genes were identified in the *P. tricornutum, F. cylindrus*, and *T. pseudonana* genomes but not the *P. multiseries* genome (Table 2.2). The sequences encoded by the two pennate diatoms are evolutionarily diverged from centric sequences (4.1-7.7% amino acid similarity) but contain conserved amino acid active sites. No chitin synthases were identified in any of the metatranscriptome datasets.

Important frustule formation processes likely require proteins whose functions are as yet unknown. Homologs of a single-copy gene encoding a protein of uncharacterized function were identified in the four diatom genomes; this gene was originally identified in *T. pseudonana* (protein identity 21613) as a gene highly upregulated both by silicic acid and iron limitation (Table 2.2) (Mock et al. 2008). The amino acid alignment was 403 amino acids long before cropping and 201 amino acids after cropping. No homologous genes were identified in other

organisms available in the NCBI nr database. One sequence was identified in the metatranscriptomes at Sta. Papa and was significantly more abundant in SOLiD sequence library derived from the control incubation compared to the iron-enriched incubation (Fig. 2.5C).

Transcriptional response of cultured isolates

Iron availability at Sta. Papa appeared to influence both transcriptional patterns and relative contribution to silica precipitation by *Pseudo-nitzschia*. To determine the relationship between transcriptional patterns and physiological responses, a laboratory isolate of *P. multiseries* was grown under iron limitation and silicic acid starvation. Nitrate-starved cultures were also grown to confirm that transcriptional responses were not related to general nutrient limitation. This species of *Pseudo-nitzschia* isolated from a coastal region has a known whole genome sequence, which enabled all genes of interest to be identified and targeted for transcriptional measurements.

Batch cultures of *P. multiseries* in nutrient replete ESAW media (Fig. 2.6A) grew at a rate of 1.9 ± 0.09 d^{-1} and the photochemical yield of photosystem II (Fv:Fm) decreased from 0.71 ± 0.01 during exponential growth to 0.43 ± 0.05 ($p<0.05$) when starved of silicic acid and to 0.47 ± 0.1 ($p<0.05$) when starved of nitrate. Samples from a previously published culturing study of *P. multiseries* (Marchetti et al. 2009) had growth rates of 1.58 ± 0.05 d^{-1} in iron-replete conditions (pFe 19) and decreased to 0.33 ± 0.01 d^{-1} in iron-limited conditions (pFe 21.4). Fv:Fm of these cultures decreased from 0.69 in iron-replete conditions to 0.43 in iron-limiting conditions.

Transcript abundance of the different SIT genes varied during iron limitation or silicic acid starvation (Fig. 2.6B). Transcript abundance of a clade A SIT gene from duplicate *P. multiseries* cultures at the onset of silicic acid starvation increased 18.7 and 24.1 fold relative to nutrient replete cells. The transcriptional response of this gene was consistently higher but not significantly different in iron-limited conditions (Fig. 2.6B) and in nitrate-starved conditions (data not shown). Transcript abundance of a clade B SIT gene from *P. multiseries* increased 5.2 ± 3.2 fold when iron-limited, but changed less than 2 fold at the onset of silicic acid starvation in both cultures. *Pseudo-nitzschia multiseries*, *F. cylindrus*, and *P. tricornutum* encode APT genes phylogenetically related to the *T. pseudonana* genes that respond to silicic acid and iron limitation (Mock et al. 2008). Both of the measured *P. multiseries* APT genes increased in

transcript abundance under silicic acid starvation (2.5 and 4.0 fold for APT A, 3.0 and 3.9 fold for APT B) but did not respond significantly to iron-limitation (Fig. 2.6B). The gene that encodes a protein of unknown function increased 2.4 and 2.8 fold in silicic acid-starved cultures and increased 3.8 ± 1.2 fold in iron-limited *P. multiseries* cultures (Fig. 2.6B). None of the genes measured in this study responded significantly to nitrate starvation (data not shown).

2.5 Discussion

Each of the diverse genera present at the iron-limited Sta. Papa can influence silica precipitation and nutrient cycling differently due to differences in cell size, abundance, and silica per cell. For example, *Pseudo-nitzschia* cells were 4-fold less abundant than small *Fragilariopsis* cells, but because *Pseudo-nitzschia* precipitated about 15-fold more silica per cell in 24 hours they contributed most to new silica precipitated by the total community. Large diatoms may have also contributed significantly to silicon cycling at Sta. Papa but were too rare to accurately quantify. As a group, these large, rare cells could contribute as much or more than *Pseudo-nitzschia* to new silica precipitation, as was found in previous studies at Sta. Papa (Boyd et al. 2005; Marchetti et al. 2006). In addition to containing larger quantities of total silica, these cells appear to be more silicified relative to their cell sizes, so changes in their proportional abundance relative to the total diatom community would effect how the community as a whole utilizes nutrients. Combining both microscopy and flow cytometry enabled us to recognize the influence of large, rare cells and more easily detect cells that are small yet highly abundant.

After iron addition, the quantity of new silica precipitated per cell changed for some genera, possibly reflecting both physiological changes to the frustule and changes in the rate of frustule precipitation. On average, *Pseudo-nitzschia* cells had a greater number of fluorescing valves after iron enrichment due to faster division rates, and also a higher fluorescence per valve. Marchetti and Harrison (2007) found that iron-replete *Pseudo-nitzschia* cells have a higher silica content than iron-limited cells, and at the same time display a different cell morphology and a decrease in the ratio of Si:N. The apparent increase in silica per cell after iron enrichment is consistent with the study by Marchetti and Harrison (2007) and suggests that similar changes in cell morphology and Si:N may also have occurred during our field incubation experiments. Even so, the changes in relative silica per cell within a genus did not compare to the difference of three orders of magnitude among genera, which will have a greater influence on bulk

measurements of community silicification, similar to what has been found in other ocean regions (Baines et al. 2010). Our study accounts for the new silica precipitated by the standing stock of cells. Any biogenic silica that rapidly cycled through the diatom community and was lost due to dissolution or grazing was not quantified; a process that may particularly affect the smaller-sized cells (Krause et al. 2010). This may cause our data to underestimate the contribution of small cells to total silica precipitation; however, overall trends are unlikely to be affected due to the vast differences in quantity of silica precipitated per cell. Experiments by Leblanc and Hutchins (2005) indicate that PDMPO fluorescent intensity has a direct relationship to the quantity of silica precipitated (Leblanc and Hutchins 2005), and this relationship varied with a standard deviation of 20% among species and mixed communities. This variability in the relationship of PDMPO fluorescence to silica precipitation is much smaller than the 1000-fold difference in PDMPO fluorescence detected among genera and the ~30-40% increase in fluorescence within the valves of a single genus responding to iron-enrichment. Further laboratory experimentation is necessary to determine the sensitivity of this stain as a quantitative measure of silica across species and within a species experiencing various nutrient-limitation conditions. However, both our data and those of LeBlanc and Hutchins (2005) demonstrate that PDMPO labeling can be used to indicate quantitative differences in silica precipitation.

Species composition also controls which diatom responses to nutrient limitation are possible at any given time or location because not all diatoms encode the same genes related to frustule formation, or transcribe these genes under the same conditions. To understand how physiological changes varied in tandem with shifting community compositions, metatranscriptome sequences were analyzed from the community present before and after iron addition at Sta. Papa and from a community in the estuarine environment of Puget Sound, where presumably iron is not limiting. A major shift was observed in the type of SIT genes present in the Puget Sound vs. the open ocean Sta. Papa. This difference likely reflects changes in community composition between the two environments because the detected SIT transcripts were derived from separate phylogenetic clades containing evolutionarily divergent species.

When the three metatranscriptomes from Sta. Papa were compared, a majority of sequences were most closely related to known *Pseudo-nitzschia* sequences. Thus, the observed abundance shift between SIT transcripts from clades A and B likely represents a physiological shift in this subset of the community. To support this interpretation, we measured the

transcriptional response of a *P. multiseries* isolate under different iron and silicic acid conditions. Iron-limited *P. multiseries* cultures increased transcript abundance of a SIT gene in clade B, the same clade of SIT genes most abundant at the iron-limited Sta. Papa, suggesting that the SIT B gene may indicate silicic acid uptake in iron-limited conditions. In the *P. multiseries* genome, this gene encodes a series of three SIT protein domains unusual for any other known SIT gene. It is unknown whether this domain structure is found in other species of *Pseudo-nitzschia* or whether these domains play a unique role in the response of *Pseudo-nitzschia* to iron-limitation. Transcripts of the SIT A gene increased in response to silicic acid starvation in cultures of *P. multiseries* and were most abundant in the community at Sta. Papa after iron-enrichment. Silicic acid concentrations remained high (21.57 μmol L^{-1}) after iron enrichment (Marchetti et al. 2012), so transcription of the SIT A gene may be indicative of multiple growth scenarios; cells growing exponentially without limitation and/or competing for available silicic acid. Transcriptional regulation of this gene may also differ between open ocean *Pseudo-nitschia* and coastal *P. multiseries*. Future studies to determine whether SIT gene clades have evolved different functions would provide a mechanism for changes in how diatom cells take up silicic acid (Brzezinski et al. 2005; Brzezinski et al. 2008). Given the large influence of *Pseudo-nitzschia* on the total amount of new silica precipitated by the community, a functional shift in silicic acid transport could have large-scale effects on silicon cycling in iron-limited regions. Since not all diatoms appear to encode this iron-responsive gene, this transcriptional response might not be detectable or relevant in all iron-limited diatom communities, which reiterates the importance of considering species composition when determining why a community responds to nutrient limitation in a particular way.

The variable responses of diatom frustules to iron limitation may be explained by genetic divergence and transcriptional diversity among diatom species, and ultimately, provide a mechanism for species-specific influences on biogeochemistry. A major mechanism for diversification appears to be through gene duplication; SITs, APTs, and chitin synthases are part of multi-copy gene families. The family of SIT genes is perhaps the most well-studied (Thamatrakoln et al. 2006; Alverson 2007) and with the addition of pennate diatom genomic sequences it is apparent that several diatom SIT gene clades diverged prior to the species themselves. Gene duplication appears to be ongoing because an individual species often encodes multiple gene copies within a single clade. Transcripts of the SIT genes in clade C have been

reported to increase in silicic acid-starved *P. tricornutum* cultures (Sapriel et al. 2009), similar to what has been described for the Thalassiosirales genes in clade E (Mock et al. 2008). The divergence of gene clades may enable the emergence of new functions for a gene. The transcription of SIT genes in clade B increased in our iron-limited *P. multiseries* cultures and has also been reported in iron-starved *P. tricornutum* cultures (Allen et al. 2008), a response that is apparently specific to this gene clade. Far from being a unique characteristic of the SIT genes, this same pattern of clade divergence was observed in the APT and chitin synthase genes and these genes may also display diverse transcriptional patterns among gene clades and species.

Notably, the gene encoding a protein with unknown function is a single copy gene in all four diatom genomes and displays a more conserved pattern of transcription. In a study of *T. pseudonana* (Mock et al. 2008), transcript abundance of the protein with ID 21613 increased 30 and 7-fold due to silicic acid and iron starvation, respectively. Transcription of this gene homolog is also induced in *P. tricornutum* by these two conditions, according to expressed sequence tag evidence (genome.jgi.org), and in our *P. multiseries* cultures under both conditions. The presence of this gene in each of the four diatom genomes and its similar transcriptional patterns suggests it may have a shared and vital role in diatom biology and perhaps frustule formation in particular. Most of the gene products hypothesized to have a role in frustule formation have an unknown function (Mock et al. 2008). Priority for the characterization of these genes should go to those that are the most informative of how diatoms influence biogeochemical cycles in different environments; particularly those that are found widely among diatom species, have measurable variation in transcription under controlled conditions, and are easily detectable in field populations. Our study of a few select genes suggests that single copy genes might have more conserved functions and transcriptional patterns across species, whereas multi-copy genes have the potential for greater diversification.

The genes selected in this study represent conserved parts of cell wall formation, some proven and some hypothesized, and the most compelling candidates to investigate frustule formation in natural communities. However, these genes were not equally detectable in natural communities. The SIT genes proved to be most informative for separating the effects of community composition and physiological responses to iron limitation. The SIT genes are multi-copy and present in diverse species, which may explain their ease of detection in field communities. Despite the fact that diatom APT and chitin synthase genes have these same

characteristics, they were not as easily detected. One difference between these gene types is the degree of transcriptional regulation. The differential transcription of SIT genes in our laboratory conditions was dramatic (24 fold at most, 4.6 fold when iron-limited), while APT genes changed very little (4 fold at most, and no response to iron-limitation). Chitin is known to be an important component of the cell wall in some genera of diatoms but not *Pseudo-nitzschia*, which lacks a chitin synthase gene. Since the frustule-related sequences detected at Sta. Papa were predominantly related to *Pseudo-nitzschia*, chitin biosynthesis in diatoms was either irrelevant at this location or impossible to detect in the less abundant species. A separate factor determining the ease of transcript detection in field communities may be the baseline transcription level of each gene, a problem that could be solved by a greater sequencing effort. The availability of additional metatranscriptomes from diverse environments will help determine which genes can be successfully used as indicators for ecological and biogeochemical processes.

The influence of species composition on silica precipitation in iron-limited environments has oceanographic implications, especially for the conceptual and numerical models of biogeochemistry in these regions. The large influence of diatom species composition should be expected from a group that evolved ~240 million years ago and has radiated into one of the most diverse groups of eukaryotes (Kooistra and Medlin 1996). Their evolutionary history has produced diatom communities composed of species with strikingly diverse physiological requirements for silicon and different responses to shifting environmental conditions. Blooms induced by iron enrichment at different locations can have different species compositions (De Baar et al. 2005) and the blooms at any one location may have shifting species composition over time (Boyd et al. 2005; Marchetti et al. 2006). Such dynamic scenarios may affect how these communities influence biogeochemical cycles. Moreover, our work and that of others suggests that the most abundant species may not have the greatest influence on silicon cycling or other biogeochemical cycles. For this reason, we must use more sophisticated techniques, and perhaps more refined models, to measure how different diatom communities alter biogeochemistry. Cellular stains that visualize physiological responses provide a powerful tool to measure the influence of species diversity, especially when combined with high throughput flow cytometry. Single-cell analyses by synchrotron x-ray fluorescence microscopy have also provided new insight into the response by individual species (Twining et al. 2004; Baines et al. 2010). Identifying genes that are readily detected in the field and indicate physiological changes in

frustule formation help characterize the dominant physiologies that influence biogeochemistry. We suggest that silicon transporters may be a valuable indicator of these processes, and additional measurements in locations with different species compositions would help clarify whether these genes can provide physiological indications of global relevance.

2.6 Acknowledgments

This study was conducted in collaboration with Adrian Marchetti, Sara Bender, Rhonda Morales, Tiffany Truong, Thomas Mock, and E. Virginia Armbrust. This work was supported through a Gordon and Betty Moore Foundation Marine Microbiology Investigator Award to E. Virginia Armbrust. I thank Marie Robert, scientists of Fisheries and Oceans Canada at the Institute of Ocean Sciences, Sidney, BC, Canada and the officers and crew of the R/V *J.P. Tully* for enabling our field work; Robin Kodner, Dave Schruth, and Chris Berthiaume for assistance and advice regarding bioinformatics; Anitra Ingalls for insightful conversations; and Franziska Lutz for assistance with phytoplankton culturing.

2.7 Bibliography

Allen, A. E., J. Laroche, U. Maheswari, M. Lommer, N. Schauer, P. J. Lopez, G. Finazzi, A. R. Fernie, and C. Bowler. 2008. Whole-cell response of the pennate diatom *Phaeodactylum tricornutum* to iron starvation. Proceedings of the National Academy of Sciences of the United States of America **105:** 10438-10443.

Altschul, S. F., W. Gish, W. Miller, E. W. Myers, and D. J. Lipman. 1990. Basic local alignment search tool. Journal of Molecular Biology **215:** 403-410.

Alverson, A. J. 2007. Strong purifying selection in the silicon transporters of marine and freshwater diatoms. Limnology and Oceanography **52:** 1420-1429.

Andersen, R. A. 2005. Algal culturing techniques. Elsevier/Academic Press.

Anthony, M. 2011. Molecular machines encoded by bacterially-derived multi-domain gene fusions that potentially synthesize, N-methylate and transfer long chain polyamines in diatoms. Febs Letters **585:** 2627-2634.

Baines, S. B., B. S. Twining, M. A. Brzezinski, D. M. Nelson, and N. S. Fisher. 2010. Causes and biogeochemical implications of regional differences in silicification of marine diatoms. Global Biogeochemical Cycles **24:** GB4031, doi: 4010.1029/2010GB003856

Benjamini, Y., and Y. Hochberg. 1995. Controlling the false discovery rate: a practical and powerful approach to multiple testing. Journal of the Royal Statistical Society. Series B (Methodological) **57:** 289-300.

Berges, J. A., D. J. Franklin, and P. J. Harrison. 2001. Evolution of an artificial seawater medium: Improvements in enriched seawater, artificial water over the last two decades. Journal of Phycology **37:** 1138-1145.

Bowler, C., A. E. Allen, J. H. Badger, J. Grimwood, K. Jabbari, A. Kuo, U. Maheswari, C. Martens, F. Maumus, R. P. Otillar, E. Rayko, A. Salamov, K. Vandepoele, B. Beszteri, A. Gruber, M. Heijde, M. Katinka, T. Mock, K. Valentin, F. Verret, J. A. Berges, C. Brownlee, J. P. Cadoret, A. Chiovitti, C. J. Choi, S. Coesel, A. De Martino, J. C. Detter, C. Durkin, A. Falciatore, J. Fournet, M. Haruta, M. J. J. Huysman, B. D. Jenkins, K. Jiroutova, R. E. Jorgensen, Y. Joubert, A. Kaplan, N. Kroger, P. G. Kroth, J. La Roche, E. Lindquist, M. Lommer, V. Martin-Jezequel, P. J. Lopez, S. Lucas, M. Mangogna, K. Mcginnis, L. K. Medlin, A. Montsant, M. P. Oudot-Le Secq, C. Napoli, M. Obornik, M. S. Parker, J. L. Petit, B. M. Porcel, N. Poulsen, M. Robison, L. Rychlewski, T. A.

Rynearson, J. Schmutz, H. Shapiro, M. Siaut, M. Stanley, M. R. Sussman, A. R. Taylor, A. Vardi, P. Von Dassow, W. Vyverman, A. Willis, L. S. Wyrwicz, D. S. Rokhsar, J. Weissenbach, E. V. Armbrust, B. R. Green, Y. Van De Peer, and I. V. Grigoriev. 2008. The *Phaeodactylum* genome reveals the evolutionary history of diatom genomes. Nature **456:** 239-244.

Boyd, P. W., R. Strzepek, S. Takeda, G. Jackson, C. S. Wong, R. M. Mckay, C. Law, H. Kiyosawa, H. Saito, N. Sherry, K. Johnson, J. Gower, and N. Ramaiah. 2005. The evolution and termination of an iron-induced mesoscale bloom in the northeast subarctic Pacific. Limnology and Oceanography **50:** 1872-1886.

Brand, L. E., R. R. L. Guillard, and L. S. Murphy. 1981. A method for the rapid and precise determination of acclimated phytoplankton reproduction rates. Journal of Plankton Research **3:** 193-201.

Brunner, E., P. Richthammer, H. Ehrlich, S. Paasch, P. Simon, S. Ueberlein, and K. H. Van Pée. 2009. Chitin-based organic networks: An integral part of cell wall biosilica in the diatom *Thalassiosira pseudonana*. Angewandte Chemie International Edition **48:** 9724-9727.

Brzezinski, M. A., C. Dumousseaud, J. W. Krause, C. I. Measures, and D. M. Nelson. 2008. Iron and silicic acid concentrations together regulate Si uptake in the equatorial Pacific Ocean. Limnology and Oceanography **53:** 875-889.

Brzezinski, M. A., J. L. Jones, and M. S. Demarest. 2005. Control of silica production by iron and silicic acid during the Southern Ocean Iron Experiment (SOFeX). Limnology and Oceanography **50:** 810-824.

Brzezinski, M. A., C. J. Pride, V. M. Franck, D. M. Sigman, J. L. Sarmiento, K. Matsumoto, N. Gruber, G. H. Rau, and K. H. Coale. 2002. A switch from $Si(OH)_4$ to NO_3 depletion in the glacial Southern Ocean. Geophysical Research Letters **29:** 1564, doi: 1510.1029/2001gl014349

Buesseler, K. O. 1998. The decoupling of production and particulate export in the surface ocean. Global Biogeochemical Cycles **12:** 297-310.

De Baar, H. J. W., P. W. Boyd, K. H. Coale, M. R. Landry, A. Tsuda, P. Assmy, D. C. E. Bakker, Y. Bozec, R. T. Barber, M. A. Brzezinski, K. O. Buesseler, M. Boye, P. L. Croot, F. Gervais, M. Y. Gorbunov, P. J. Harrison, W. T. Hiscock, P. Laan, C. Lancelot, C. S. Law, M. Levasseur, A. Marchetti, F. J. Millero, J. Nishioka, Y. Nojiri, T. Van

Oijen, U. Riebesell, M. J. A. Rijkenberg, H. Saito, S. Takeda, K. R. Timmermans, M. J. W. Veldhuis, A. M. Waite, and C. S. Wong. 2005. Synthesis of iron fertilization experiments: From the iron age in the age of enlightenment. Journal of Geophysical Research-Oceans **110:** C09S16, doi:10.1029/2004JC002601

De La Rocha, C. L., D. A. Hutchins, M. A. Brzezinski, and Y. Zhang. 2000. Effects of iron and zinc deficiency on elemental composition and silica production by diatoms. Marine Ecology Progress Series **195:** 71-79.

Durkin, C. A., T. Mock, and E. V. Armbrust. 2009. Chitin in diatoms and its association with the cell wall. Eukaryotic Cell **8:** 1038-1050.

Edgar, R. C. 2004. MUSCLE: multiple sequence alignment with high accuracy and high throughput. Nucleic Acids Research **32:** 1792-1797.

Field, C. B., M. J. Behrenfeld, J. T. Randerson, and P. Falkowski. 1998. Primary production of the biosphere: Integrating terrestrial and oceanic components. Science **281:** 237-240.

Frigeri, L. G., T. R. Radabaugh, P. A. Haynes, and M. Hildebrand. 2006. Identification of proteins from a cell wall fraction of the diatom *Thalassiosira pseudonana*. Molecular & Cellular Proteomics **5:** 182-193.

Guillard, R. R., and J. H. Ryther. 1962. Studies of marine planktonic diatoms.1. *Cyclotella nana* Hustedt, and *Detonula confervacea* (Cleve) Gran. Canadian Journal of Microbiology **8:** 229-239.

Hildebrand, M., K. Dahlin, and B. E. Volcani. 1998. Characterization of a silicon transporter gene family in *Cylindrotheca fusiformis*: Sequences, expression analysis, and identification of homologs in other diatoms. Molecular and General Genetics MGG **260:** 480-486.

Hutchins, D. A., and K. W. Bruland. 1998. Iron-limited diatom growth and Si : N uptake ratios in a coastal upwelling regime. Nature **393:** 561-564.

Ikeguchi, Y., M. C. Bewley, and A. E. Pegg. 2006. Aminopropyltransferases: Function, structure and genetics. Journal of Biochemistry **139:** 1-9.

Knott, J. M. 2009. Biosynthesis of long-chain polyamines by crenarchaeal polyamine synthases from *Hyperthermus butylicus* and *Pyrobaculum aerophilum*. Febs Letters **583:** 3519-3524.

Knott, J. M., P. Romer, and M. Sumper. 2007. Putative spermine synthases from *Thalassiosira pseudonana* and *Arabidopsis thaliana* synthesize thermospermine rather than spermine. Febs Letters **581:** 3081-3086.

Kooistra, W. H. C. F., and L. K. Medlin. 1996. Evolution of the diatoms (Bacillariophyta): IV. A reconstruction of their age from small subunit rRNA coding regions and the fossil record. Molecular Phylogenetics and Evolution **6:** 391-407.

Krause, J. W., M. A. Brzezinski, M. R. Landry, S. B. Baines, D. M. Nelson, K. E. Selph, A. G. Taylor, and B. S. Twining. 2010. The effects of biogenic silica detritus, zooplankton grazing, and diatom size structure on silicon cycling in the euphotic zone of the eastern equatorial Pacific. Limnology and Oceanography **55:** 2608-2622.

Kroger, N., R. Deutzmann, C. Bergsdorf, and M. Sumper. 2000. Species-specific polyamines from diatoms control silica morphology. Proceedings of the National Academy of Sciences of the United States of America **97:** 14133-14138.

Kroger, N., R. Deutzmann, and M. Sumper. 1999. Polycationic peptides from diatom biosilica that direct silica nanosphere formation. Science **286:** 1129-1132.

Leblanc, K., and D. A. Hutchins. 2005. New applications of a biogenic silica deposition fluorophore in the study of oceanic diatoms. Limnology and Oceanography:Methods **3:** 462-476.

Marchetti, A., and P. J. Harrison. 2007. Coupled changes in the cell morphology and the elemental (C, N, and Si) composition of the pennate diatom *Pseudo-nitzschia* due to iron deficiency. Limnology and Oceanography **52:** 2270-2284.

Marchetti, A., M. S. Parker, L. P. Moccia, E. O. Lin, A. L. Arrieta, F. Ribalet, M. E. P. Murphy, M. T. Maldonado, and E. V. Armbrust. 2009. Ferritin is used for iron storage in bloom-forming marine pennate diatoms. Nature **457:** 467-470.

Marchetti, A., D. M. Schruth, C. A. Durkin, M. S. Parker, R. B. Kodner, C. T. Berthiaume, R. Morales, A. E. Allen, and E. V. Armbrust. 2012. Comparative metatranscriptomics identifies molecular bases for the physiological responses of phytoplankton to varying iron availability. Proceedings of the National Academy of Sciences **109:** E317-E325.

Marchetti, A., N. D. Sherry, H. Kiyosawa, A. Tsuda, and P. J. Harrison. 2006. Phytoplankton processes during a mesoscale iron enrichment in the NE subarctic Pacific: Part I - Biomass and assemblage. Deep-Sea Research II **53:** 2095-2113.

Marchetti, A., D. E. Varela, V. P. Lance, Z. Johnson, M. Palmucci, M. Giordano, and E. V. Armbrust. 2010. Iron and silicic acid effects on phytoplankton productivity, diversity, and chemical composition in the central equatorial Pacific Ocean. Limnology and Oceanography **55:** 11-29.

Martin, J. H. 1990. Glacial-interglacial CO_2 change: The iron hypothesis. Paleoceanography **5:** 1-13.

Matsen, F. A., R. B. Kodner, and E. V. Armbrust. 2010. pplacer: linear time maximum-likelihood and Bayesian phylogenetic placement of sequences onto a fixed reference tree. BMC Bioinformatics **11:** 538, doi:510.1186/1471-2105-1111-1538

Matsumoto, K., J. L. Sarmiento, and M. A. Brzezinski. 2002. Silicic acid leakage from the Southern Ocean: A possible explanation for glacial atmospheric pCO(2). Global Biogeochemical Cycles **16:** 1031, doi: 1010.1029/2001gb001442

Minguet, E. G., F. Vera-Sirera, A. Marina, J. Carbonell, and M. A. Blazquez. 2008. Evolutionary diversification in polyamine biosynthesis. Molecular Biology and Evolution **25:** 2119-2128.

Mock, T., M. P. Samanta, V. Iverson, C. Berthiaume, M. Robison, K. Holtermann, C. Durkin, S. S. Bondurant, K. Richmond, M. Rodesch, T. Kallas, E. L. Huttlin, F. Cerrina, M. R. Sussmann, and E. V. Armbrust. 2008. Whole-genome expression profiling of the marine diatom *Thalassiosira pseudonana* identifies genes involved in silicon bioprocesses. Proceedings of the National Academy of Sciences of the United States of America **105:** 1579-1584.

Moore, J. K., S. C. Doney, D. M. Glover, and I. Y. Fung. 2002. Iron cycling and nutrient-limitation patterns in surface waters of the World Ocean. Deep-Sea Research Part II **49:** 463-507.

Nelson, D. M., P. Treguer, M. A. Brzezinski, A. Leynaert, and B. Queguiner. 1995. Production and dissolution of biogenic silica in the ocean- Revised global estimates, comparison with regional data and relationship to biogenic sedimentation. Global Biogeochemical Cycles **9:** 359-372.

Robinson, M. D., and A. Oshlack. 2010. A scaling normalization method for differential expression analysis of RNA-seq data. Genome Biology **11:** R25, doi: 10.1186/Gb-2010-1111-1183-R1125

Rozen, S., and H. Skaletsky. 2000. Primer3 on the WWW for general users and for biologist programmers. Methods Mol Biol **132:** 365-386.

Sapriel, G., M. Quinet, M. Heijde, L. Jourdren, V. Tanty, G. Z. Luo, S. Le Crom, and P. J. Lopez. 2009. Genome-wide transcriptome analyses of silicon metabolism in *Phaeodactylum tricornutum* reveal the multilevel regulation of silicic acid transporters. Plos One **4:** e7458, doi: 7410.1371/Journal.Pone.0007458

Scheffel, A., N. Poulsen, S. Shian, and N. Kroeger. 2011. Nanopatterned protein microrings from a diatom that direct silica morphogenesis. Proceedings of the National Academy of Sciences **108:** 3175-3180.

Stamatakis, A., T. Ludwig, and H. Meier. 2005. RAxML-III: a fast program for maximum likelihood-based inference of large phylogenetic trees. Bioinformatics **21:** 456-463.

Takeda, S. 1998. Influence of iron availability on nutrient consumption ratio of diatoms in oceanic waters. Nature **393:** 774-777.

Thamatrakoln, K., A. J. Alverson, and M. Hildebrand. 2006. Comparative sequence analysis of diatom silicon transporters: Toward a mechanistic model of silicon transport. Journal of Phycology **42:** 822-834.

Thamatrakoln, K., and M. Hildebrand. 2007. Analysis of *Thalassiosira pseudonana* silicon transporters indicates distinct regulatory levels and transport activity through the cell cycle. Eukaryotic Cell **6:** 271-279.

Twining, B. S., S. B. Baines, and N. S. Fisher. 2004. Element stoichiometries of individual plankton cells collected during the Southern Ocean Iron Experiment (SOFeX). Limnology and Oceanography **49:** 2115-2128.

Wenzl, S., R. Hett, P. Richthammer, and M. Sumper. 2008. Silacidins: Highly acidic phosphopeptides from diatom shells assist in silica precipitation in vitro. Angewandte Chemie-International Edition **47:** 1729-1732.

Table 2.1 *Pseudo-nitzschia multiseries* gene transcripts measured by RT-qPCR, their protein identity, and the sequence of the PCR primers used.

Gene	Predicted function	Protein identity	PCR Primers
SIT A	silicon transport	338021	F 5'-TCGGTCTTTTGGAGGGTATG-3' R 5'-GCAATGACGAAGAAGCACAA-3'
SIT B	silicon transport	338018	F 5'-CAATCTTTTTCTGGGGACGA-3' R 5'- GCGATCTGCATACCTTCCAT-3'
APT A	polyamine synthesis	338026	F 5'-CCATTGTTGGAGGAGGAGAA-3' R 5'-ACTCCAGAAGGGCAAAACCT-3'
APT B	polyamine synthesis	338056	F 5'-GTCCTCAAGCACAAGGGAGT-3' R 5'-GGTCGTCAGTGCAGTCGTT-3'
unknown function	unknown	262167	F 5'-GCTTCCAGACCAAGAAGTGC-3' R 5'-CCACTCGGTGCTCAGTAGGT-3'
Actin	cytoskeleton, cell motility	22272	F 5' -TGACTGAGCGTGGTTACTC- 3' R 5' -ACCATCAGGCAATTCAAAGGAC-3'

Table 2.2 Presence (+) or absence (-) of genes related to frustule formation in four diatom genomes.

Gene	Silicic acid Transporter				Aminopropyltransferase						Unknown function	Chitin synthase			
Clade	a	b	c	d	a	b	c	d	e	other		a	b	c	d
Thalassiosira pseudonana	-	-	-	+	-	-	-	+	+	+	+	+	+	+	-
Phaeodactylum tricornutum	-	+	+	-	-	-	-	-	-	+	+	-	-	-	+
Fragilariopsis cylindrus	+	+	+	-	+	+	+	-	-	+	+	-	-	-	+
Pseudo-nitzschia multiseries	+	+	-	-	+	+	-	-	-	+	+	-	-	-	-

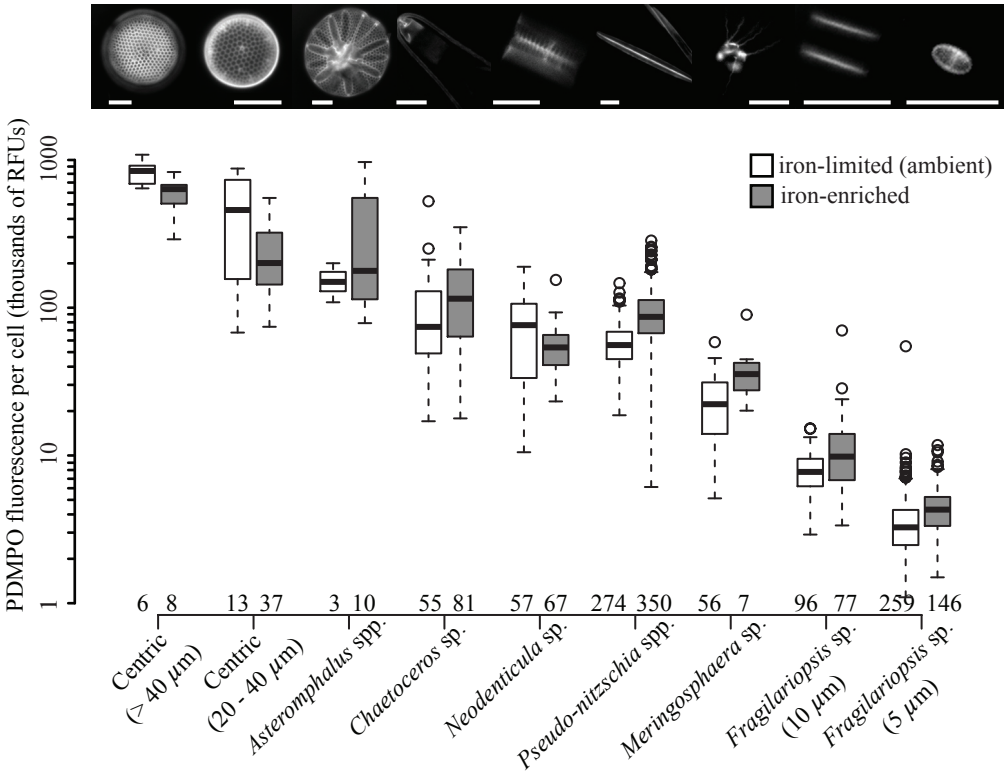

Figure 2.1 Boxplot of integrated fluorescence of individual cells at Sta. Papa incubated with PDMPO for 24 hours and quantified with epifluorescent microscopy. Note that the y-axis is a log scale. Example micrographs along the top include a 10 micron scale bar. Numbers above the x-axis indicate the number of cells quantified in each condition.

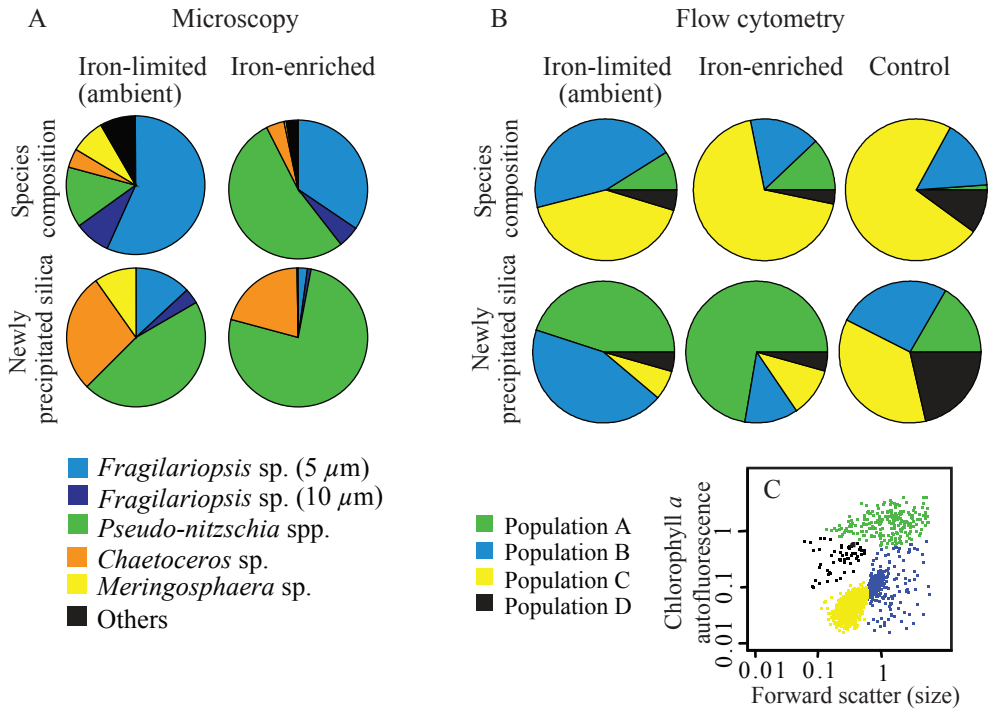

Figure 2.2 Relative contribution of different silicifying phytoplankton at Sta. Papa to total new silica precipitated determined by (A) microscopy and (B) flow cytometry of communities incubated in the presence of PDMPO for 24 hours. (A) Abundance of actively growing cells in the iron-limited (top left pie) and the iron fertilized (top right pie) communities was multiplied by the mean of the integrated fluorescence of individual cell types (see Fig. 1) to determine the contribution of each cell type to the total new silica precipitated by the community (bottom pies). (B) The sum of PDMPO fluorescence of individual particles determined the contribution of each population to total new silica precipitation. An unamended control incubation was also analyzed by flow cytometry. (C) An example cytogram indicates how the four flow cytometry populations were defined.

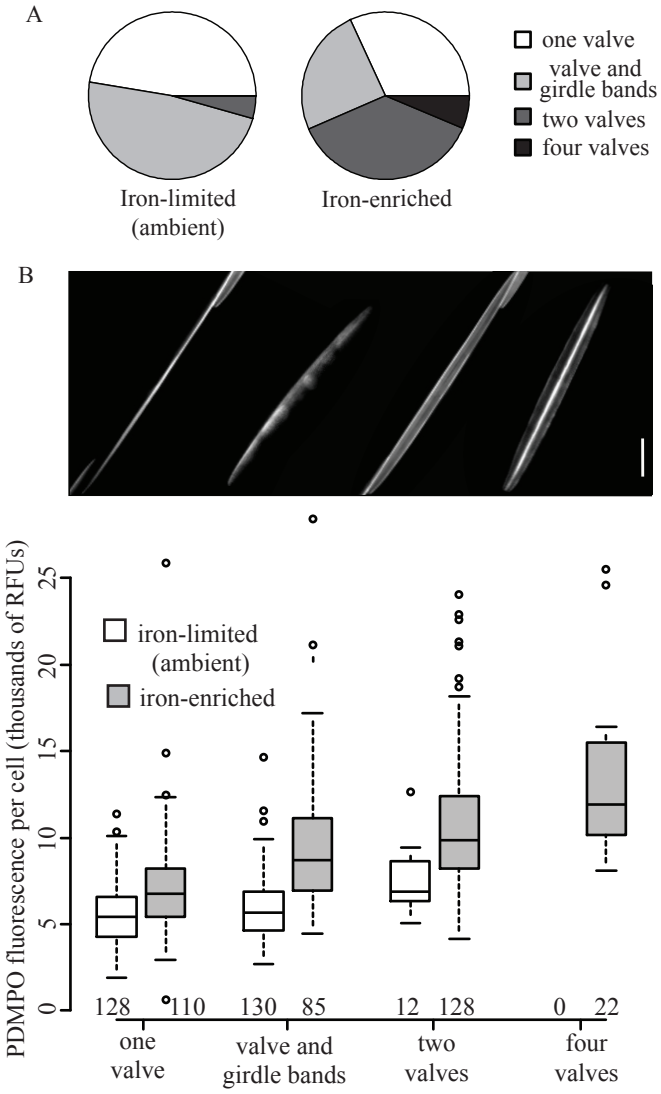

Figure 2.3 (A) Proportion of *Pseudo-nitzschia* cells with various parts of their frustule labeled with PDMPO before and after iron enrichment. Cells identified with four fluorescing valves were in the midst of dividing but had not separated. (B) Boxplot of integrated fluorescence of individual *Pseudo-nitzschia* cells with various parts of their frustule labeled with PDMPO before and after iron-enrichment. Example micrographs are along the top and the scale bar indicates 10 microns. Numbers above the x-axis indicate the number of cells quantified in each condition.

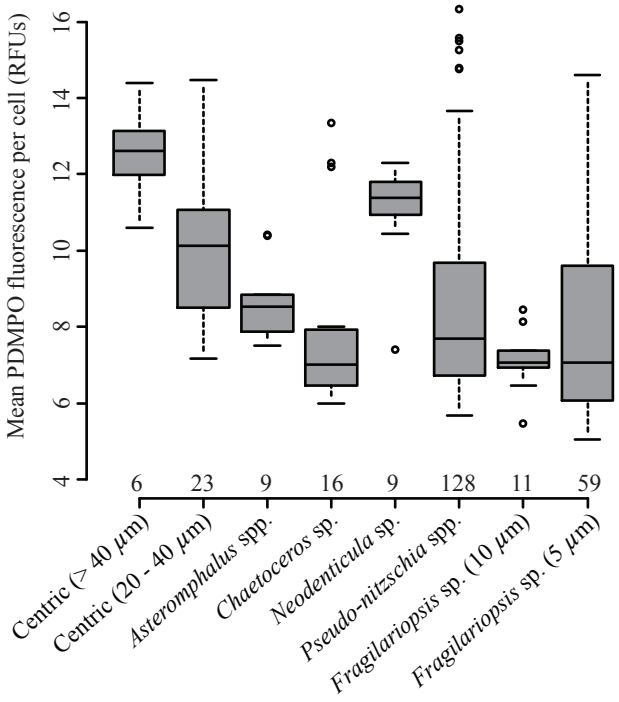

Figure 2.4 Boxplot of the mean fluorescent intensity of fully labeled diatom cells after iron enrichment. Mean fluorescence is a proxy for relative silicification per unit surface area because it is the sum of total cell fluorescence normalized to the two dimensional surface area measured. Numbers above the x-axis indicate the number of cells quantified. Significant differences in the distributions exist among the diatom genera.

Figure 2.5 Maximum likelihood phylogenetic trees of translated (A) silicic acid transporter genes (B) aminopropyltransferase genes, and (C) a gene with unknown function. Colored circles on the trees represent transcript fragments from three metatranscriptomes whose placement on the tree were determined by pplacer (Matsen et al. 2010). Trees include all known sequences from diatom genomes and any other known sequences most closely related to the predicted products of environmental transcripts. Larger circles outlined in black represent metatranscriptome sequences with significant transcriptional support from SOLiD sequencing. These circles correspond to pie charts to the right of the tree showing the shift in relative abundance of transcripts at Sta. Papa in the ambient iron-limited (amb) vs. the iron-enriched incubation (left pie chart) and in the control (cont) vs. the iron-enriched incubation (right pie chart). Grey bars indentify the upper-most and lower-most transcripts that correspond with pie charts in each clade. *Pseudo-nitzschia* genes selected for RT-qPCR are highlighted in bold. Genes from diatom species with available genome sequences are followed by the protein identity number, and include species *Fragilariopsis cylindrus*, *Phaeodactylum tricornutum*, *Thalassiosira pseudonana*, and *Pseudo-nitzschia multiseries*. EST sequences from Pseudo-nitzschia granii isolated from this experiment are also included. (A) includes diatom sequences from the NCBI database *Chaetoceros muellerii* (ABA54411), *Paralia sulcata* (ABB81822), *Nitzschia* sp.(ABB81821), *Navicula pelliculosa* (ABB81811), *Porosira glacialis* (ABF50389), and *Porosira pseudodenticulata* (ABF50390). (B) includes sequences from the NCBI database representing additional lineages (NP_731384, XP_960907, XP_460017, NM_102230, BT000742, ABB13960, CAF31140, NP_376216, YP_004447, NP_568376, and AJ009865). Bootstrap values are indicated on branches and the scale bar indicates amino acid changes per site.

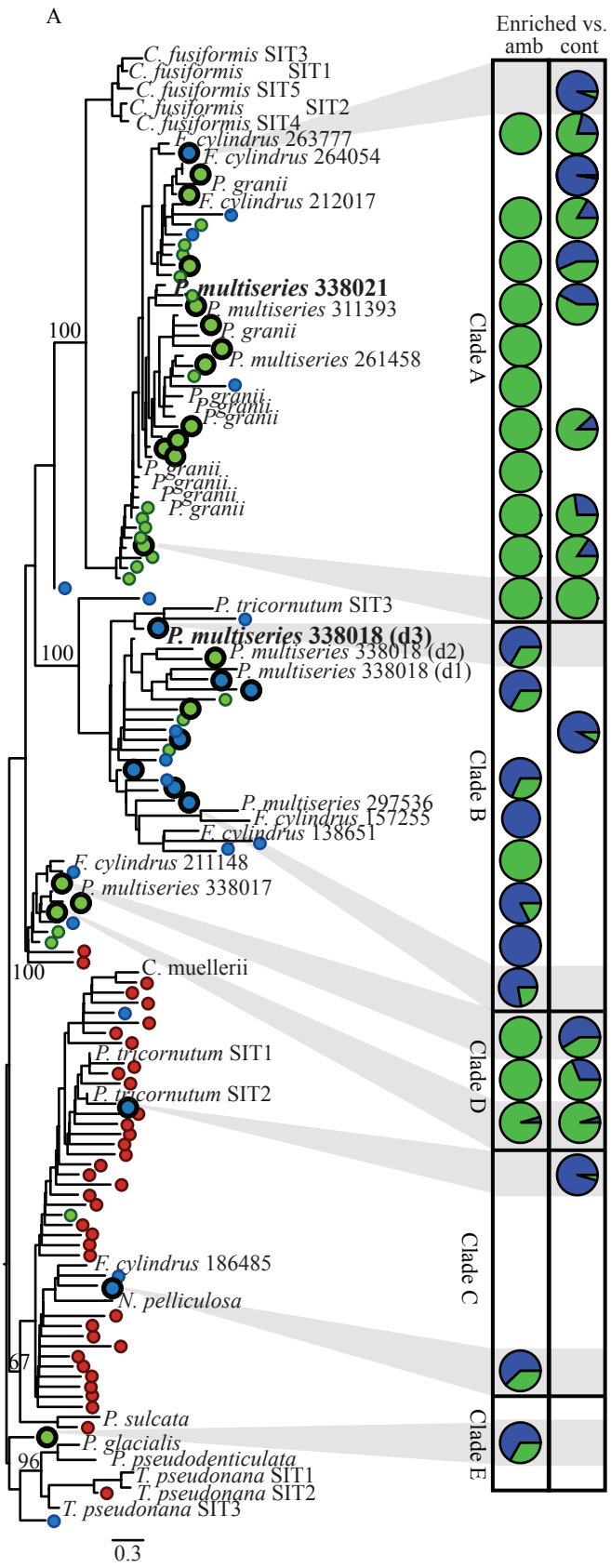
A
Enriched vs.
amb cont
C. fusiformis SIT3
C. fusiformis SIT1
C. fusiformis SIT5
C. fusiformis SIT2
C. fusiformis SIT4
F. cylindrus 263777
F. cylindrus 264054
P. granii
F. cylindrus 212017
P. multiseries 338021
P. multiseries 311393
P. granii
P. multiseries 261458
P. granii
P. granii
P. granii
P. granii
P. granii
P. granii
P. granii
P. tricornutum SIT3
P. multiseries 338018 (d3)
P. multiseries 338018 (d2)
P. multiseries 338018 (d1)
P. multiseries 297536
F. cylindrus 157255
F. cylindrus 138651
F. cylindrus 211148
P. multiseries 338017
C. muellerii
P. tricornutum SIT1
P. tricornutum SIT2
F. cylindrus 186485
N. pelliculosa
P. sulcata
P. glacialis
P. pseudodenticulata
T. pseudonana SIT1
T. pseudonana SIT2
T. pseudonana SIT3
100
100
100
67
96
0.3
Clade A
Clade B
Clade C
Clade D
Clade E

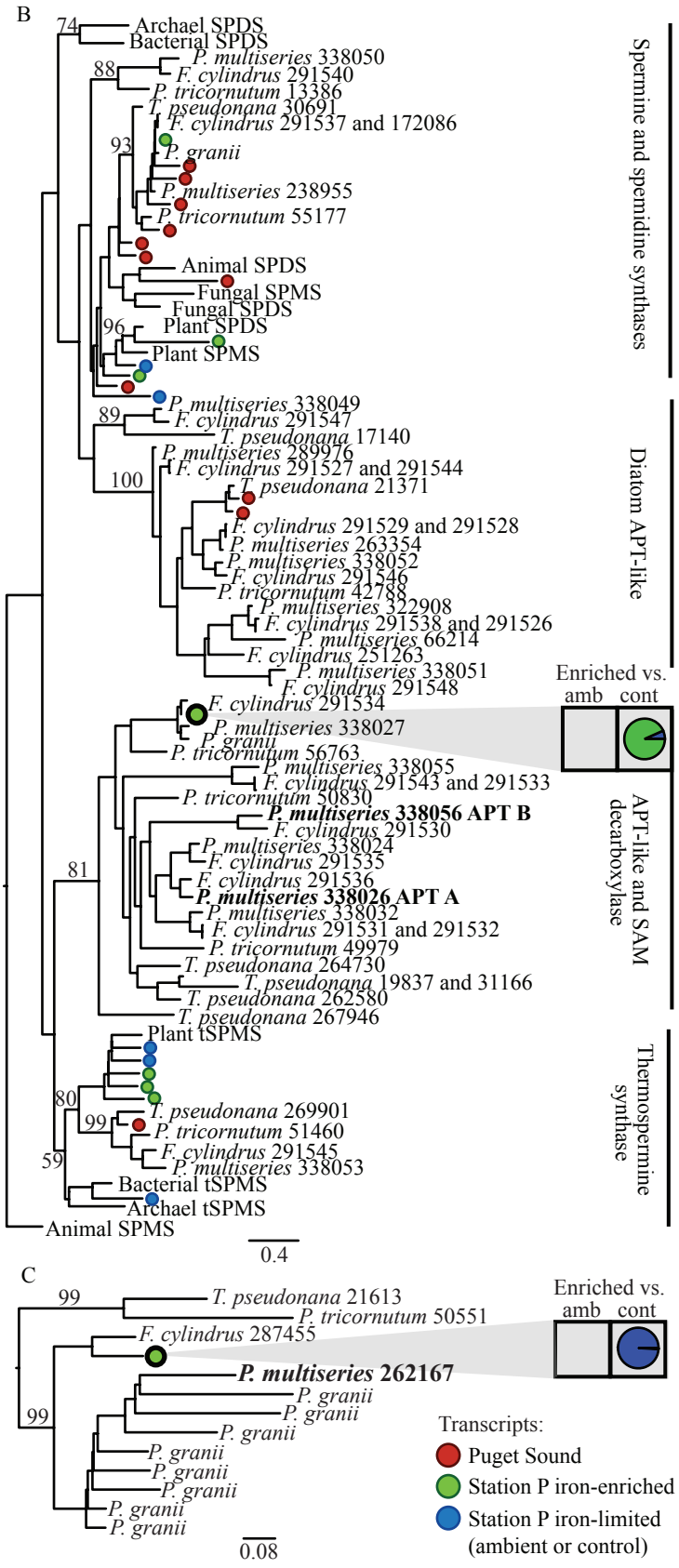
B
74
Archael SPDS
Bacterial SPDS
88
P. multiseries 338050
F. cylindrus 291540
P. tricornutum 13386
T. pseudonana 30691
F. cylindrus 291537 and 172086
93
P. granii
P. multiseries 238955
P. tricornutum 55177
Animal SPDS
Fungal SPMS
Fungal SPDS
96
Plant SPDS
Plant SPMS
P. multiseries 338049
89
F. cylindrus 291547
T. pseudonana 17140
P. multiseries 289976
F. cylindrus 291527 and 291544
100
T. pseudonana 21371
F. cylindrus 291529 and 291528
P. multiseries 263354
P. multiseries 338052
F. cylindrus 291546
P. tricornutum 42788
P. multiseries 322908
F. cylindrus 291538 and 291526
P. multiseries 66214
F. cylindrus 251263
P. multiseries 338051
F. cylindrus 291548
F. cylindrus 291534
P. multiseries 338027
P. granii
P. tricornutum 56763
P. multiseries 338055
F. cylindrus 291543 and 291533
P. tricornutum 50830
P. multiseries 338056 APT B
F. cylindrus 291530
81
P. multiseries 338024
F. cylindrus 291535
F. cylindrus 291536
P. multiseries 338026 APT A
P. multiseries 338032
F. cylindrus 291531 and 291532
P. tricornutum 49979
T. pseudonana 264730
T. pseudonana 19837 and 31166
T. pseudonana 262580
T. pseudonana 267946
Plant tSPMS
80
99
T. pseudonana 269901
P. tricornutum 51460
F. cylindrus 291545
59
P. multiseries 338053
Bacterial tSPMS
Archael tSPMS
Animal SPMS
0.4
Spermine and spemidine synthases
Diatom APT-like
APT-like and SAM decarboxylase
Thermospermine synthase
Enriched vs.
amb cont
C
99
T. pseudonana 21613
P. tricornutum 50551
F. cylindrus 287455
P. multiseries 262167
P. granii
P. granii
99
P. granii
P. granii
P. granii
P. granii
P. granii
P. granii
0.08
Enriched vs.
amb cont
Transcripts:
Puget Sound
Station P iron-enriched
Station P iron-limited
(ambient or control)

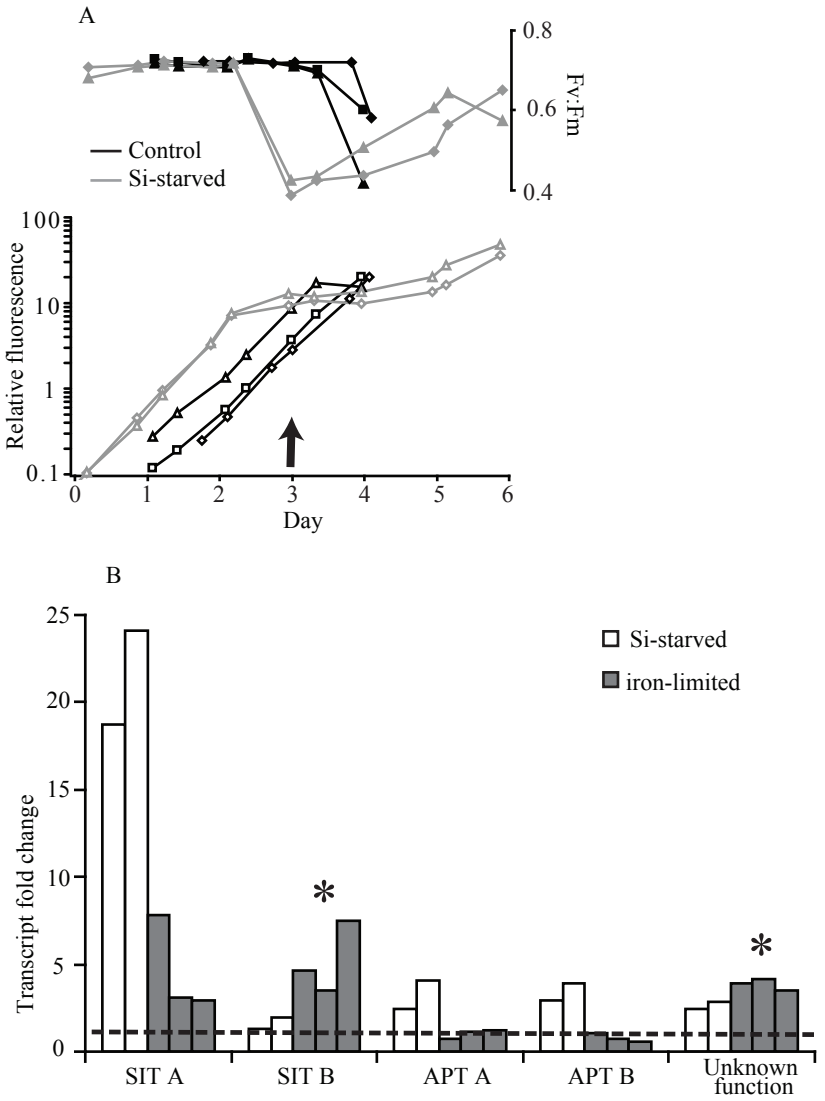

Figure 2.6 Response of *Pseudo-nitzschia multiseries* to silicic acid starvation and iron limitation. (A) Change in relative chlorophyll *a* fluorescence (open symbols) and Fv:Fm (filled symbols) of *P. multiseries* cultures grown in nutrient replete (black lines) or low silicic acid (grey lines) media. Arrow at day 3 indicates when half the culture volume was filtered and silicic acid was replenished to the remaining silicic acid-depleted cultures. (B) Transcript fold-change of genes transcribed by *P. multiseries* cultures experiencing silicic acid starvation (white) or iron limitation (grey). All genes are normalized to actin transcripts and transcript fold-change is relative to transcription under nutrient replete conditions. The dashed line denotes a ratio of 1 which indicates no differential transcript abundances between nutrient-replete and nutrient-limited or starved conditions. Asterisks indicate a significant increase of average transcript abundance in the triplicate iron-limited cultures relative to nutrient-replete conditions. Significance could not be assessed for duplicate silicic acid starved cultures. None of these genes had a significant change of transcript copy number due to nitrate starvation (data not shown).

Chapter 3

Silicic acid supplied to coastal diatom communities influences cellular silicification and the potential export of carbon

3.1 Abstract

Microcosm experiments were conducted along the Washington and Oregon coast in May 2009, May 2010, and July 2010 to determine whether variation in the supply of silicic acid from the Columbia River could influence the silicification and sinking potential of coastal diatom blooms. The microcosm communities incubated with added nitrate or nitrate and silicic acid similarly increased in abundance indicating that growth of the communities was limited by the availability of nitrate. The communities that grew in the presence of more silicic acid were more silicified. No differences were detected in the community compositions of the more- or less-silicified blooms. Isolates of *Minutocellus*, *Cylindrotheca*, *Thalassiosira*, and *Odontella* were obtained from the microcosm experiment in May 2010 and maintained in the laboratory in 20 μmol L^{-1} silicic acid. All three diatoms contained ~2.5 times more silica per cell when the silicic acid concentration in the seawater media was increased to 80 μmol L^{-1} silicic. The increase in silicification is likely caused by diffusion into the cell, a hypothesis with support because no change was observed in RT-qPCR measurements of the transcript abundance of the silicon transporter genes under both growth conditions. The intensity of a fluorescent cellular stain (PDMPO) that incorporates into newly precipitated silica was strongly correlated to the silica content among species, but was not capable of detecting the physiological changes in silicification within a species. The sinking rate increased by about 2 fold for cells that contained about 2.5 times as much silica. These data suggest that variation in silicic acid supply will alter the silicification of coastal diatom blooms and the potential sink of carbon from coastal zones.

3.2 Introduction

Diatoms are responsible for an estimated 75% of the primary production that occurs in coastal regions (Nelson et al. 1995). Their requirement for silicon to form their cell walls (frustules) dominates the silicon cycle and links this cycle with the marine carbon cycle. Silicon enters the marine system at the continental margins, where an estimated 5 Tmol of Si drain from

rivers into the coastal oceans every year and is eventually transformed into the silica frustules of blooming diatoms (Treguer et al. 1995). The heavy silica frustules act as a ballast that helps to sink the carbon fixed by diatoms into deeper waters where it is separated from the atmosphere (Buesseler 1998). This tendency to sink is a pathway for long-term net carbon removal from the atmosphere, a factor influencing global climate. Changes in the supply and utilization of silicic acid in coastal regions could influence the carbon cycle of these regions, and perhaps their relative contribution in global carbon budgets. Characterizing the response of diatoms to variations in silicic acid concentration will help to constrain how biological variability influences the coastal carbon cycle.

Diatoms transport silicic acid into their cells with silicic acid transporter (SIT) proteins that are embedded in the outer membrane of the cell and are typically uptake limited below about 1-14 μmol L^{-1} silicic acid, depending on the diatom species (Martin-Jezequel et al. 2000). When the availability of silicic acid is at uptake limiting concentrations, diatoms can maintain their growth rates by reducing their cellular silica content, enabling additional cell divisions with a less silicified frustule before nutrients are depleted entirely (Paasche 1973; Harrison et al. 1977). The utilization of silicic acid can be explained in most cases by Michaelis-Menten uptake kinetics, which determine the efficiency of silicic acid uptake at low concentrations and determine the rate of maximum uptake when silicic acid concentrations saturate transporters. Deviations from Michaelis-Menten kinetics, where uptake rates continue to increase linearly with increasing supply of silicic acid, have been observed in natural communities (Brzezinski and Nelson 1996; Leblanc et al. 2005), and in laboratory isolates (Thamatrakoln and Hildebrand 2008; Finkel et al. 2010). Under some conditions, diatoms increase silicification when silicic acid concentrations are orders of magnitude above typical uptake-limiting concentrations (Finkel et al. 2010). The physiological condition of the cells appears to determine whether maximum uptake is observed and at what concentration maximum uptake is reached (Harrison et al. 1976; Thamatrakoln and Hildebrand 2008). In this way, the supply of silicic acid can change the silicification of individual cells, and thus their potential to export of carbon, either because uptake limitation reduces cellular silicification or because non-saturable uptake increases cellular silicification. It is hypothesized that these two modes of silicic acid uptake are controlled by a switch between SIT mediated uptake and internally controlled diffusion (Thamatrakoln and

Hildebrand 2008). These two mechanisms of uptake could have large biogeochemical consequences in coastal oceans, where silicic acid concentrations can be highly variable.

Diatom blooms in the coastal waters of Washington and Oregon experience fluctuating concentrations of silicic acid supplied by upwelling deep water and out-flowing freshwater from the Columbia River. The growth of phytoplankton in this region is fueled by the upwelling of nitrate-rich deep water (Kudela and Peterson 2009). Compared to upwelling, the Columbia River supplies a relatively small amount of nitrate to coastal communities (Bruland et al. 2008; Hickey and Banas 2008) but is a major source of silicic acid, with concentrations ranging from 140 to 240 μmol L^{-1}. Although nitrate availability controls primary production in this region, silicic acid is predicted to be secondarily limiting (Kudela and Peterson 2009) and the river water potentially creates highly variable concentrations of silicic acid available to phytoplankton blooms. These conditions could produce diatom communities with highly variable silicification, but to date these physiological changes have not been investigated. If silicification, and thus the sinking potential, of coastal communities changes with silicic acid supply, the river may have a large influence on the fate of coastal primary production and determine whether this region is a net source or sink of carbon dioxide to the atmosphere, a status that is under debate (Borges et al. 2005; Hales et al. 2005; Ianson et al. 2009).

This study tests the hypothesis that high concentrations of silicic acid, like those supplied by the Columbia River, will increase the relative silicification of coastal phytoplankton communities and lead to a more efficient export of organic matter to deeper waters. A change in the silica content of phytoplankton in waters with high productivity and nutrients may be possible due to the flexibility in silicification observed in the presence of both very low and very high silicic acid concentrations (Paasche 1973; Finkel et al. 2010). Alternatively, variations in silicic acid concentration could favor different diatom species assemblages, affecting the silicification of the community as a whole, without altering the silica content of individuals. This study uses the transcription of silicon transporters to indicate the mechanism of silicic acid uptake and a fluorescent cellular stain to indicate changing silicification in coastal communities. Measured changes in diatom sinking rates directly connect these physiological changes to their biogeochemical consequences.

3.3 Methods

Locations of microcosm seawater collection

Four separate microcosm incubation experiments were conducted on three research cruises; two incubation experiments were conducted aboard the R/V New Horizon between 12-26 May 2009, one incubation experiment was conducted aboard the R/V Wecoma between 21-27 May 2010, and another aboard the R/V Wecoma between 29 July – 3 August 2010. Seawater was collected in 10 L niskin bottles attached to a CTD rosette off shore of the Columbia River (CR) mouth (46.497° N 124.464° W) on 15 May 2009 from a depth of 7 m. On 18 May 2009 water was similarly collected from station LP-17 along the La Push line (47.917° N 125.083° W) from a depth of 2 m. On 22 May 2010 and 30 July 2010 water was collected from station NH-20 along the Newport Hydroline (44.65° N 124.53° W) from a depth of 5 m (Fig. 3.1).

Microcosm incubation experiments

Ten liter cubitainers were filled with seawater collected in separate Niskin bottles from a single cast. For both the LP-17 and CR incubation experiments, triplicate cubitainers were amended with nitrate and/or silicic acid to produce added concentrations of 40 μmol L^{-1} Na_2SiOH_3, 20 μmol L^{-1} $NaNO_3$, or both 40 μmol L^{-1} Na_2SiOH_3 and 20 μmol L^{-1} $NaNO_3$. Three cubitainers were left as unamended controls, for a total of four different incubation treatments (control, +Si, +Nitrate, +2:1 Si:N). In the incubation experiments conducted at NH-20 in May 2010 and at NH-20 in July 2010, triplicate cubitainers were amended with either 20 μmol L^{-1} Na_2SiOH_3, 20 μmol L^{-1} $NaNO_3$, 20 μmol L^{-1} Na_2SiOH_3 and 20 μmol L^{-1} $NaNO_3$, or 80 μmol L^{-1} Na_2SiOH_3 and 20 μmol L^{-1} $NaNO_3$ for a total of five different treatments including unamended controls (control, +Si, +nitrate, +1:1 Si:N, +4:1 Si:N) (Table 3.1). A separate set of triplicate cubitainers were collected to determine the initial water conditions and were immediately processed for chemical and biological measurements (*see* incubation-related Methods below). The remaining cubitainers were incubated in deck-top incubators with continuously circulating seawater and covered with neutral density screening to reduce irradiance to 30% of ambient light. Seawater was incubated on-deck for 2.5 days in both the LP-17 and CR incubation experiments and for 3 days in the two NH-20 incubation experiments in May and July 2010 incubations.

BSi, chlorophyll *a*, and nutrient measurements of microcosm incubation experiments

The cells contained in 350-500 mL of seawater from each incubation treatment were collected onto a 5 μm polycarbonate filter (Millipore) and stored at 4 ºC until analysis on-shore. Filters were dried in a 55 ºC oven, biogenic silica was dissolved in 0.2 N NaOH at 95 ºC for 1 hour and concentrations were quantified by the ammonium molybdate method described by Brzezinski and Nelson (1986).

To quantify chlorophyll *a* concentrations in deck-board incubations, cells contained in 350-500 mL of seawater were collected onto 5 μm polycarbonate filters and stored at 4 ºC in 90% acetone for 24 h. The fluorescence of the extracted chlorophyll *a* was measured ship-board with a Trilogy fluorometer (Turner) previously calibrated with a chlorophyll *a* standard (Turner Designs Liquid Primary Chlorophyll A Standard). Differences in chlorophyll *a* and BSi concentrations among incubation treatments were determined using an analysis of variance (ANOVA) and a post-hoc Tukey's test.

About 50 mL of seawater was filtered through a 0.2 μm syringe filter to determine the concentration of dissolved nutrients remaining after incubation, or in the initial ambient seawater, and was measured with a Technicon autoanalyzer II system by the University of Washington marine chemistry laboratory.

Community composition in microcosm incubation experiments

To identify the actively growing diatoms in the natural phytoplankton community at the end of each incubation experiment, 125 mL of seawater was incubated with 0.125 μmol L^{-1} 2-(4-pyridyl)-5{[4-dimethylaminoethyl-aminocarbamoyl)-methoxy]phenyl}oxazole (PDMPO), a fluorescent label of newly precipitated silica, in deck-top incubators for 24 h. After 24 h, 1.8 mL was preserved in 0.2 mL of fixative (10% formaldehyde, 0.5% glutaraldehyde, 40% phosphate buffered saline solution) (Andersen 2005), flash frozen in liquid nitrogen, and stored at -80 ºC until later enumeration and quantification by flow cytometry. The cells in the remaining volume of incubated seawater were collected onto a 0.2 μm black polycarbonate filter and preserved in immersion oil on a microscope slide beneath a cover slip. The edges of the cover slip were sealed with nail polish and slides were stored at 4 ºC.

PDMPO labeled cells from the incubations were quantified on an Influx flow cytometer (BD). PDMPO fluorescence was detected at 460 nm (50 nm bandpass) after excitation with a

355 nm UV laser. Chlorophyll *a* was detected at 692 nm (40 nm bandpass) after excitation with a 488 nm Coherent laser. The volume analyzed was determined by a flow meter (Sensirion) attached to the sample line. Populations of actively silicifying phytoplankton were identified using tools in the FlowCore and Splancs libraries in R. Silicifying populations were identified and quantified first by their PDMPO fluorescence and further by their chlorophyll *a* and forward scatter characteristics. A preserved seawater sample without PDMPO labeling was similarly analyzed to identify background fluorescence in the PDMPO bandwidth.

Diatom genera labeled with PDMPO during the incubation experiment at NH-20 in May 2010 were identified and enumerated by epifluorescence microscopy using a Nikon Eclipe 80i microscope equipped with a Nikon Digital Sight-Qi1monochrome camera using Nikon Imaging Software (NIS) Elements. Micrographs were taken from between 68 and 121 fields distributed across the preserved filter. Cells were identified to the level of genus or morphological groups and concentrations were determined by the total area of the filter analyzed vs. the total volume of seawater filtered.

Community composition data from both microscopy and flow cytometry were separately analyzed in Plymouth Routines In Multivariate Ecological Research (PRIMER) software to determine the significance of changes in composition among incubations treatments. Genera with low abundance (<10 cells counted) in most treatments were grouped into a single category. Samples with similar community compositions were identified based on Bray-Curtis similarity matrix and using the Simprof clustering algorithm with group-averaged linking of clusters. An analysis of similarity (ANOSIM) was used to identify whether the community composition among replicates of a treatment were more similar to one another than to bottles of another treatment. Similarities in community composition among each incubation bottle were visualized using a multi-dimensional scaling analysis.

Culturing conditions of diatom isolates

Seawater samples were brought back to shore and diatoms were isolated from the community that bloomed after incubations at NH-20 in May 2010. Cells were identified using an Eclipse TS100 inverted microscope (Nikon), isolated with a micropipette, and transferred into natural seawater from Puget Sound amended with f/2 nutrient concentrations (Guillard and Ryther 1962). Diatom cultures included *Odontella sp.*, *Minutocellus sp.*, *Cylindrotheca sp.*, and

Thalassiosira sp. and were maintained at 13 ºC on a 12hr light:12 hr dark cycle. The resulting unialgal isolates were maintained in polycarbonate plastic tubes (Millipore) in 30 mL of ESAW artificial seawater (Berges et al. 2001) amended with f/2 concentrations of vitamins and trace metals, 36 μmol L^{-1} NaH_2PO_4, 20 μmol L^{-1} $NaNO_3$, and either 20 μmol L^{-1} or 80 μmol L^{-1} Na_2SiOH_4. All nutrient stock solutions were prepared in polycarbonate plastic bottles to avoid silicic acid contamination. Growth was monitored by the increase of chlorophyll *a* autofluorescence with an AU flourometer (Turner) and cultures were transferred to new media by the middle of the exponential growth phase. Cultures were considered acclimated to the seawater media when the growth rates were not significantly different for three consecutive transfers (Brand et al. 1981).

Acclimated cultures were inoculated into polycarbonate bottles containing 2 L of artificial seawater amended with the same nutrient concentrations that the cells were acclimated to. Growth, as inferred from chlorophyll *a* autofluorescence, was monitored daily during the dark cycle. At the middle of the exponential growth phase and 2 h into the light cycle, media was filtered through a 0.2 μm syringe filter to determine the concentration of dissolved nitrate and silicic acid remaining in the media, as described above. At the same time, the cells in 100 mL of culture were collected on a GFF filter (Whatman) previously combusted at 450 °C for 4.5 h. An additional 100 mL of culture were filtered through a 0.6 μm polycarbonate filter (Millipore) to collect BSi. Triplicate solutions of cell-free seawater media, each amended with nutrients separately, were also filtered through 0.6 μm polycarbonate filters to collect silica that had chemically precipitated in the media containing both 20 and 80 μmol L^{-1} silicic acid. All filters were dried in a 55 ºC oven. The quantity of POC and PON collected on the GFF filters were measured with an elemental analyzer (Elementar) by the UC Davis stable isotope laboratory. BSi and chemically precipitated silica were measured as described above for field samples.

Cell abundance of laboratory cultures

To determine the concentration of cells in cultures acclimated to either 20 μmol L^{-1} or 80 μmol L^{-1} silicic acid, 1.8 μL of culture was preserved in fixative and frozen as described above for field samples. The concentration of *Minutocellus* sp., *Cylindrotheca* sp., and *Thalassiosira* sp. were enumerated by flow cytometry. Cells were identified by their chlorophyll *a*

fluorescence and the volume measured was determined by the flow meter as described above. *Odontella* cells in 1 mL of the preserved culture were counted on a sedwick rafter because these cells were too large to be quantified by flow cytometry.

Fluorescent quantification of silica in laboratory cultures

PDMPO fluorescence was used as a proxy to determine the quantity of silica per cell of isolates cultured in either 20 μmol L^{-1} or 80 μmol L^{-1} silicic acid. A 30 mL aliquot of each diatom culture was incubated with 0.25 μmol L^{-1} PDMPO and incubated for 3-9 days, depending on the species. This incubation length was chosen so that cells would divide multiple times in the presence of PDMPO, and thus the frustules of most of the cells would be fully labeled. After incubation, cells were fixed and frozen as described above. The fluorescent intensity of PDMPO per cell was detected by flow cytometry and analyzed with libraries in R as described above. Differences in the PDMPO fluorescence of cells acclimated to 20 μmol L^{-1} vs. 80 μmol L^{-1} silicic acid were tested using a Kolmogorov-Smirnov test and a Bonferroni correction for multiple comparisons was applied with the p.adjust function in R.

Gene identification and PCR primer design

Silicon transporter (SIT) gene sequences were identified from transcriptomes of the *Odontella* and *Cylindrotheca* isolates (CAMERA). A hidden markov model (HMM) profile was constructed based on an alignment of amino acid sequences from previously identified silicon transporters (Durkin et al. 2012). The software HMMer was used to identify SIT sequences in the *Odontella* and *Cylindrotheca* transcriptomes. Sequences were placed on a phylogenetic tree (Durkin et al. 2012) using pplacer software (Matsen et al. 2010) to identify the phylogenetic clade of each sequence. Actin gene sequences were similarly identified using an alignment of translated actin gene sequences identified in the genomes of *Fragilariopsis cylindrus* (protein ID 222562), *Pseudo-nitzscha multiseries* (protein ID 22272), and *Thalassiosira pseudonana* (protein ID 269504) (http://genome.jgi-psf.org). PCR primers were designed for identified SIT and actin encoding genes using Primer 3 (Rozen and Skaletsky 2000) to amplify a 100-200 bp region.

RNA extraction and quantification of transcript abundance

Cells in 300-400 mL of *Cylindrotheca* and *Odontella* cultures were collected on 0.6 μm polycarbonate filters, immediately frozen in liquid nitrogen, and stored at -80 ºC. Ribonucleic acid (RNA) was extracted from the cells on frozen filters using the Totally RNA extraction kit (Invitrogen). The RNA was incubated with dioxyribonuclease (DNase) I (Ambion) at 37 ºC for 2 h and purified with DNase inactiviation reagent. A 2 μL aliquot of RNA was reserved for quantitative polymerase chair reaction (qPCR) (*see* paragraph below) to ensure that RNA was free of DNA contamination. Two micrograms of total RNA was reverse transcribed into cDNA using Superscript III First Strand Synthesis System for reverse transcription quantitative polymerase chain reaction (RT-qPCR) (Invitrogen). Final aliquots of cDNA were diluted to a volume of 100 μL.

Relative transcript abundance of each gene was determined by RT-qPCR reactions consisting of 2 μL cDNA, 0.8 μmol L^{-1} forward and reverse primer, and 15 μL of iTaq Sybergreen Supermix with ROX (Biorad). Reactions were carried out on a Step One Plus thermocycler (Applied Biosystems) with an initial incubation at 95 ºC for 3 minutes followed by 45 cycles of 95 ºC for 10 s, 60 ºC for 30 s, and 72 ºC for 50 s, followed by a step-wise increase in melting temperature to verify the presence of a single melt peak fluorescence signal. All SIT gene transcripts were amplified at the same time as the actin sequences. Amplification efficiencies were calculated for each reaction using LinReg (Ramakers et al. 2003) and threshold cycle numbers were calculated using Step One software (Applied Biosystems). The amplification efficiencies from all reactions were averaged to determine a single efficiency for each gene. Relative transcript abundance was calculated using the equation $(E_{actin}{}^{CT\ actin})/(E_{target}{}^{CTtarget})$ where E_{actin} is the amplification efficiency of actin, E_{target} is the target gene efficiency, CT_{actin} is the threshold cycle number of actin, and CT_{target} is the threshold cycle number of the target gene (Pfaffl 2001). Differences in relative transcript abundance of SIT genes in cells acclimated to 20 μmol L^{-1} vs. 80 μmol L^{-1} silicic acid were tested using a t test.

Sinking rates of laboratory cultures

The influence of changing cellular silica content on the sinking rate was assessed for *Thalassiosira* sp. and *Odontella* sp., the isolates with largest cell size and silica content. Thirty milliliters of triplicate cultures of *Thalassiosira* sp. and duplicate cultures of *Odontella* sp.

acclimated to either 20 μmol L^{-1} or 80 μmol L^{-1} silicic acid were concentrated into a pellet by centrifugation at 650 x g for 10 minutes. Overlying seawater media was removed and cells were fixed by resuspending in 5 mL of 100% methanol and stored at 4° C until the sinking experiments were conducted. Prior to measurement, cells were pelleted by centrifugation, methanol was removed, and the cells were resuspended in artificial seawater with salinity 26 psu. Each diatom sample was examined by light microscopy to ensure that cells remained intact after preservation. Sinking rates of dead, intact diatoms represent the maximum sinking rate, since living cells use biological mechanisms, such as buoyant vacuoles, to counteract the force of sinking.

Sinking rates were measured in a weakly stratified water column (28-32 psu) 7 cm in diameter and 36 cm tall. Preserved diatoms resuspended in 26 psu seawater were introduced into a layer separated from the top of the water column by a gate valve. The valve was opened for 30 minutes to allow diatoms to sink. A USB camera (Logitech, QuickCam Pro9000) equipped with 60 mm Marco lens (Cannon) with a field of view of 10.05 x 7.5 mm were taken 18 cm below the surface of the water column to ensure that sinking particles had reached terminal velocities. Ten minutes of video were recorded each hour over the course of 12 h. One additional clip of the large *Odontella* cells was recorded after the first 0.5 h. Video clips were analyzed with customized software avidemux2.4 to subtract background, threshold for size and brightness, and extract pixel coordinates. The coordinates were then calibrated and reassembled into individual trajectories with Tracker3D (Chan and Grunbaum 2010). The sinking speed of each particle detected was calculated from the vertical distance between the start and end point of each path divided by the total frames observed multiplied by the frame rate (5 frames per second). Particles with a velocity less than 0.1 m d^{-1} were assumed to be background particles suspended in the media and were eliminated from further statistical analysis. Differences in the distribution of sinking speeds among samples were examined with a Kolmogorov-Smirnov test and a Bonferroni correction for multiple comparisons was applied with the p.adjust function in R.

3.4 Results

Biogenic silica and chlorophyll *a* changes in microcosm experiments

The effect of silicic acid concentration on community silicification was tested in four different microcosm incubation experiments. Two experiments were conducted several days

apart during the same cruise in May 2009 with water from different locations (CR and LP-17). A third incubation experiment was conducted in May 2010 with water from NH-20, and a fourth incubation experiment was conducted with water from this same location in July 2010 (Fig. 3.1) The similar response to nutrient amendments indicates that growth of all four phytoplankton communities was limited by nitrate (Table 3.1, Fig. 3.2), despite differences in initial chlorophyll *a*, BSi, and nutrient characteristics. Silicic acid amendments did not promote further consumption of nitrate in most cases or a greater production of chlorophyll *a* when added in combination with nitrate, but the added silicic acid did cause the four communities to produce higher concentrations of biogenic silica. A further increase in the ratio of added silicic acid to nitrate did not result in a higher production of BSi.

At LP-17, the initial nitrate concentration was relatively high (7.3 μmol L^{-1}), silicic acid concentration was moderate (12.7 μmol L^{-1}), and chlorophyll *a* and biogenic silica concentrations were relatively low (0.7 ± 0.03 μg L^{-1} and 0.4 ± 0.05 μmol L^{-1} respectively) (Table 3.1, Fig. 3.2A). These initial conditions supported growth during the 2.5 day incubation in the unamended control and +Si treatments, after which the seawater was depleted of nitrate (<1 μmol L^{-1}), the concentration of chlorophyll *a* nearly tripled, the concentration of biogenic silica increased nearly 10 fold. When this seawater was incubated with 20 μmol L^{-1} added nitrate (+Nitrate), silicic acid concentrations were drawn down to 1.8 ± 0.96 μmol L^{-1}, the concentration of chlorophyll *a* was four times higher than in the control or +Si treatments and the concentration of biogenic silica was 1.4 times higher. Additions of 40 μmol L^{-1} silicic acid and 20 μmol L^{-1} nitrate (+2:1 Si:N treatment) resulted in similar final chlorophyll *a* concentrations as in +Nitrate treatment, but the concentration of BSi was 1.4 times higher and 2 times higher compared to the control or +Si incubations.

A comparable response was observed in the incubations conducted at CR, although the initial nitrate concentration was much lower (<1 μmol L^{-1}) and did not support increases in chlorophyll *a* concentration in either the control or +Si incubation treatments (Fig. 3.2B). BSi concentrations did increase, however, in both treatments compared to the initial condition. Chlorophyll *a* concentration increased about 7 fold in the +Nitrate treatment relative to the control incubation with the calculated drawdown of nitrate significantly higher than in the control treatment. The concentration of BSi in the +2:1 Si:N treatment was 1.9 fold higher than the control or +Si treatments and 1.2 fold higher than the +Nitrate treatment. Final silicic acid

concentrations were relatively low in the seawater incubated in the +Nitrate treatment (4.63 ± 1.02) but higher than the same treatment conducted at LP-17 (1.8 ± 0.96 μmol L^{-1}).

In 2010, an incubation treatment with higher silicic acid (80 μmol L^{-1}) and the same nitrate amendment (20 μmol L^{-1}) (+4:1 Si:N treatment) was added to the suite of conducted treatments (Table 3.1, Fig. 3.2C, 3.2D). The initial concentration of silicic acid at NH-20 in May was moderately high (9.2 ± 0.56 μmol L^{-1}) and available nitrate was low (1.3 ± 0.04 μmol L^{-1}). These initial conditions did not support an increase in chlorophyll *a* or BSi concentrations in either the control or +Si treatments (Fig. 3.2C). However, the calculated drawdown of silicic acid was significantly higher in the +Si treatment than in the control treatment ($p < 0.05$). The addition of nitrate enabled a 2.5 fold increase in the concentration of chlorophyll *a* compared to the control treatment and an increase nitrate drawdown, but no difference in the concentration of BSi. When either 1:1 or 4:1 silicic acid:nitrate was added, no additional increase in chlorophyll *a* concentration was observed compared to the +Nitrate treatment. Instead, the concentration of BSi nearly doubled in both the +1:1 Si:N and +4:1 Si:N treatments. The +1:1 and +4:1 Si:N treatments were not different from each other, but the final concentrations of silicic acid and nitrate were highly variable in the replicates of the +4:1 Si:N treatment.

The incubation conducted at NH-20 in July 2010 was different from the previous three incubations because the initial phytoplankton community appeared to be at the end of a large bloom: the initial chlorophyll *a* and BSi concentrations were high (15.5 ± 0.5 μg L^{-1} and 8.9 ± 0.27 μmol L^{-1} respectively) (Fig 3.2D), nitrate concentrations were low (0.41 ± 0.11 μmol L^{-1}), and silicic acid concentrations were moderate (9.1 ± 0.66 μmol L^{-1}). The community declined after incubating in the control and +Si treatments, as indicated by the approximately 3 fold decrease in the concentration of chlorophyll *a*. The concentration of BSi increased about 1.5 fold in both these treatments, and the calculated drawdown of silicic acid was significantly higher in the +Si treatment than in the control ($p<0.05$). When nitrate was amended to the seawater, the original biomass of the community was mostly maintained, as indicated by only a 6% reduction in the concentration of chlorophyll *a*, a 1.9 fold increase from the control treatment. The concentration of BSi was not different in the +Nitrate treatment compared to the control and the concentration of silicic acid was low (2.2 ± 0.5 μmol L^{-1}) at the end of the incubation. As was found in the three previous microcosm experiments, the addition of both nitrate and silicic acid increased the concentration of BSi compared to the +Nitrate treatment (1.4

fold in this incubation) despite the lack of an increase in chlorophyll *a* concentration. As observed in May 2010 (Fig. 3.2C), the concentration of BSi in the +4:1 Si:N treatment was not different from the concentration in the +1:1 Si:N treatment.

Community composition of microcosm experiments determined by flow cytometry

Changes in diatom community composition or increases in the silica per cell of individual diatoms could underlie the observed increases in biogenic silica concentrations in the treatments with both nitrate and silicic acid added. To determine the role of community composition in driving these changes, the actively growing component of the diatom community at NH-20 in May was quantified by flow cytometry (Fig 3.3). Cells with detectable PDMPO fluorescence were categorized into four populations according to chlorophyll *a* fluorescence and forward light scatter, a proxy for cell size, and enumerated (Fig. 3.3A).

Population 1 had the highest chlorophyll *a* fluorescence and forward scatter, followed by populations 2, 3, and 4. All populations increased in abundance in the control incubation compared to the initial conditions (Fig 3.3B). Diatom community composition was not significantly different between the control and +Si treatments (ANOSIM, R=0.074). Both treatments were significantly different from the initial sample (R=0.889). The abundance of diatoms increased in the +Nitrate, +1:1 Si:N, and +4:1 Si:N treatments relative to control. The diatom communities in the +Nitrate and +1:1 Si:N treatments were significantly different from the control treatment (R=0.704 and 0.963 respectively). The community composition in the replicates of the +4:1 Si:N treatment was more variable (Fig 3.3B and C) and as a group was not different from the control, +Nitrate, or +1:1 Si:N treatments (R=0.148, 0, and 0.111 respectively) but was significantly different from the +Si treatment (R=0.519). Bray-Curtis similarity analyses indentified one cluster that included +Nitrate, +1:1 Si:N, and +4:1 Si:N replicates, a second cluster that included Control, +Si, and one +Nitrate and +4:1 Si:N replicate, and a third cluster defined by the initial community (Fig. 3.3C). Thus flow cytometric-based measures of community composition of the different samples were not correlated the observed differences in BSi concentrations between the + Nitrate and the 1:1 and 4:1 Si:N treatments (Fig. 3.2).

Community composition of microcosm experiment determined by microscopy

To determine whether the changes in community composition detected by flow cytometry reflect comparable changes at the resolution of species composition, the actively growing component of the diatom community was identified by microscopy from the May NH-20 incubations (Fig. 3.4A). This incubation was chosen for a more detailed enumeration of community composition because isolates were obtained from this community and the response of members of the natural community could be further explored in controlled laboratory experiments. The initial community was composed primarily of the genera *Bacteriostrum* (57±14 cell mL^{-1}), followed by *Guinardia* (55±22 cell mL^{-1}), large (10-100 μm) centrics including *Thalassiosira* (52±8 cell mL^{-1}), *Minutocellus* (46±26 cell mL^{-1}), *Chaetoceros* (25±41 cell mL^{-1}), *Pseudo-nizschia* (2±1 cell mL^{-1}), and *Cylindrotheca* (1±1 cell mL^{-1}) (Fig 3.4B). A category of small (~5 μm) diatoms with both centric and oval morphologies was also abundant (133±44 cell mL^{-1}) and was likely a combination of both a small *Thalassiosira*-like diatom and a small morphotype of *Minutocellus*. Other genera detected with low concentrations in all treatments include *Rhizoselenia*, *Asteromphalus*, *Nitzschia*-like pennates, *Actinoptycus*, *Skeletonema*, *Thalassionema*, *Asterionellopsis*, *Odontella*, and *Coretheron*. The initial concentration of these genera was 28±10 cell mL^{-1} when grouped together.

The abundance of *Bacteriastrum*, *Guinardia*, *Pseudo-nitzschia*, and *Minutocellus* similarly increased (between 5.5 and 6 fold) in the unammended control treatment (Fig 3.4A), with an increase in abundance also observed in the small centric diatoms (2.7 fold) and *Cylindrotheca* (24 fold). The abundance of *Chaetoceros* and the large centric diatoms was variable among replicates and no changes were detected between the initial conditions and the control treatment. The composition of the community in the control incubation bottles was significantly different from the initial community (ANOSIM, R=0.889) (Fig 3.4C). The community composition of the +Si treatment was not different than the control incubation (R=0), whereas the diatom communities that grew in the +Nitrate, +1:1 Si:N, and +4:1 Si:N incubation treatments were significantly different from the control incubation (R=0.63, 0.519, and 0.778 respectively). Relative to the control incubation, the +Nitrate, +1:1 Si:N, and +4:1 Si:N treatments all shared a similar increase in the abundance of *Bacteriastrum* cells (~2 fold), large centric diatoms (~3.6 fold), and *Chaetoceros* cells (4.25-5 fold). Although the +1:1 Si:N treatment produced a community with higher concentrations of biogenic silica than the +Nitrate

treatment (Fig 3.2C), the community compositions were not significantly different from one another (R=0.185). The community that grew in the +4:1 Si:N treatment displayed more variability among triplicate incubations and as a group had a significantly different diatom community than the +Nitrate treatment (R=0.963), but not strongly different than the +1:1 Si:N treatment (R=0.37). All treatments that were amended with nitrate were identified in a single cluster based on the Bray-Curtis similarities of their community compositions (Fig 3.4C), whereas the initial, control, and some +Si treatments were placed in separate clusters. Together, these data indicate that the diatom community composition in the nitrate treatment and the nitrate and silicic acid treatments were not significantly different relative to the control treatment.

Changes in cellular silicification of laboratory cultures

The observed differences in community composition did not explain the changes in community silicification. The influence of silicic acid concentration on the silica content of individual cells was therefore assessed in laboratory experiments with diatoms isolated from the NH-20 incubations in May 2010. The growth rates of cultures acclimated to 20 μmol L^{-1} or 80 μmol L^{-1} silicic acid were the same for *Odontella* (0.21±0.006 d^{-1} vs. 0.26±0.08 d^{-1}), *Minutocellus* (0.72±0.15 d^{-1} vs. 0.66±0.06 d^{-1}), and *Thalassiosira* (0.5±0.07 d^{-1} vs. 0.45±0.08 d^{-1}) cultures. *Cylindrotheca* grew at 0.26±0.04 d^{-1} when acclimated to 20 μmol L^{-1} silicic acid and 0.61±0.24 d^{-1} when acclimated to media containing 80 μmol L^{-1} silicic acid. The *Cylindrotheca* cultures were acclimated 1-3 months apart and the observed changes in growth rate may be an artifact of the length of time in culture. The *Minutocellus* isolate displayed variable sizes and morphologies over time in culture, but all replicate cultures were of a small (~5 μm) oval morphology at the time when cultures were acclimated (Fig. 3.5 micrograph inset). All cultures quantified by flow cytometry had similar forward scatter characteristics among replicates and between treatments, except for one *Thalassiosira* culture acclimated to 20 μmol L^{-1} silicic acid (data not shown). The mean forward scatter of this culture, a proxy for cell size, was ~25% larger than the other replicate cultures of this species in both treatments. This replicate was removed from further analysis to ensure that comparisons of cellular silica content were not influenced by differences in cell sizes among replicate cultures.

Isolates were maintained in semi-continuous bath cultures and transferred to new media before experiencing nutrient starvation. The concentration of nitrate in 17 out of 22 cultures at

the time of measurement was >7 μmol L^{-1}. Two *Minutocellus* cultures, 2 *Odontella* cultures, and 1 *Thalassiosira* culture had between 2 and 3 μmol L^{-1} nitrate remaining. When seawater media contained initial silicic acid concentration of 20 μmol L^{-1}, the concentration of at the time of measurement was approximately 15 μmol L^{-1} in all cultures except two of the *Odontella* replicates, which had approximately 8 μmol L^{-1} silicic acid remaining. When seawater media contained initial silicic acid concentrations of 80 μmol L^{-1}, the concentration at the time of measurement was > 40 μmol L^{-1} in all cultures.

To eliminate the influence of chemical precipitate on the estimation of silica per cell, the mean concentration of precipitated silica in the media before the addition of diatoms was subtracted from the quantity of biogenic silica measured in each diatom culture. Chemical precipitation of silica was detected in the media amended with 20 μmol L^{-1} and 80 μmol L^{-1} silicic acid at an average concentration of 2.28 ± 1.2 μmol L^{-1} and 6.23 ± 0.77 μmol L^{-1}, respectively. One replicate *Thalassiosira* culture acclimated to 80 μmol L^{-1} silicic acid contained 4.9 fold less silica per cell than the other replicates of that growth treatment most likely caused by an error in the measurement of BSi; this replicate was removed from further analysis.

All diatom cultures increased their silica content per cell between 2.3 and 2.7 fold when acclimated to media containing 80 μmol L^{-1} silicic acid vs. 20 μmol L^{-1} silicic acid (Fig 3.5A). Cellular silicification increased the most in *Minutocellus* (0.056±0.004 pmol $cell^{-1}$ to 0.16±0.03 pmol $cell^{-1}$), followed by *Thalassiosira* (0.54 pmol $cell^{-1}$ to 1.36 pmol $cell^{-1}$), *Odontella* (37.8±1.3 pmol $cell^{-1}$ to 93.3±27.3 pmol $cell^{-1}$), and *Cylindrotheca* (0.27±0.01 pmol $cell^{-1}$ to 0.64±0.19 pmol $cell^{-1}$).

PDMPO as a proxy for silicification

The utility of PDMPO fluorescent intensity as a quantitative measure of the silica content of individual cells growing in variable silicic acid concentrations was tested with the laboratory isolates. *Minutocellus* had the lowest PDMPO fluorescence per cell (mode=0.006 RFUs). The fluorescence of *Cylindrotheca* was 5.4 fold higher than *Minutocellus* (mode=0.027 RFUs), and the fluorescence of *Thalassiosira* was 13.8 fold higher than *Minutocellus* (mode=0.069 RFUs) (Fig. 3.6). The difference in PDMPO fluorescence among species is strongly correlated with the cellular silica content measured in these species (Fig. 3.7), although the absolute differences are not the same. *Odontella* cells were too large to be analyzed by flow cytometry.

Isolates acclimated to media with either 20 μmol L^{-1} or 80 μmol L^{-1} silicic acid displayed small differences in PDMPO fluorescence per cell (Fig 3.6), and when data from all replicates of a treatment were pooled together, the distribution of PDMPO fluorescence between treatments was significantly different ($p<0.05$). The distribution of PDMPO fluorescent intensities increased in *Minutocellus*, *Cylindrotheca*, and *Thalassiosira* cultures acclimated to 80 μmol L^{-1} silicic acid compared to cells acclimated to media containing 20 μmol L^{-1} silicic acid , with mode fluorescence increasing 1.2, 1.1, and 1.3 fold, respectively. This is smaller than the approximately 2.5 fold increase for silica per cell measured in the same cultures (Fig. 3.7). The relationship of PDMPO fluorescence to cellular silica content differs between cells acclimated to media containing 80 μmol L^{-1} silicic acid versus 20 μmol L^{-1} silicic acid (Fig. 3.7).

Transcription of silicic acid transporter genes

The potential mechanism of changing silicification of diatom isolates was assessed by measuring the transcript abundance of SIT genes. A total of 14 and 54 separate SIT gene fragments were identified in the *Cylindrotheca* and *Odontella* transcriptomes, respectively, with total translated sequence lengths between 37 and 469 amino acids, spanning different regions of the aligned sequences. The translated sequences of *Cylindrotheca* were most closely related to clades A and B of a previously constructed SIT phylogenetic tree (Durkin et al. 2012). *Odontella* sequences were most closely related to clades A, B, C, and D. It is unknown whether the fragments detected within a single clade represent different copies of closely related genes or different regions of the same gene sequence and for this reason a single transcript sequence from each clade was selected for primer design and RT-qPCR.

The relative transcript abundance of both SIT A and SIT B genes in *Cylindrotheca* were down regulated 1.5±0.16 and 2.5±1.0 fold ($p<0.05$), respectively, in cells acclimated to media with 80 μmol L^{-1} silicic acid relative to cells acclimated to media with 20 μmol L^{-1} silicic acid. The relative transcript abundance of SIT genes in *Odontella* cultures did not change significantly in cells acclimated to media containing 80 μmol L^{-1} silicic acid vs. cells acclimated to media containing 20 μmol L^{-1}silicic acid (Fig 3.8).

Sinking rates of laboratory isolates

Preserved cells were used for sinking experiments to ensure that all measurements were made of cells acclimated at the same time with similar cells sizes between conditions. A total of 6755 observations of sinking *Thalassiosira* cells were made, with between 235 and 2831 observations per sample. A total of 1363 observations of sinking *Odontella* cells were made, with between 206 and 642 observations per sample. Data from all replicates of a single treatment were pooled together to account for the observed variations among replicates.

The largest proportion of *Thalassiosira* cells sank at a speed of 0.175 m d^{-1} when acclimated to seawater media with 20 μmol L^{-1} silicic acid (Fig 3.9A). When *Thalassiosira* cells were acclimated to 80 μmol L^{-1} silicic acid, the sinking speeds increased ($p<0.05$); a large proportion of cells (mode) sank at speeds between 0.275 and 0.325 m d^{-1}. This represents a 60-90% increase in sinking speed of cells growing in higher concentrations of silicic acid.

The sinking speed of *Odontella* cells were more broadly distributed than *Thalassiosira* cells, likely because both single cells and cells in chains of two were observed in the preserved samples. On average, *Odontella* cells sank 2.2 times faster than *Thalassiosira* cells (Fig 3.9B). The faster sinking population is likely composed of the doublet chains, which sank 2-3 times faster than the singlets. When *Odontella* cells were cultured in media containing 20 μmol L^{-1} silicic acid, the majority (mode) of singlet and doublet cells sank at a speed of 0.25 m d^{-1} and 0.75 m d^{-1}, respectively. When these cells were cultured in media containing 80 μmol L^{-1} silicic acid, the majority of these cells sank at a speed of 0.55 and 1.05 m d^{-1}. This represents a 120% increase in sinking rates by the presumed singlet cells and a 40% increase in the sinking rate of the presumed doublet cells, respectively. When data from all replicates of a treatment were pooled together, the distribution of sinking velocities between treatments was significantly different ($p<0.05$).

3.5 Discussion

The high concentration of silicic acid supplied by the Columbia River to the coastal ocean likely supports a more silicified phytoplankton community, increasing the sinking potential of coastal production. Four separate deck-board seawater incubations consistently resulted in more heavily silicified communities when silicic acid was supplied in addition to nitrate. The consistent result is striking because these four incubations occurred at different

times and locations, and with different initial nutrient conditions and phytoplankton communities.

One explanation for the observed changes in community silicification is that communities growing without additional silicic acid became uptake limited. When the concentration of silicic acid is at uptake limiting levels, the SIT proteins are substrate limited and transport less silicic acid into the cell. The cell can maintain its growth rate and compensating for the reduced supply of silicic acid by reducing cellular silicification. A shared characteristic among all nitrate-only incubation treatments was the relatively low final concentrations of silicic acid (1.8-7.1 μmol L^{-1}), levels that often limit the uptake rate of silicic acid (Martin-Jezequel et al. 2000). The communities did not appear to have reduced their growth rates since the abundance of diatoms was not different in the treatments with only nitrate added compared to the treatments with both silicic acid and nitrate added. This suggests that the communities growing in the treatments amended only with nitrate may have reduced their silicic acid requirements to maintain their growth rates. These incubation conditions exposed communities to a pulse input of nutrients and are analogous to the natural coastal environment, where episodic weather events provide a pulse supply of nutrients throughout the upwelling season (Hickey and Banas 2003). As phytoplankton communities draw down a finite nutrient supply in water not influenced by the Columbia River, they might experience silicic acid concentrations that limit the uptake rate; a condition when the rate of incorporation of silicic acid into the frustule cannot keep up with the rate of cell division and therefore the frustule becomes less silicified. Communities incubated with nitrate had 18-41% less BSi than communities amended with both nitrate and silicic acid. This response is comparable the 13-46% reduction in cellular silica previously observed in laboratory batch cultures that depleted the available silicic acid (Harrison et al. 1977). Silicic acid uptake limitation of coastal communities could account for the observed changes in silicification, which means that the community silicification would have decreased when silicic acid concentrations were depleted at the end of the +Nitrate incubations. In an alternative scenario, where uptake limitation was not responsible for decreased silicification, cellular silicification could have immediately increased at the beginning of the incubation with both silicic acid and nitrate added. The closest indication of whether this second mechanism could be responsible for the observed patterns occurred in May 2010, when final silicic acid concentrations in the nitrate treatment were the highest (7.1 μmol L^{-1}) and the community was

still less silicified than in the treatments with both nitrate and silicic acid added. It is therefore possible that silicification increased in the treatments with both nitrate and silicic acid added, rather than decreased in the treatment with only nitrate added.

Although uptake limitation at low silicic acid concentrations could have caused a decrease in community silicification, it is physiologically possible for diatoms growing in high concentrations of silicic acid to increase silicic acid uptake and silicification. Diatoms isolated from one of the field incubations were cultured to simulate a persistently high nutrient coastal environment with different concentrations of silicic acid. Silicic acid never became depleted to typically uptake-limiting concentrations in these semi-continuous batch cultures, and diatoms cultured in seawater with a higher silicic acid concentration precipitated more silica per cell than the same cells cultured in lower silicic acid concentrations. This result is consistent with the results of a culturing study by Finkel et al. (2010), who observed an increase in silica content, and a linear increase in silicic acid uptake, when silicic acid concentrations increased between 20 and 1100 μmol L^{-1}. This effect on silicification could be a consequence of chemical diffusion of silicic acid into the cell or an alternative mechanism of uptake. Thamatrakoln and Hildebrand (2008) also observed a linear increase in uptake rates in the diatom *Thalassiosira pseudonana* as silicic acid concentrations increased above 30 μmol L^{-1} and attributed this to diffusion. Diatoms acclimated to high silicic acid concentrations appear to have a high potential capacity for uptake probably because internally controlled mechanisms enable non-saturable uptake (Thamatrakoln and Hildebrand 2008). The results of our culturing study confirm that utilization of silicic acid above uptake saturating concentrations is biologically possible in the diatoms growing in the field incubations because experiments were conducted on cells isolates from one of these incubations. However, the utilization of silicic acid did appear to be saturable in the natural communities because the increase in community silicification with silicic acid supply did not continue to increase as more silicic acid was supplied. The community that grew in the amendment of silicic acid four times greater than the nitrate amendment was not more silicified than the community that grew after adding the same amount of silicic acid as nitrate. The seemingly different response in the field community compared to laboratory isolates maybe be caused by the difference in time scales over which cells were grown, the initial physiological condition of the cells, and the physiological differences between acclimated vs. not-acclimated growth.

Changes in community composition, instead of uptake limitation, could also be responsible for changes in community silicification because the cellular silica content of different diatom species can be vastly different (Brzezinski 1985). The same community composition was observed between the treatments that had the same concentration of chlorophyll *a* but different concentrations of BSi. A previous study in this region determined that the composition of diatoms growing inside the Columbia River plume was not different than those growing outside of the plume (Frame and Lessard 2009). The results of our incubations that simulate the nutrient conditions of river-influenced water are consistent with the study by Frame and Lessad (2009), and suggest that the river water has a larger effect on physiology than community composition.

Since the river-influenced environment could have a large affect on diatom physiology, detecting the physiological state of the phytoplankton community is necessary to measure and predict the effects of changing conditions. Detecting changes in gene transcription is a promising method of indicating the physiological state of individual cells and natural communities (Marchetti et al. 2010). A previous study of the iron-limited NE Pacific ocean found that changes in SIT gene transcription correlated with changes in iron-availability and thus may be an indicator of changing silicic acid uptake by iron-limited diatoms (*see* Chapter 2 of this thesis). Laboratory studies have correlated SIT transcript abundance with the timing of silicic acid uptake (Thamatrakoln and Hildebrand 2007) and silicic acid starvation (Mock et al. 2008; Sapriel et al. 2009). The present study found no clear correlation between changes in SIT gene transcription and cellular silicification by cells dividing exponentially in seawater with two different silicic concentrations. This supports the hypothesis that increased silicification at high concentrations of silicic acid is a result of diffusion instead of transporter-mediated uptake. Additional measurements of SIT transcription at different parts of the light cycle would be necessary to fully eliminate SITs as part of the mechanism of increasing silicification, since the cultures in this study were likely partially synchronized by the light:dark growth condition. These results suggest that SITs will not be sensitive indicators of excess silicic acid uptake in natural environments because field measurements are also often collected at a single point in time in populations with different growth rates and partially synchronized by the day:night cycle. While SIT gene transcription is a promising indicator of silica metabolism in other environments, additional characterization is necessary to determine whether these genes are useful indicator of the physiological changes controlled by silicic acid concentrations in this coastal environment.

PDMPO is another potentially useful tool for detecting and quantifying changes in silicification of the coastal communities. In this study, PDMPO labeling enabled the identification of diatoms within the mixed phytoplankton community by flow cytometry. Since diatom populations can have similar fluorescence and light scattering characteristics to other phytoplankton types, PDMPO fluorescence is an effective way to identify the cells with a different ecological and biogeochemical role and assess the composition of this community in a more high-throughput way than by microscopy. Previous studies have suggested that the fluorescence intensity of this stain can also be used as a quantitative measure of the amount of silica precipitated (Leblanc and Hutchins 2005) and has been applied in this way to quantify silica precipitation in the diatom populations of the NE Pacific (*see* Chapter 2 of this thesis). The quantitative measurements of PDMPO fluorescence in laboratory cultures in the present study further validate the quantitative relationship between PDMPO fluorescence and silica content among species, but this relationship changes with the physiological state of the diatoms. A slight increase in the fluorescence of PDMPO was detected within a single species when silica content also increased, but the scales of the changes were not comparable. This decoupling between silica precipitation and PDMPO fluorescence might be explained by the different mechanisms responsible for PDMPO vs. silicic acid incorporation into the cell. Silicic acid enters the cell through active transport or diffusion and accumulates in the silica deposition vesicle (SDV). PDMPO enters the cell through passive diffusion through the cell membrane; it is preferentially incorporated into the SDV because of its acidity and is not related to the concentration of silicon (Shimizu et al. 2001). PDMPO likely correlates strongly with silica content among species because of the corresponding differences in SDV size, and thus silicon-accumulation capacity. A physiological change that alters the concentration of silicon in the SDV is unlikely to proportionally influence the concentration of PDMPO in the SDV. PDMPO is a useful tool for assessing changes in the community composition of silicifying phytoplankton and measuring the relative differences in silica content among different species, but it is not a sensitive indicator of changing community silicification caused by the physiological response to silicic acid availability.

Diatoms precipitate a more heavily silicified frustule in response to changing silicic acid supply and, consequently, they sink faster. *Thalassiosira* cells cultured in high silicic acid concentrations were 2.5 times more silicified than cells cultured in lower concentrations; and

these heavier cells sank about twice as fast. The much larger *Odontella* cells also contained about 2.5 times more silica when growing in higher silicic acid concentrations and sank between 1.5 and 2.2 times faster. The increase in silicification was a consistent change in the four species examined, and the increase in sinking rates was consistent in both of the species measured. This suggests that these results can be applied to diverse diatom populations in similar growth conditions, including species that are difficult to study in the laboratory. The absolute export potential of a community will depend on the community composition since sinking rates are vastly different among dominant species; however the relative change in export of the community as a result of changing silicic acid concentrations appears to be independent of diatom species composition since all species observed in this study had similar responses.

This study indicates that the efficiency with which diatom organic matter reaches deeper waters is dependant upon the concentrations of silicic acid in coastal waters. Our data suggest that using a single, unchanging diatom sinking rate to model this region will not accurately capture the dynamic physiological changes that occur in this river-influenced system, and this could influence whether this region is estimated as a net source or sink of carbon dioxide to the atmosphere. Whether it is accurate to apply these results to characterize the broader coastal region requires further investigation. Identifying and developing useful indicators of these physiological processes will enable a better assessment and parameterization of the biological processes controlling the carbon cycle in coastal environments. The carbon cycle in this region maybe be particularly sensitive to changes in silicic acid supply, which is affected both by changes in coastal upwelling and river outflow. Damming of the Columbia River has already created major changes in the supply of silicic acid to the coast, with a reduced supply in the summer months and a larger and more northward supply in the winter months (Whitney et al. 2005). This has likely reduced the silicification of summertime blooms, and their role in carbon export.

3.6 Acknowledgments

This study was conducted in collaboration with Sara Bender, Kit Yu Karen Chan, Kelsey Gaessner, Daniel Grünbaum, E. Virginia Armbrust. This work was supported through a Gordon and Betty Moore Foundation Marine Microbiology Investigator Award to E. Virginia Armbrust and also by an award from the National Science Foundation to the Center for Coastal Margin

Observation and Prediction. I would like to thank the crew of the R/V New Horizon and the R/V Wecoma and the scientist who accommodated this work out at sea and enabled its success. In particular, I would like to thank Byron Crump, Lydie Herfort, Tawnya Peterson, and Fred Prahl. Gwenn Hennon and Francois Ribalet conducted incubations and collected samples in May 2010, which were a central part of this study. Francois Ribalet, Jarred Swalwell, and Rhonda Morales provided invaluable advice regarding flow cytometry analysis.

3.7 Bibliography

Andersen, R. A. 2005. Algal culturing techniques. Elsevier/Academic Press.

Berges, J. A., D. J. Franklin, and P. J. Harrison. 2001. Evolution of an artificial seawater medium: Improvements in enriched seawater, artificial water over the last two decades. Journal of Phycology **37:** 1138-1145.

Borges, A. V., B. Delille, and M. Frankignoulle. 2005. Budgeting sinks and sources of CO2 in the coastal ocean: Diversity of ecosystems counts. Geophys. Res. Lett. **32:** L14601

Brand, L. E., R. R. L. Guillard, and L. S. Murphy. 1981. A method for the rapid and precise determination of acclimated phytoplankton reproduction rates. Journal of Plankton Research **3:** 193-201.

Bruland, K. W., M. C. Lohan, A. M. Aguilar-Islas, G. J. Smith, B. Sohst, and A. Baptista. 2008. Factors influencing the chemistry of the near-field Columbia River plume: Nitrate, silicic acid, dissolved Fe, and dissolved Mn. Journal of Geophysical Research-Oceans **113:** C00B02

Brzezinski, M. A. 1985. The Si:C:N Ratio of Marine Diatoms: Interspecific Variability and the Effect of Some Environmental Variables. Journal of Phycology **21:** 347-357

Brzezinski, M. A., and D. M. Nelson. 1986. A Solvent-Extraction Method for the Colorimetric Determination of Nanomolar Concentrations of Silicic-Acid in Seawater. Marine Chemistry **19:** 139-151

---. 1996. Chronic substrate limitation of silicic acid uptake rates in the western Sargasso Sea. Deep Sea Research Part II: Topical Studies in Oceanography **43:** 437-453

Buesseler, K. O. 1998. The decoupling of production and particulate export in the surface ocean. Global Biogeochemical Cycles **12:** 297-310.

Chan, K. Y. K., and D. Grunbaum. 2010. Temperature and diet modified swimming behaviors of larval sand dollar. Marine Ecology-Progress Series **415:** 49-59

Durkin, C. A., A. Marchetti, S. J. Bender, T. Truong, R. Morales, T. Mock, and E. V. Armbrust. 2012. Frustule-related gene transcription and the influence of diatom community composition on silica precipitation in an iron-limited environment Limnology and Oceanography **In press:**

Finkel, Z. V., K. A. Matheson, K. S. Regan, and A. J. Irwin. 2010. Genotypic and phenotypic variation in diatom silicification under paleo-oceanographic conditions. Geobiology **8:** 433-445

Frame, E. R., and E. J. Lessard. 2009. Does the Columbia River plume influence phytoplankton community structure along the Washington and Oregon coasts? Journal of Geophysical Research-Oceans **114:** C00B09

Guillard, R. R., and J. H. Ryther. 1962. Studies of marine planktonic diatoms.1. *Cyclotella nana* Hustedt, and *Detonula confervacea* (Cleve) Gran. Canadian Journal of Microbiology **8:** 229-239.

Hales, B., T. Takahashi, and L. Bandstra. 2005. Atmospheric CO2 uptake by a coastal upwelling system. Global Biogeochemical Cycles **19:** GB1009

Harrison, P. J., H. L. Conway, and R. C. Dugdale. 1976. Marine diatoms grown in chemostats under silicate or ammonium limitation. I. Cellular chemical composition and steady-state growth kinetics of *Skeletonema costatum*. Marine Biology **35:** 177-186

Harrison, P. J., H. L. Conway, R. W. Holmes, and C. O. Davis. 1977. Marine Diatoms Grown in Chemostats under Silicate or Ammonium Limitation .3. Cellular Chemical Composition and Morphology of Chaetoceros-Debilis, Skeletonema-Costatum, and Thalassiosira-Gravida. Marine Biology **43:** 19-31

Hickey, B., and N. Banas. 2003. Oceanography of the U.S. Pacific Northwest Coastal Ocean and estuaries with application to coastal ecology. Estuaries and Coasts **26:** 1010-1031

Hickey, B. M., and N. S. Banas. 2008. Why is the Northern End of the California Current System So Productive? Oceanography **21:** 90-107

Ianson, D., R. A. Feely, C. L. Sabine, and L. W. Juranek. 2009. Features of Coastal Upwelling Regions that Determine Net Air-Sea CO2 Flux. Journal of Oceanography **65:** 677-687

Kudela, R. M., and T. D. Peterson. 2009. Influence of a buoyant river plume on phytoplankton nutrient dynamics: What controls standing stocks and productivity? Journal of Geophysical Research-Oceans **114:** C00B11

Leblanc, K., and D. A. Hutchins. 2005. New applications of a biogenic silica deposition fluorophore in the study of oceanic diatoms. Limnology and Oceanography:Methods **3:** 462-476.

Leblanc, K., A. Leynaert, C. Fernandez I, P. Rimmelin, T. Moutin, P. Raimbault, J. Ras, and B. Quéguiner. 2005. A seasonal study of diatom dynamics in the North Atlantic during the POMME experiment (2001): Evidence for Si limitation of the spring bloom. J. Geophys. Res. **110:** C07S14

Marchetti, A., D. E. Varela, V. P. Lance, Z. Johnson, M. Palmucci, M. Giordano, and E. V. Armbrust. 2010. Iron and silicic acid effects on phytoplankton productivity, diversity, and chemical composition in the central equatorial Pacific Ocean. Limnology and Oceanography **55:** 11-29.

Martin-Jezequel, V., M. Hildebrand, and M. A. Brzezinski. 2000. Silicon metabolism in diatoms: Implications for growth. Journal of Phycology **36:** 821-840

Matsen, F. A., R. B. Kodner, and E. V. Armbrust. 2010. pplacer: linear time maximum-likelihood and Bayesian phylogenetic placement of sequences onto a fixed reference tree. BMC Bioinformatics **11:** 538, doi:510.1186/1471-2105-1111-1538

Mock, T., M. P. Samanta, V. Iverson, C. Berthiaume, M. Robison, K. Holtermann, C. Durkin, S. S. Bondurant, K. Richmond, M. Rodesch, T. Kallas, E. L. Huttlin, F. Cerrina, M. R. Sussmann, and E. V. Armbrust. 2008. Whole-genome expression profiling of the marine diatom *Thalassiosira pseudonana* identifies genes involved in silicon bioprocesses. Proceedings of the National Academy of Sciences of the United States of America **105:** 1579-1584.

Nelson, D. M., P. Treguer, M. A. Brzezinski, A. Leynaert, and B. Queguiner. 1995. Production and dissolution of biogenic silica in the ocean- Revised global estimates, comparison with regional data and relationship to biogenic sedimentation. Global Biogeochemical Cycles **9:** 359-372.

Paasche, E. 1973. Silicon and Ecology of Marine Plankton Diatoms .1. Thalassiosira-Pseudonana (Cyclotella-Nana) Grown in a Chemostat with Silicate as Limiting Nutrient. Marine Biology **19:** 117-126

Pfaffl, M. W. 2001. A new mathematical model for relative quantification in real-time RT-PCR. Nucleic Acids Research **29:** e45

Ramakers, C., J. M. Ruijter, R. H. L. Deprez, and A. F. M. Moorman. 2003. Assumption-free analysis of quantitative real-time polymerase chain reaction (PCR) data. Neuroscience Letters **339:** 62-66

Rozen, S., and H. Skaletsky. 2000. Primer3 on the WWW for general users and for biologist programmers. Methods Mol Biol **132:** 365-386.

Sapriel, G., M. Quinet, M. Heijde, L. Jourdren, V. Tanty, G. Z. Luo, S. Le Crom, and P. J. Lopez. 2009. Genome-wide transcriptome analyses of silicon metabolism in *Phaeodactylum tricornutum* reveal the multilevel regulation of silicic acid transporters. Plos One **4:** e7458, doi: 7410.1371/Journal.Pone.0007458

Shimizu, K., Y. Del Amo, M. A. Brzezinski, G. D. Stucky, and D. E. Morse. 2001. A novel fluorescent silica tracer for biological silicification studies. Chemistry & Biology **8:** 1051-1060

Thamatrakoln, K., and M. Hildebrand. 2007. Analysis of *Thalassiosira pseudonana* silicon transporters indicates distinct regulatory levels and transport activity through the cell cycle. Eukaryotic Cell **6:** 271-279.

---. 2008. Silicon uptake in diatoms revisited: A model for saturable and nonsaturable uptake kinetics and the role of silicon transporters. Plant Physiology **146:** 1397-1407

Treguer, P., D. M. Nelson, A. J. Vanbennekom, D. J. Demaster, A. Leynaert, and B. Queguiner. 1995. The Silica Balance in the World Ocean - a Reestimate. Science **268:** 375-379

Whitney, F. A., W. R. Crawford, and P. Harrison. 2005. Physical processes that enhance nutrient transport and primary productivity in the coastal and open ocean of the subarctic NE Pacific. Deep-Sea Research Part Ii-Topical Studies in Oceanography **52:** 681-706

Table 3.1 Location, treatments, and nutrient concentrations of all deck-board incubations conducted along the Washington and Oregon coast. Nutrient drawdown (in μM) was calculated from the difference between the initial+amended concentration and the final concentration.

Location	Date	Incubation (days)	Treatment	Na_2SiO_3 added (μM)	Na_2NO_3 added (μM)	Silicic acid (μM)	Nitrate (μM)	NH_4 (μM)	Phosphate (μM)	$Si(OH)_4$ drawdown	NO_3 drawdown
LP-17 47.917° N 125.083° W	18 May 2009	0	Initial	0	0	12.7	7.3	0.6	.8	—	—
		2.5	Control	0	0	4.22 ± 0.66	0.15 ± 0.2	0.41 ± 0.36	0.15 ± 0..01	8.4 ± 0.66	7.1 ± 0.2
		2.5	+Si	40	0	44.65 ± 7.39	0.47 ± 0.43	0.34 ± 0.42	0.24 ± 0.03	8 ± 7.4	6.8 ± 0.43
		2.5	+N	0	20	1.8 ± 0.96	16.41 ± 2.95	0.21 ± 0.05	0.05 ± 0.05	11 ± 1	11 ± 3
		2.5	+ 2:1 Si:N	40	20	45.32 ± 3.85	18.79 ± 2.64	0.19 ± 0.02	0.08 ± 0.03	7.4 ± 3.8	8.5 ± 2.6
CR 46.497° N 124.464° W	15 May 2009	0	Initial	0	0	8.92 ± 2	0.36 ± 0.18	0.6 ± 0.11	0.21 ± .04	—	—
		2.5	Control	0	0	8.38 ± 0.62	0.09 ± 0.14	0.39 ± 0.45	0.11 ± 0.02	0.54 ± 0.62	0.28 ± 0.14^{+}
		2.5	+Si	40	0	45.86 ± 12.8	0.03 ± 0.04	0.17 ± 0.09	0.06 ± 0.02	3.06 ± 12.8	0.33 ± 0.04^{+}
		2.5	+N	0	20	4.63 ± 1.02	11.64 ± 5.89	0.58 ± 0.26	0.02 ± 0.02	3.9 ± 1.1	8.7 ± 5.9*
		2.5	+ 2:1 Si:N	40	20	34.1 ± 8.34	10.59 ± 2.44	0.33 ± 0.19	0.01 ± 0.01	15 ± 8.3	9.8 ± 2.4*
NH-20 44.65° N 124.53° W	22 May 2010	0	Initial	0	0	9.3 ± 0.56	1.3 ± 0.04	0.3 ± 0.02	0.9 ± 0.0	—	—
		3	Control	0	0	8.0 ± 0.32	0.07 ± 0.03	0.09 ± 0.02	0.25 ± 0.02	1.3 ± 0.32	1.28 ± 0.03^{+}
		3	+Si	20	0	27 ± 0.44	0.21 ± 0.05	0.1 ± 0.03	0.24 ± 0	2.7 ± 0.44^{*+}	1.1 ± 0.05^{+}
		3	+N	0	20	7.1 ± 0.38	14 ± 0.42	0.41 ± 0.21	0.1 ± 0.01	2.2 ± 0.39	7.6 ± 0.42*
		3	+ 1:1 Si:N	20	20	23 ± 2.5	10 ± 1.2	0.05 ± 0	0.05 ± 0	6 ± 2.5^{*+}	11 ± 1.2^{*+}
		3	+ 4:1 Si:N	80	20	88 ± 7.8	13 ± 1	0.34 ± 0.24	0.08 ± 0	1.2 ± 7.8	8 ± 1*
NH-20 44.65° N 124.53° W	30 July 2010	0	Initial	0	0	9.1 ± 0.66	0.41 ± 0.11	0.09 ± 0.06	0.25 ± 0.03	—	—
		3	Control	0	0	3.0 ± 0.33	0.2 ± 0.06	0.04 ± 0.006	0.06 ± 0.02	6.1 ± 0.33	0.22 ± 0.06^{+}
		3	+Si	20	0	21 ± 0.7	0.15 ± 0.02	0.04 ± 0.01	0.06 ± 0.007	7.8 ± 0.7^{*+}	0.26 ± 0.02^{+}
		3	+N	0	20	2.2 ± 0.5	0.2 ± 0.03	0.36 ± 0.17	0.11 ± 0.01	6.9 ± 0.5	20 ± 0.03*
		3	+ 1:1 Si:N	20	20	11 ± 0.58	0.1 ± 0.04	0.61 ± 0.18	0.07 ± 0.03	18 ± 0.58^{*+}	20 ± 0.04*
		3	+ 4:1 Si:N	80	20	75 ± 2.9	0.25 ± 0.18	0.27 ± 0.13	0.17 ± 0.11	14 ± 2.9^{*+}	20 ± 0.18*

* = different from control treatment

+ = different from +Nitrate treatment

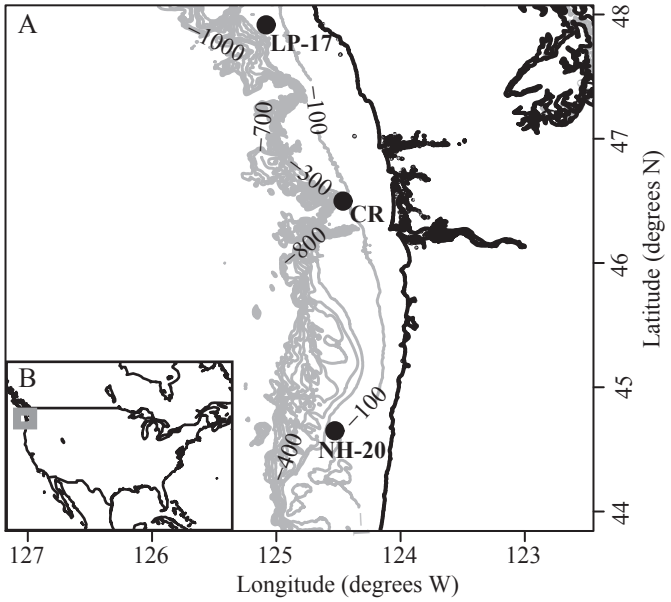

Figure 3.1 A) Map of the study region. Locations where water was collected for deck-board incubations are marked with circles and labeled. One hundred meter isobaths are shown in grey down to 1000 m. The inset (B) indicates the location of the study region (grey square) relative to the North American continent.

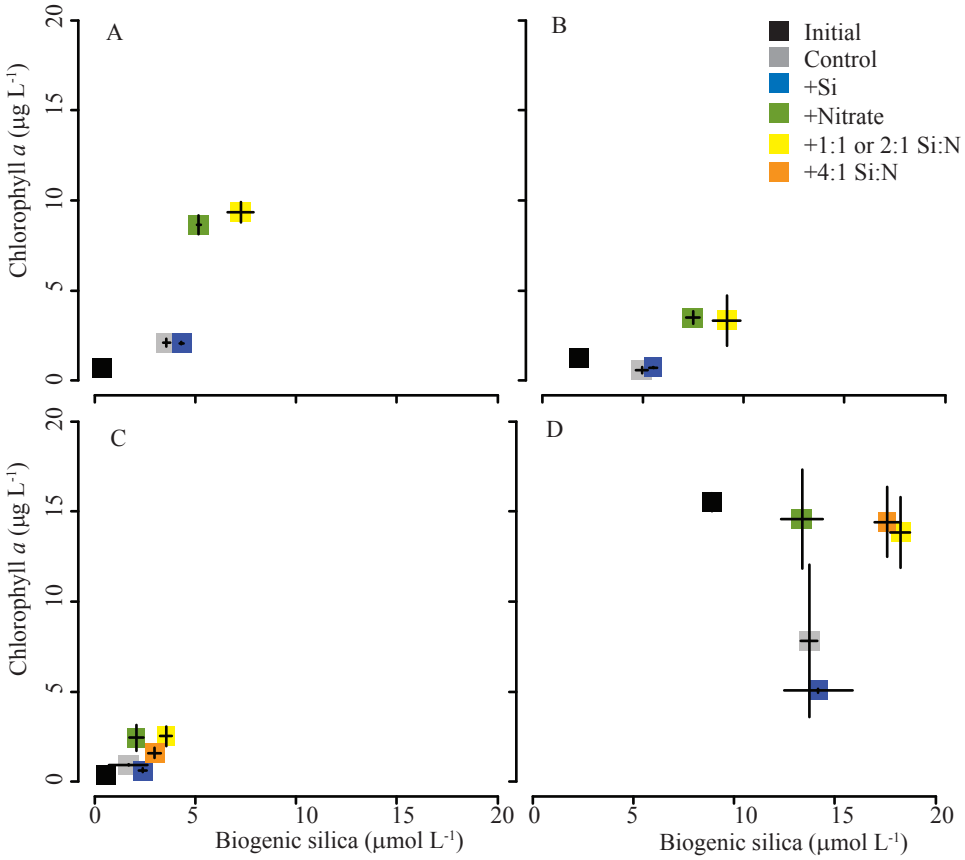

Figure 3.2 Chlorophyll a vs. biogenic silica concentrations in the water sampled from (A) LP-17, (B) CR, (C) NH-20 in May 2010, and (D) NH-20 in July 2010. Initial concentrations from the ambient seawater are indicated by black squares and the concentrations after incubation in various treatments are represented by the colored squares as indicated in the key. Error bars indicate the standard deviation of triplicate incubation bottles.

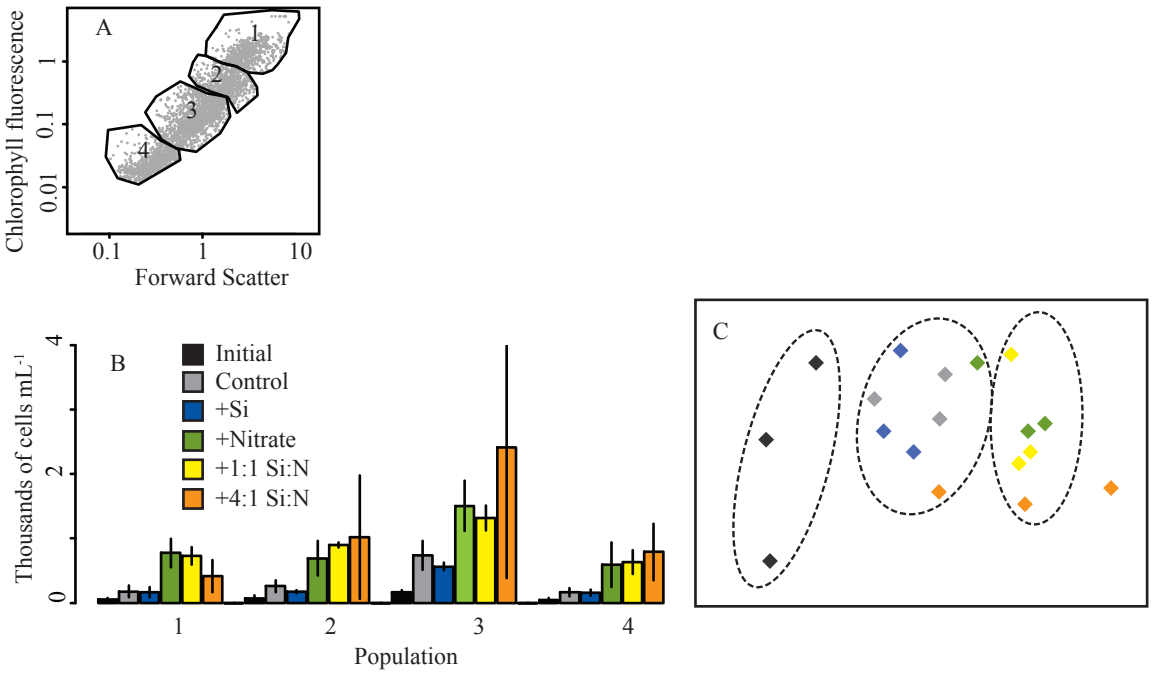

Figure 3.3 Diatom community composition in treatments from all incubation sets as determined by flow cytometry of PDMPO labeled cells. A) Example cytogram of chlorophyll *a* fluorescence vs. forward light scatter of PDMPO labeled cells (grey dots) and how each population was defined (black polygons). B) Abundance of PDMPO labeled populations in the May2010 NH-20 incubation treatments. C) Multidimentional scaling analysis visualizing the similarity of the community composition in each incubation bottle. Dashed circles identify clusters of bottles with similar community compositions according to a Simprof clustering algorithm.

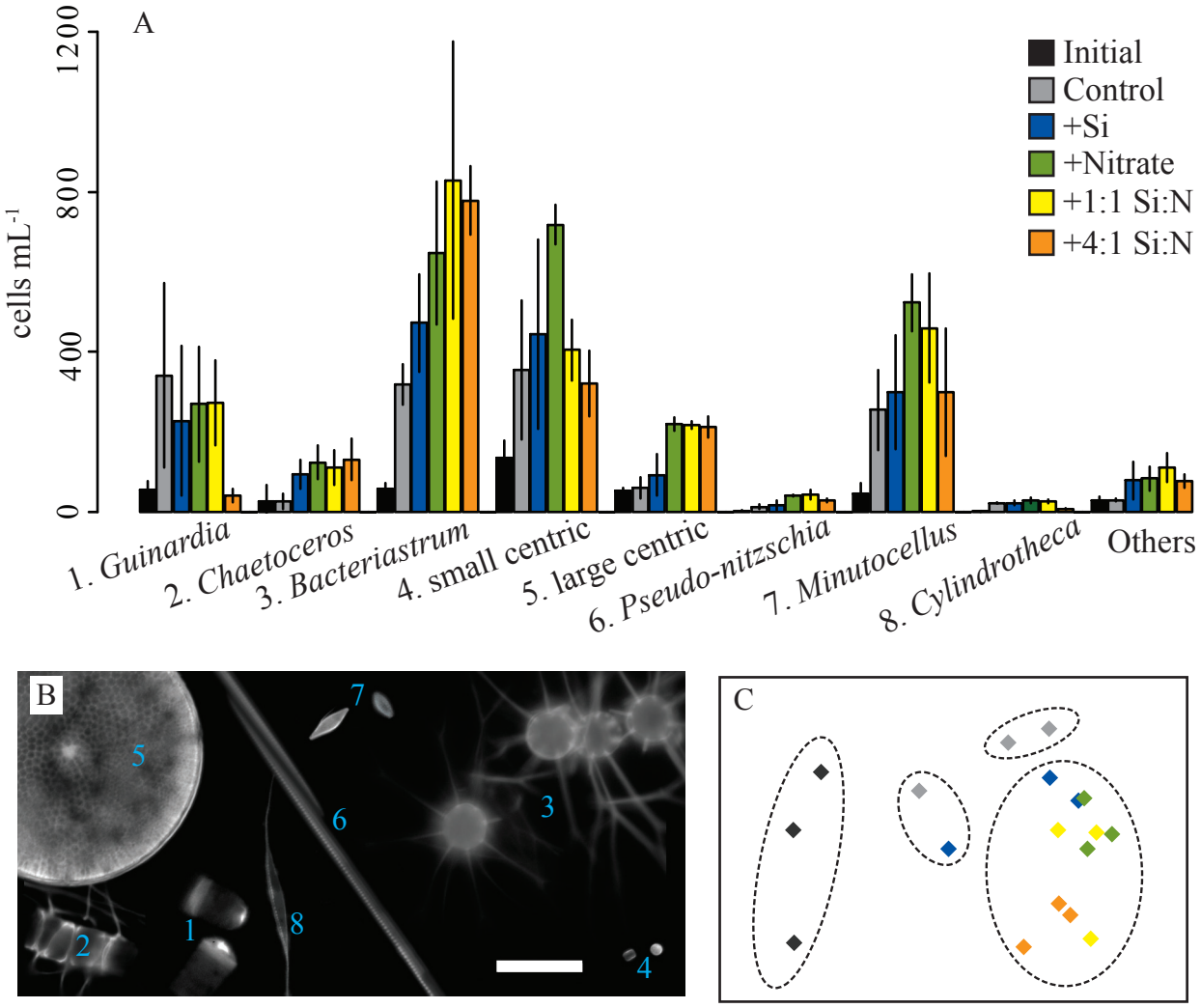

Figure 3.4 Diatom community composition in the May 2010 incubation with seawater collected at station NH-20, identified by microscopy of PDMPO labeled cells. A) Abundance of the dominant categories of diatoms in the initial water sample and after incubation treatments. Error bars indicate the standard deviation of triplicate bottles. Numbers in front of category labels along the x-axis correspond to micrographs labeled in panel B. B) A collage of epifluorescence micrographs of the cells identified in the incubation treatments. The scale bar is 20 µm. C) Multidimensional scaling analysis spatially displaying the similarity of the community compositions among treatments. Each diamond represents the composition of a single incubation bottle and colors correspond to the key in panel A. Dashed circles identify clusters of bottles with similar community compositions according to a Simprof clustering algorithm.

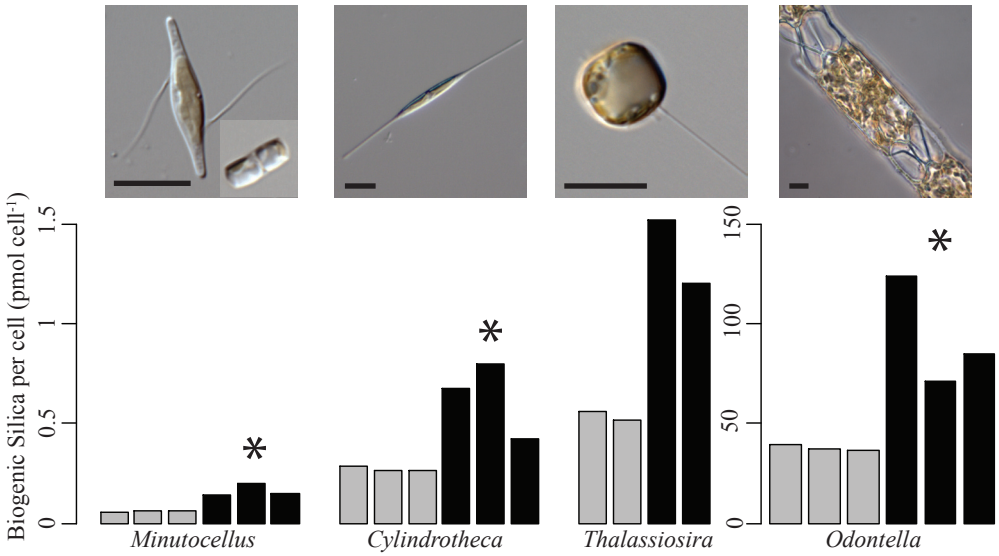

Figure 3.5 The silica per cell of cultured isolates acclimated to media containing 20 µmol L^{-1} silicic acid (grey bars) or 80 µmol L^{-1} silicic acid (black bars). Example light micrographs of each culture are along the top. *Minutocellus* cultures displayed a small centric-like morphology at the time of acclimated growth (inset in *Minutocellus* micrograph). Scale bars in each micrograph are 10 µm. Asterisks above the bars of the 80 µmol L^{-1} silicic acid growth treatment indicate significant differences ($p<0.05$) from the 20 µmol L^{-1} silicic acid growth treatment. Significance could not be assessed for duplicate *Thalassiosira* cultures.

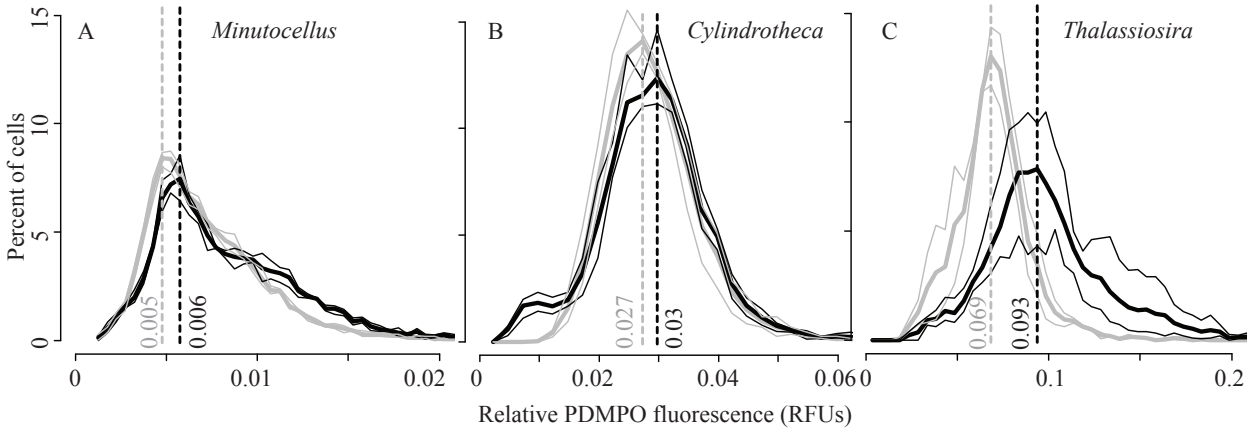

Figure 3.6 Histograms of the relative fluorescence of PDMPO labeled (A) *Minutocellus*, (B) *Cylindrotheca*, and (C) *Thalassiosira* cultures acclimated to either 20 µmol L^{-1} silicic acid (grey lines) or 80 µmol L^{-1} silicic acid (black lines) quantified on a flow cytometer. Thick lines represent the average of replicate cultures from each treatment and the thin lines indicate the variability among replicates as the maximum and minimum percent of cells observed. Dashed lines at the labeled fluorescent values denote the most frequently observed fluorescence (mode) in each growth treatment.

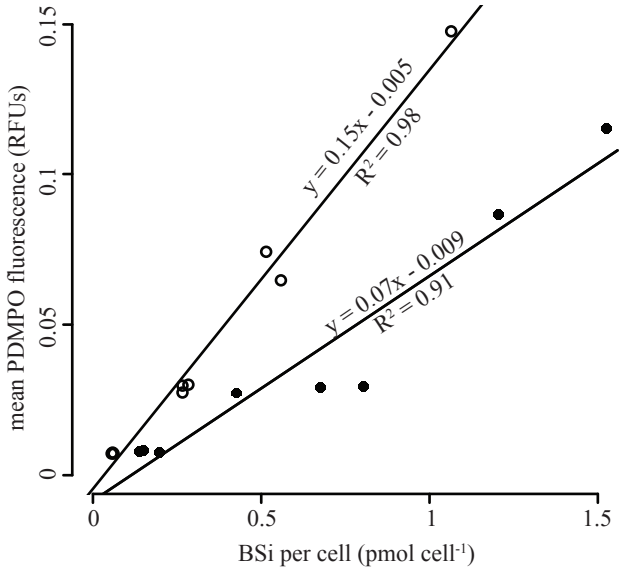

Figure 3.7 Linear regression of the average PDMPO fluorescence of each culture measured by flow cytometry (see Fig. 3.7) vs. the silica per cell of these cultures (see Fig.3.5). Open circles are cultures acclimated to 20 µmol L^{-1} silicic acid and black circles are the same isolates acclimated to 80 µmol L^{-1} silicic acid. Measurements are of replicate *Minutocellus*, *Cylindrotheca*, and *Thalassiosira* cultures. The regression of each growth treatment is labeled on the lines.

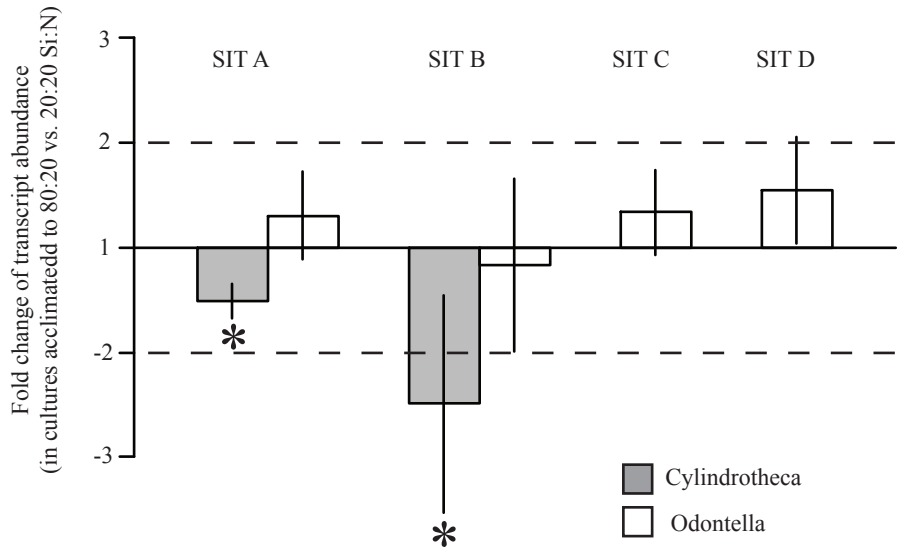

Figure 3.8 Fold change of the relative transcript abundance of evolutionarily diverged silicon transporters from clades A and B in *Cylindrotheca* cultures (grey bars) and clades A, B, C, and D in *Odontella* cultures (white bars) acclimated to media containing 80 µmol L^{-1} silicic acid relative to the transcript abundance in cultures acclimated to media containing 20 µmol L^{-1} silicic acid. All SIT gene transcripts were first normalized to the transcript abundance of actin in the same treatment before normalizing the relative transcript abundance in each treatment to one another. Horizontal dashed lines denote a ratio of ±2, a common threshold for determining significant transcript fold change. Error bars are the standard deviation of measurements in triplicate cultures and asterisks indicate a statistically significant difference between growth treatments ($p<0.05$).

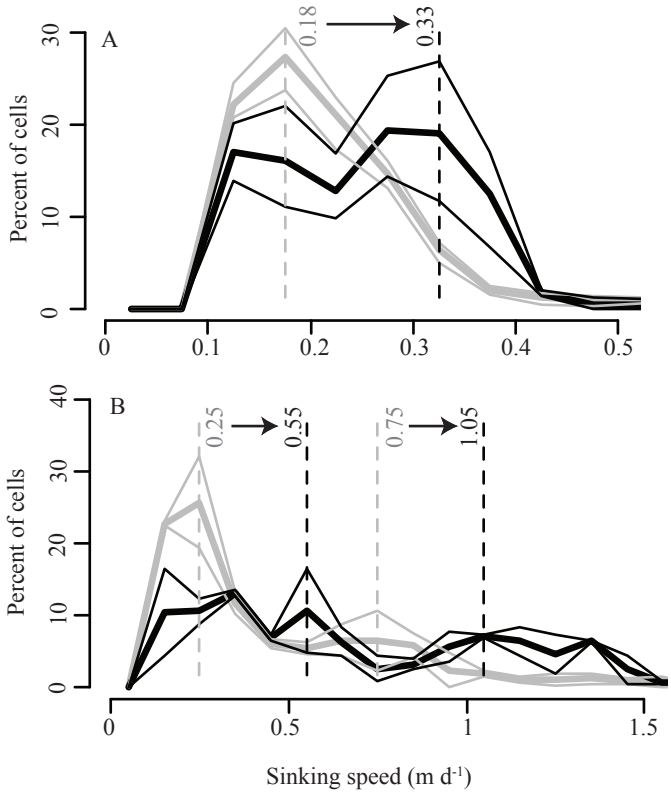

Figure 3.9 Histogram of observed sinking speeds normalized to the number to total observed (A) *Thalassiosira* and (B) *Odontella* cells acclimated to media containing either 20 µmol L^{-1} silicic acid (grey lines) or 80 µmol L^{-1} silicic acid (black lines). Thick lines represent the average of triplicate *Thalassiosira* cultures and duplicate *Odontella* cultures from each t reatment and the thin lines indicate the variability among replicates as the maximum and minimum percent of cells observed. Dashed lines at the labeled velocities denote the most frequently observed sinking speed (mode), and arrows indicate the shift in this speed between growth treatments. Two modes are identified in the *Odontella* samples to distinguish between the sinking speeds of single cells and what are likely to be short chains of cells.

Conclusion

Diatoms are an important link between the global carbon and silicon cycles, and the response of these microscopic organisms to different environmental conditions can alter global scale processes. This thesis focused on the formation of the silica frustules, the definitive characteristic of diatoms, because this silica requirement gives diatoms an ecological role and biogeochemical influence that is different from other phytoplankton groups. Despite the ecological and biogeochemical influence frustule formation can have on both local and global scales, many of the mechanisms controlling frustule formation have yet to be discovered and characterized. Detecting how frustule formation responds to changing environmental conditions is also complicated by the diversity in natural communities.

Chapter one of this thesis focused on how the diatom cell wall changes in response to different nutrient conditions and a previously unknown component of the frustule was discovered. With the help of newly available diatom genomes and transcriptomes, chitin was discovered in the cell wall of several diatom species. This work changes the known chemical composition of the frustule and suggests that chitin may be involved in frustule formation. This previously unknown part of the frustule could be an important part of how frustule formation changes in environments with limited availability of iron or silicic acid.

In chapter two, the role of chitin and other parts of frustule formation was studied in natural communities experiencing iron-limitation. This was the first time molecular methods were applied to studying frustule formation in natural communities. Species composition particularly influenced silica precipitation by the community because of the evolved differences in chemical composition and genetic potential. Surprisingly, not all genes with a vital role in frustule formation were equally or easily detected in natural diatom communities. Silicon transporters were the most abundant transcripts detected, and when put in the evolutionary context of their gene family, showed transcriptional changes indicative of a potential functional shift in how diatoms take up silicic acid from iron-limited waters. This is the first molecular evidence of a biological mechanism that could be responsible for altering the distribution of silicon throughout the global ocean.

The third chapter addressed the biogeochemical role of diatoms in coastal upwelling environments with the goal of improved parameterization of coastal biogeochemistry. In this study, the silicification of diatoms blooming in response to nitrate was influenced by the supply of silicic acid. When studied in laboratory cultures, a similar response was detected in all species examined, suggesting that the biological mechanism responsible for changing silicification is widespread among diatom species. Although silicon transporters were sensitive indicators of changing utilization of silicic acid in chapter two, their transcription patterns did not indicate that they were the mechanism responsible for the changes in silicification measured in chapter 3. This supports the hypothesis that alternative mechanisms of silicic acid uptake, like diffusion, are an important part of silicic acid utilization. This change in silica content was directly connected to biogeochemical consequences by measuring the sinking rate of diatom cultures. Cells that took up silicic acid at higher concentrations, probably by diffusion, were more silicified and had faster sinking rates. This physiological response to changing silicic acid concentrations could have a large influence on the degree to which diatom production makes coastal regions a net carbon sink.

This work has explored how microscopic engineers influence global processes, and how they fit into the interconnected system of biology, chemistry, geology, and physics of the planet. Diatoms have long been an inspiration because of their beauty, but also an inspiration because of their larger role in connecting the earth’s systems.

CURRICULUM VITA

Colleen Andrea Durkin

Education

PhD Oceanography, University of Washington August 2012
Advisor: E. Virginia Armbrust
Dissertation Title: Environmentally induced changes to the diatom cell wall and the implications of these changes on biogeochemical cycles

M.S. Oceanography, University of Washington 2008
Advisor: E.Virginia Armbrust
Presentation and Paper Title: Chitin in diatoms and its association with the cell wall.

B.S Biology and Oceanography, University of Washington 2004
Magna cum laudae
Thesis title: Predator avoidance as a possible driver of diel vertical migration.

Research

2005-2012 Research Associate University of Washington, Oceanography
Conducted dissertation research on how the diatom cell wall changes in response to nutrient conditions and how these changes influence biogeochemistry.

2004 Research Intern EAWAG, Duebendorf, Switzerland
Collected and identified *Daphnia* zooplankton species from regional lakes

2003-2004 Undergraduate Researcher NOAA Northwest Fisheries Science Center
Collected juvenile salmon from the waters of Puget Sound and screened them for bacterial kidney disease using epifluorescent microscopy.

2004 Senior Thesis University of Washington, Oceanography
Designed, conducted, and presented a study addressing the drivers of diel vertical migration by dinoflagellates in Puget Sound, Washington.

2003 Research Apprentice Friday Harbor, University of Washington
Designed and conducted a study of the population genetics of the intertidal snail *Littorina* during a 3 month apprenticeship course entitled Marine Molecular Ecology.

2002-2003 Undergraduate Researcher University of Washington, Botany
Cultured diverse dinoflagellate species and tested the distribution of a gene among these species using PCR

Research Cruises

Nov 2010 R/V Thomas G. Thompson 2 days PI: Dr. E. Virginia Armbrust
Puget Sound educational and research cruise
Program: University of Washington Oceans and Human Health

Sept 2010	R/V Wecoma	1 week	PI: Dr. Fred Prahl
	Coastal to open ocean transects along the WA and OR and in the Columbia River		
	Program: Coastal Margin Observation and Prediction		
March 2010	M/V Alta and the Barkley Star	1 week	PI: Dr. Richard Keil
	Survey of the basins and inlets of Barkley Sound on Vancouver Island		
	Program: University of Washington Ocean 444 senior thesis projects		
Oct 2009	R/V Thomas G. Thompson	2 days	PI: Dr. E. Virginia Armbrust
	Puget Sound educational and research cruise		
	Program: University of Washington Oceans and Human Health		
Sept 2009	R/V New Horizon	2 weeks	PI: Dr. Tawnya Peterson
	Coastal to open ocean transects along WA and OR and in the Columbia River		
	Program: Coastal Margin Observation and Prediction		
May 2009	R/V New Horizon	2 weeks	PI: Dr. Byron Crump
	Coastal to open ocean transects along WA and OR and in the Columbia River		
	Program: Coastal Margin Observation and Prediction		
May 2008	CCGS John P. Tully	3 weeks	PI: Marie Robert
	Transect from Sydney, B.C. to Station P in the NE subarctic Pacific Ocean		
	Program: Institute of Ocean Sciences Canada, Line P		

Teaching

Advisor to undergraduate researchers 2006-2012

- Teach and train undergraduate laboratory assistants
- Encourage them to develop skills necessary to do science and participate in collaborative research
- Total undergraduates advised: 4

Invited lecturer October 2011
Ocean 530: Biological Oceanography, lecture title: “Nutrients and Phytoplankton”

Teaching Assistant Jan-June 2010
Ocean 443: Design of Oceanographic Field Experiments

Teaching Assistant
Ocean 444: Advanced Field Oceanography

Communicating Ocean Science course
Ocean 592: Communicating Ocean Science March-June 2008
Taught oceanography lessons to first graders

Teaching Assistant Sept-Dec 2006
Ocean 430: Biological Oceanography

Public Outreach 2005-present

- Laboratory tours, presentations, and demonstrations for visiting primary and middle school students
- Invited lecturer/teacher at local elementary and high schools

Additional Relevant Experiences

- SOLAS Summer School 2011, Cargese, Corsica
- Science Film Workshop 2011, Friday Harbor, Washington
- Science Communication Fellowship 2011, Pacific Science Center, Seattle, Washington

Publications

Durkin, C.A., A. Marchetti, S.J. Bender, T. Truong, R. Morales, and E.V. Armbrust. 2012. Diverse patterns of silica precipitation and frustule-related gene transcription among iron-limited diatoms. Limnology and Oceanography In press

Marchetti, A.M., D.M. Schruth, **C.A. Durkin**, M.S. Parker, R. Kodner, C.T. Berthiaume, R. Morales, A.E. Allen, and E.V. Armbrust. 2012. Comparative metatranscriptomics identifies molecular bases for the physiological responses of phytoplankton to varying iron availability. PNAS. 109: E317-E325.

Rhodes, L.D., C.A. Rice, C.M. Greene, D.J. Teel, S.L. Nance, P. Moran, **C.A. Durkin**, and S.B. Gezhegne. 2011. Nearshore ecosystem predictors of a bacterial infection in juvenile Chinook salmon. Marine Ecology Progress Series 432: 161-172

Ribalet, F., A. Marchetti, K.A. Hubbard, K. Brown**, C.A. Durkin**, R. Morales, Marie Robert, Jarred E. Swalwell, Philippe D. Tortell, and E. Virginia Armbrust. 2010. Unveiling a phytoplankton hotspot at a narrow boundary between coastal and offshore waters. PNAS. 107: 16571-16576.

Durkin, C.A, T. Mock, and E.V. Armbrust. 2009. Chitin in diatoms and its association with the cell wall. Eukaryotic Cell. 8: 1038-1050.

Mock, T., M. P. Samanta, V. Iverson, C. Berthiaume, M. Robison, K. Holtermann, **C. Durkin**, S.S. BonDurant, K. Richmond, M. Rodesch, T. Kallas, E. L. Huttlin, F. Cerrina, M. R. Sussmann, and E. V. Armbrust. 2008. Whole-genome expression profiling of the marine diatom Thalassiosira pseudonana identifies genes involved in silicon bioprocesses. PNAS 105:1579-1584.

Bowler, C., A. E. Allen, J. H. Badger, J. Grimwood, K. Jabbari, A. Kuo, U. Maheswari, C. Martens, F. Maumus, R. P. Otillar, E. Rayko, A. Salamov, K. Vandepoele, B. Beszteri, A. Gruber, M. Heijde, M. Katinka, T. Mock, K. Valentin, F. Verret, J. A. Berges, C. Brownlee, J.-P. Cadoret, A. Chiovitti, C. J. Choi, S. Coesel, A. De Martino, J. C. Detter**, C. Durkin**, A. Falciatore, J. Fournet, M. Haruta, M. J. J. Huysman, B. D. Jenkins, K. Jiroutova, R. E. Jorgensen, Y. Joubert, A. Kaplan, N. Kroger, P. G. Kroth, J. La Roche, E. Lindquist, M. Lommer, V. Martin-Jezequel, P. J. Lopez, S. Lucas, M. Mangogna, K. McGinnis, L. K. Medlin, A. Montsant, M.-P. O.-L. Secq, C. Napoli, M. Obornik, M. S. Parker, J.-L. Petit, B. M. Porcel, N. Poulsen, M. Robison, L. Rychlewski, T. A. Rynearson, J. Schmutz, H. Shapiro, M. Siaut, M. Stanley, M. R. Sussman, A. R. Taylor, A. Vardi, P. von Dassow, W. Vyverman, A. Willis, L. S. Wyrwicz, D. S. Rokhsar, J. Weissenbach, E. V. Armbrust, B. R. Green, Y. Van de Peer, and I. V. Grigoriev. 2008. The Phaeodactylum genome reveals the evolutionary history of diatom genomes. Nature 456: 239-244.

Rhodes, L.D**., C.A. Durkin**, S.L. Nance, C.A. Rice. 2006. Prevalence and analysis of *Renibacterium salmoninarum* infection among juvenile Chinook salmon *Oncorhynchus tshawytscha* in North Puget Sound. Diseases of Aquatic Organisms 71: 179–190.

Meeting Presentations

2012 Uptake limitation of silicic acid in coastal diatoms controls cellular silicification
AGU/ASLO Ocean Science Meeting,Salt Lake City, Utah
Durkin, C.A., S.J. Bender, K. Gaessner, E.V. Armbrust

Identifying shared responses to nitrate starvation among three diatoms using whole-cell transcriptomics
AGU/ASLO Ocean Science Meeting,Salt Lake City, Utah
S.J. Bender, **C.A Durkin**, D. Schruth, R.L. Morales, E.V. Armbrust

2011 Excessive silicic acid supply leads to increased silicification in coastal diatoms
Eastern Pacific Ocean Conference, Fallen Leaf Lake, California
Durkin, **C.A.,** S.J. Bender, K. Gaessner, E.V. Armbrust

2011 Diversity in iron-limited diatoms has varied effects on silicon cycling
PSA Annual Meeting, Seattle, Washington
Durkin, C.A., A. Marchetti, S.J. Bender, T. Truong, R. Morales, E.V. Armbrust

2010 Common cell wall related genes in diatoms and their potential use as biological indicators in changing ocean environments
AGU/ASLO Ocean Science Meeting, Portland, Oregon
Durkin, C.A., S.J. Bender, T. Truong, A. Marchetti, E.V. Armbrust

Taxonomic and metabolic shifts in an iron-stimulated eukaryotic marine plankton community from the NE Pacific Ocean revealed through comparative metatranscriptomics
AGU/ASLO Ocean Science Meeting, Portland, Oregon

Marchetti, A,D Schruth, **C Durkin**, C Berthiaume, R Morales, MS Parker, R Kodner, EV Armbrust

2009 Contribution of different diatom genera to total community silicification in a coastal to open ocean transect and in response to iron fertilization.
ASLO Aquatic Science Meeting, Nice, France
Durkin, CA, A Marchetti, R Morales, EV Armbrust

Patchiness and diel variability of phytoplankton communities in the subarctic pacific ocean revealed by continuous-monitoring flow cytometry.
ASLO Aquatic Science Meeting, Nice, France
Ribalet, F., R. Morales, J. Swalwell, A. Marchetti, **C.A. Durkin**, D. Schruth, G. van den Engh, E.V. Armbrust.

2009 Biogeochemical implications of diatom growth, silicification, and species composition in iron limited environments.
Graduate Climate Conference, Pack Forest, Washington
Durkin C.A., A. Marchetti, R. Morales, E.V. Armbrust

2008 Chitin as a component of the diatom cell wall.
AGU/ASLO Ocean Science Meeting, Orlando, Florida
Durkin, CA, T. Mock, R. Marohl, E.V. Armbrust

Whole genome expression profiling of the marine diatom Thalassiosira pseudonana: New insites into the molecular underpinnings of global-scale processes.
AGU/ASLO Ocean Science Meeting, Orlando, Florida
Mock, T, MP Samanta, V Iverson, C Berthiaume, M Robison, K Holtermann**, C Durkin**, S Splinter BonDurant, K Richmond, M Rodesch

2007 Unexpected presence, diversity, and expression of chitin synthase genes in diatoms.
ASLO Aquatic Sciences Meeting, Santa Fe, New Mexico
Durkin, C. A., T. Mock, E.V. Armbrust